FACULTY OF CHEMISTRY

DEPARTMENT OF PHYSICAL CHEMISTRY AND TECHNOLOGY OF POLYMERS

Modulating cell adhesion through electroactive, chemical, and topographical cues for biomedical applications

Modulowanie adhezji komórkowej poprzez bodźce elektroaktywne, chemiczne i topograficzne w zastosowaniach biomedycznych

mgr. Sara Shakibania

Supervisor: dr hab. inż. Katarzyna Krukiewicz, prof. PŚ

Acknowledgment

I would like to express my deepest gratitude to my supervisor for her invaluable mentorship, continuous support, and encouragement throughout my PhD journey. Her expertise, constructive advice, and trust in my abilities have greatly contributed to my academic and personal development and have been instrumental in the successful completion of this thesis.

I am sincerely grateful to my family (Homeira, Ghasem, and Sina) for their unconditional love, endless encouragement, and unwavering belief in me. Their support has been my greatest source of strength throughout this journey.

I would also like to express my heartfelt gratitude to my boyfriend, Patryk, for his patience, understanding, and constant encouragement. His support during both the challenging and rewarding moments of my PhD has meant more to me than words can express.

I would also like to express my heartfelt gratitude to my dear friends (Sahar, Minoo and Mehraban) for their friendship, kindness, and support throughout my PhD journey.

My sincere thanks also go to Manus J. P. Biggs, Daria Niewolik, Małgorzata Bogusz, Marcin Basiaga, Katarzyna Jaszcz, Barbara Bednarczyk-Cwynar, Magdalena Skonieczna, Wiktoria Lipińska, Katarzyna Grochowska, Jakub Karczewski, Joanna Knapczyk-Korczak, Urszula Stachewicz, Jadranka Travas-Sejdić, Alireza Akbarinejad, Yang Hui, Peng Du, Rodney O'Connor, and Martin Bača for their collaboration, valuable discussions, technical assistance, and support throughout different stages of this research.

Finally, I would like to thank the members of the Bioélectronique (BEL) Group at the University of Mines Saint-Étienne and Advanced Materials and Bioelectronics Lab at the University of Auckland for their support during my research stay. I am truly grateful to everyone who contributed, directly or indirectly, to the successful completion of this thesis.

Abstract

Cell adhesion plays a critical role in regulating cellular survival, proliferation, migration, and tissue regeneration, making it a key factor in the performance of biomedical implants and tissue-engineered scaffolds. However, inadequate interactions at the cell–material interface often led to fibrosis, scarring, insufficient tissue integration, or implant failure. Therefore, understanding how material surface properties influence cellular behavior is essential for the development of advanced biomaterials for regenerative medicine and tissue engineering applications.

This thesis investigates the modulation of cell adhesion through electroactive, chemical, and topographical cues by tailoring the properties of biomaterial surfaces. Different surface engineering strategies have been explored to examine how parameters such as surface charge, wettability, roughness, topography, electrochemical properties, and bioactive chemistry affect cell–material interactions. Nanoscale topographical engineering of titanium surfaces revealed that nanoarchitectures strongly influence cellular morphology, adhesion, migration, and network formation. Chemical functionalization of the titanium surface using bioactive polymer coatings enabled selective modulation of cellular adhesion while simultaneously promoting bioactivity and mineralization. Conducting polymer coatings improved electrochemical performance by increasing electroactive surface area, reducing impedance, and enhancing charge transfer at the electrode–tissue interface, while also supporting neural cell adhesion and neurite outgrowth. Electroactive modifications of electrospun polymeric scaffolds demonstrated that altering surface charge and conductivity significantly improved cellular attachment, and cell spreading.

Overall, this work demonstrates that cellular responses can be effectively directed through precise control of surface properties. By integrating electroactive materials, chemical modifications, and nanoscale topographical features, this thesis contributes to the development of multifunctional biomaterial interfaces with improved performance for biomedical implants, neural interfaces, and tissue scaffolds.

Streszczenie

Adhezja odgrywa kluczową rolę w regulacji zachowania komórek, tj. ich przeżycia, proliferacji, migracji, oraz regeneracji tkanek, stanowiąc jeden z najważniejszych czynników determinujących skuteczność implantów biomedycznych i rusztowań do inżynierii tkankowej. Jednak oddziaływania pomiędzy komórkami z biomateriałem często prowadzą do włóknienia, powstawania blizn, niewystarczającej integracji z tkanką lub niepowodzenia implantacji. Dlatego zrozumienie wpływu właściwości powierzchni materiałów na zachowanie komórek jest niezbędne do opracowania zaawansowanych biomateriałów przeznaczonych do zastosowań w medycynie regeneracyjnej i inżynierii tkankowej.

Niniejsza rozprawa doktorska skupia się na modulowaniu adhezji komórek za pomocą bodźców elektroaktywnych, chemicznych oraz topograficznych poprzez modyfikację powierzchni biomateriałów. Zastosowano różne strategie inżynierii powierzchni w celu zbadania, w jaki sposób takie parametry jak ładunek powierzchniowy, zwilżalność, chropowatość, topografia, właściwości elektrochemiczne oraz bioaktywna funkcjonalizacja chemiczna wpływają na oddziaływania pomiędzy komórkami a materiałem. Modyfikacja powierzchni tytanu wykazała, że nanostruktury w istotny sposób wpływają na morfologię komórek, ich adhezję, migrację oraz tworzenie sieci komórkowych. Chemiczna funkcjonalizacja powierzchni tytanu z wykorzystaniem bioaktywnych powłok polimerowych umożliwiła selektywną modulację adhezji komórek, jednocześnie zwiększając bioaktywność powierzchni i wspomagając proces mineralizacji. Powłoki z polimerów przewodzących poprawiły właściwości elektryczne poprzez zwiększenie powierzchni elektroaktywnej, zmniejszenie impedancji oraz usprawnienie przeniesienia ładunku pomiędzy elektrodą a tkanką, jednocześnie sprzyjając adhezji komórek nerwowych i wzrostowi neurytów. Elektroaktywna modyfikacja elektroprzędzonych rusztowań polimerowych wykazała, że zmiana ładunku powierzchniowego i przewodności istotnie poprawia adhezję komórek oraz promuje ich wzrost.

Podsumowując, niniejsza praca wykazuje, że odpowiedzi komórkowe mogą być skutecznie ukierunkowane poprzez kontrolowanie właściwości powierzchni. Integracja materiałów elektroaktywnych, modyfikacji chemicznych oraz nanotopograficznych cech powierzchni, przedstawiona w tej pracy, okazała się skuteczna do opracowania wielofunkcyjnych interfejsów biomateriałowych o ulepszonych właściwościach, przeznaczonych do zastosowań w implantach biomedycznych, interfejsach nerwowych oraz inżynierii tkankowej.

Abbreviations

AFM	atomic force microscopy
ALP	alkaline phosphatase
CAM	cell adhesion molecule
CNS	central nervous system
CPE	constant phase element
CPs	conducting polymers
CSC	charge storage capacity
CSF	cerebrospinal fluid
CV	cyclic voltammetry
CVD	chemical vapor deposition
DA	degree of acetylation
DMSO	dimethyl sulfoxide
ECM	extracellular matrix
EDS	energy-dispersive X-ray spectroscopy
EIS	electrochemical impedance spectroscopy
FA	focal adhesion
FAK	focal adhesion kinase
FD	fractal dimension
FESEM	field-emission scanning electron microscopy
GAGs	glycosaminoglycans
HA	hydroxyapatite
hASCs	human adipose-derived stem cells
HPECs	human prostate epithelial cells
HUVEC	human umbilical vein endothelial cells
iCVD	initiated chemical vapor deposition
IEP	isoelectric point
ILK	integrin-linked kinase
LbL	layer-by-layer

NGCs	nerve guidance conduits
NHDF	normal human dermal fibroblasts
NMR	nuclear magnetic resonance
PANI	polyaniline
PBS	phosphate-buffered saline
PCL	polycaprolactone
PDA	polydopamine
PECVD	plasma-enhanced chemical vapor deposition
PEDOT:PSS	poly(3,4-ethylenedioxythiophene):polystyrene sulfonate
PEG	poly(ethylene glycol)
PGs	proteoglycans
piCVD	photoinitiated chemical vapor deposition
PKC	protein kinase C
PLCL	poly(L-lactide-*co*-ε-caprolactone)
PLGA	poly(L-lactide-*co*-glycolide)
PNS	peripheral nervous system
PPy	polypyrrole
PVA	poly(vinyl alcohol)
PVDF	poly(vinylidene fluoride)
Ra	average roughness
RGD	Arg–Gly–Asp
SAMs	self-assembled monolayers
SBF	simulated body fluid
SCI	spinal cord injury
TBI	traumatic brain injury
TCP	tissue culture plastic
TiND	titanium nanodimples
UV-Vis	ultraviolet–visible spectrophotometry
VM	ventral mesencephalon

WCA	water contact angle
XPS	X-ray photoelectron spectroscopy

Contents

Chapter 1 12
1. Introduction 12
1.1. Cell adhesion 13
1.2. Mechanism of cell adhesion 13
1.3. Protein adsorption at the biomaterial interface 15
1.4. Mechanotransduction 17
1.5. Cell signaling after adhesion 20
1.6. Physicochemical factors affecting cellular responses 22
1.6.1. Surface chemistry 22
1.6.2. Surface roughness 24
1.6.3. Surface topography 24
1.6.4. Surface wettability 25
1.6.5. Surface charge 26
1.6.6. Electroactive properties 29
1.7. Surface engineering strategies for modulating cell adhesion 30
1.7.1. Surface nanostructurization 30
1.7.2. Bioactive coatings 31
1.7.3. Electrodeposition 32
1.7.4. Electrospinning 35
1.8. Biomedical applications 36
1.8.1. Neural tissue engineering 37
1.8.2. Neural stimulation 39
1.8.3. Skull implants 41
1.9. Hypothesis and objectives 44
Chapter 2 46
2. Materials and methods 46
2.1. Chemicals 47
2.2. Cells 47
2.3. Biological reagents 47
2.4. Consumables 48
2.5. Laboratory equipment 48
2.6. Software and programmes 48

2.7. Surface modification approaches 49
2.7.1. Topographical modification of Ti surface 49
2.7.2. Fabrication of PEDOT and PANI-based coatings 49
2.7.3. Preparation of PEG-DBB 50
2.7.4. Preparation of nanofibers via electrospinning 51
2.8. Surface characterization 52
2.8.1. Morphological characterisation 52
2.8.2. Chemical characterization 54
2.8.3. Mechanical characterization 54
2.8.4. Electrochemical characterization 55
2.8.5. Hydrolytic degradation 55
2.8.6. Bioactivity of the coatings 56
2.8.7. Biological characterization 56
2.9. Statistical analysis 59
Chapter 3 60
3. Results and Discussion 60
3.1. Influence of surface topography on cell adhesion behaviour 61
3.1.1. Aims and objectives 61
3.1.2. Fabrication and surface characterization of TiND 62
3.1.3. Biocompatibility of unmodified and modified Ti surfaces 65
3.1.4. Effect of nanodimples on cell morphology 66
3.1.5. Effect of nanodimples on focal adhesion formation 71
3.1.6. Perspectives and limitations 73
3.1.7. Conclusions 74
3.2. Effect of bioactive coatings on cell adhesion 75
3.2.1. Aim and objectives 75
3.2.2. Formation of PVA-based electrospun fibers 76
3.2.3. Chemical analysis of PVA-based electrospun fibers 78
3.2.4. Cell viability 79
3.2.5. Cell adhesion 81
3.2.6. Proof-of-concept: modification of titanium surface 83
3.2.7. Support in bone remodeling 84
3.2.8. Perspectives and limitations 86

3.2.9. Conclusion 87
3.3. Electroactive modulation of cellular adhesion 89
3.3.1. Aims and objectives 89
3.3.2. Electrodeposition of conducting polymers 90
3.3.3. Electrochemical characterization 92
3.3.4. Surface characterization 95
.3.3.5 Biological Characterization 101
3.3.6. Perspectives and limitations 105
3.3.7. Conclusion 106
3.4. Modification of nonconductive polymers using conducting polymers 107
3.4.1. Aims and objectives 107
3.4.2. Fabrication of fibers 108
3.4.3. Morphology of fibers 109
3.4.4. Physicochemical characterization 112
3.4.5. Cell viability and morphology 115
3.4.6. Cell attachment 119
3.4.7. *In vitro* degradation studies 122
3.4.8. Perspectives and limitations 125
3.4.9. Conclusions 126
Chapter 4 127
4. Conclusions 127
4.1. Conclusion 128
4.2. Applicability of results 132
4.3. Limitations 133
Chapter 5 135
5. Scientific output 135
5.1. Overview of Scientific Output 136
5.2. Journal Publications 137
5.3. Other publication 142
5.4 International Research Internships 144
5.5. Conference Contributions 145
5.6. Research Grants and Competitive Funding 147
5.7. Patent Applications 147

References.....148

Chapter 1

1. Introduction

1.1. Cell adhesion

Cell adhesion is a fundamental requirement for the survival of anchorage-dependent cells and represents an early and critical step preceding essential cellular processes such as proliferation, migration, and differentiation [1]. Accordingly, the initial attachment of cells to a substrate is widely regarded as a key indicator of their capacity to interact with and respond to their surrounding microenvironment. The strength and stability of cell adhesion, as well as subsequent cellular behaviors including proliferation and differentiation, are strongly influenced by the physicochemical properties of biomaterial surfaces [2], with surface topography playing a particularly important role in modulating these responses [3].

1.2. Mechanism of cell adhesion

The extracellular matrix (ECM) is a fundamental extracellular component of tissues and organs, providing a complex nanoarchitectural environment that surrounds and supports cells. It is a highly hydrated network composed of cell-secreted proteins, including collagen, fibronectin, and elastin, as well as macromolecules such as polysaccharides, hyaluronan, glycosaminoglycans (GAGs), and proteoglycans (PGs). In addition, the ECM incorporates a variety of bioactive soluble factors, including ions, growth factors, cytokines, and hormones, which collectively regulate cellular behavior and tissue homeostasis [4]. Cell adhesion refers to the ability of cells to attach either to other cells or to the ECM through the transmission of intracellular and extracellular forces. This process is fundamental for tissue formation, regeneration, and maintenance of tissue homeostasis. It plays a key role in intercellular communication and in regulating essential cellular functions such as differentiation, cell cycle progression, migration, and survival [5]. Cell–matrix adhesion is primarily mediated by integrin receptors, which are transmembrane proteins that connect extracellular ligands to the intracellular cytoskeleton. In contrast, cell–cell adhesion is governed by specific adhesion molecules located at the cell surface. Integrins link ECM components to the actin cytoskeleton through focal adhesion complexes, which serve as mechanical and signaling hubs that maintain cellular architecture and regulate processes such as migration, proliferation, and differentiation [6].

Cell adhesion can be classified into two main types: passive adhesion, typically observed *in vitro* under static culture conditions, and dynamic adhesion, occurring *in vivo* under physiological conditions involving fluid flow, such as blood circulation [7]. *In vitro* cell

adhesion can be described in three successive stages. Initially, cells establish weak interactions with the substrate surface, followed by cell spreading and flattening (**Figure 1**). This is subsequently accompanied by the formation and maturation of focal adhesions that anchor the cell firmly to the substrate [6].

The biological effects of biomaterials and their interactions with cellular functions are commonly investigated using *in vitro* models, which provide simplified and experimentally controllable systems that approximate key aspects of the *in vivo* environment. In these models, cells are seeded onto biomaterial surfaces to investigate processes such as initial attachment, spreading, proliferation, and subsequent cell–material interactions. However, cellular responses may differ substantially between two-dimensional and three-dimensional environments, as 3D scaffolds provide a more physiologically relevant architecture that enables complex cell–matrix interactions and the spatial distribution and remodeling of ECM proteins [8].

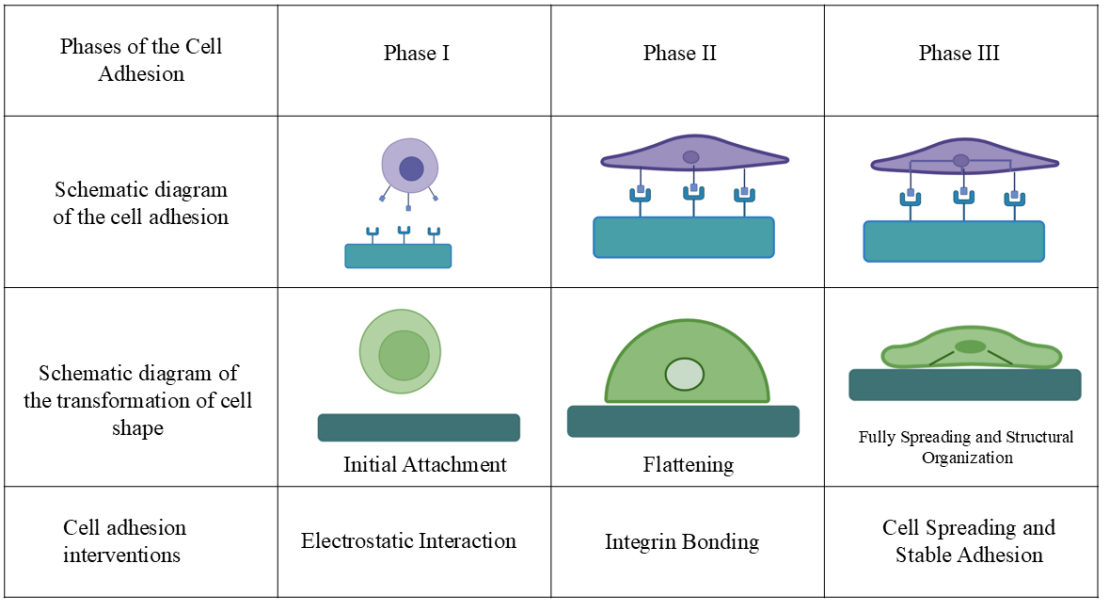


Figure 1. Stages of *in vitro* cell adhesion, illustrating initial substrate attachment, cell spreading, and focal adhesion formation during the establishment of stable cell–substrate interactions (adapted and reprinted with permission from [6] and recreated in BioRender).

1.3. Protein adsorption at the biomaterial interface

Protein adsorption is the first biological event that occurs when a biomaterial comes into contact with physiological fluids, leading to the formation of an interfacial protein layer that mediates subsequent cell–material interactions [9]. Upon implantation, material surfaces are rapidly conditioned by proteins derived from blood and interstitial fluids, meaning that cells do not interact directly with the bare substrate but instead with this adsorbed protein layer [10]. The composition of this layer is highly dynamic. In the initial stage, adsorption is mainly governed by protein transport to the surface via diffusion. As time progresses, however, competitive interactions between proteins with different surface affinities become increasingly important. This can lead to a continuous exchange process in which initially adsorbed proteins are displaced by others with higher affinity, a phenomenon commonly known as the Vroman effect [11]. First described by Leo Vroman and Ann Adams in the late 1960s, this effect describes the time-dependent and competitive nature of protein adsorption from complex biological fluids. Abundant plasma proteins with relatively low surface affinity adsorb rapidly at early time points due to diffusion-controlled transport. Over time, these proteins are progressively replaced by less abundant species with higher binding affinity, resulting in a continuously evolving surface composition governed by both transport kinetics and competitive adsorption processes (**Figure 2**) [12]. By the time cellular components reach the biomaterial surface, it is therefore typically covered by a pre-adsorbed protein layer rather than being exposed directly. As a result, cellular responses are determined by interactions with this protein-coated interface rather than the underlying material itself [11].

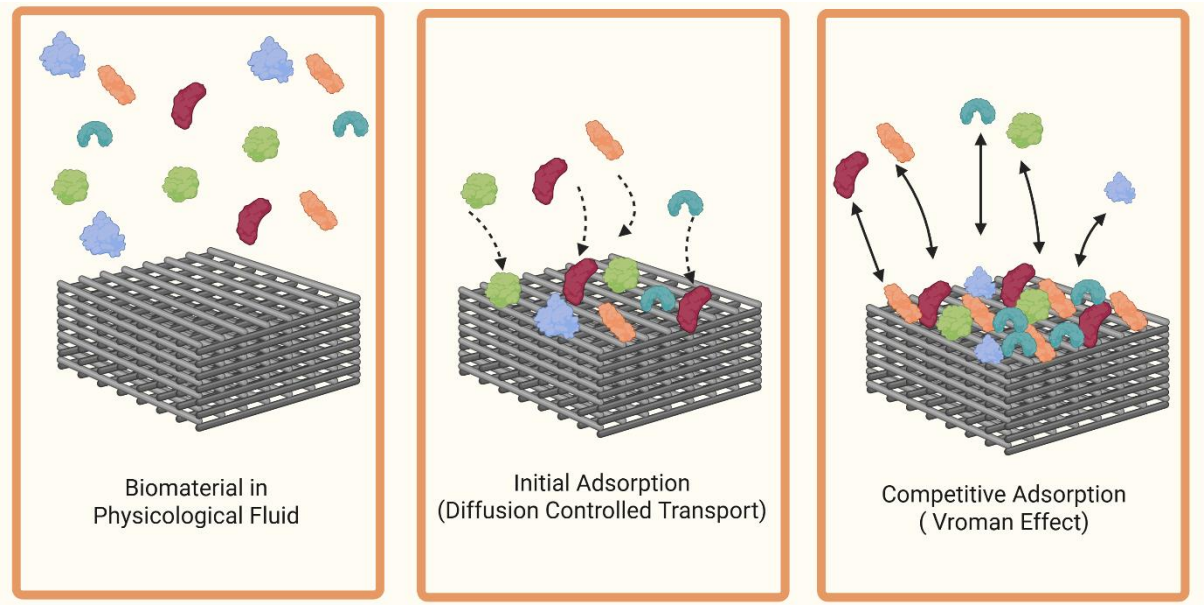


Figure 2. Schematic illustration of Vroman Effect which shows the time-dependent and competitive nature of protein adsorption from complex biological fluids on the surface of the biomaterial. Created in BioRender.

Among the adsorbed proteins, ECM adhesion proteins such as fibronectin and vitronectin play a central role in regulating cell attachment, morphology, and migration. These early adhesion events are critical for downstream biological processes such as cell survival, proliferation, and differentiation, and ultimately influence tissue healing. The extent, composition, and stability of protein adsorption are influenced by multiple factors, including the physicochemical properties of the biomaterial surface, the structural and chemical characteristics of the proteins, and competitive interactions among proteins present in the surrounding medium [10] [11, 13]. Protein adsorption is primarily driven by interfacial forces such as hydrophobic interactions mediated by structured water layers, hydration forces arising from water organization at the interface, and electrostatic interactions between charged groups on both the protein and the material surface. Together, these interactions determine the amount, orientation, and stability of adsorbed proteins [14].

Surface chemistry plays a crucial role in determining not only the quantity but also the biological functionality of adsorbed proteins. Hydrophobic surfaces often promote higher protein adsorption but may induce conformational changes or unfavorable orientations that mask cell-binding motifs, thereby reducing biological activity. On the other side, highly hydrophilic surfaces, such as hydrogels, can also exhibit reduced protein and peptide

adsorption due to the formation of a strongly hydrated layer at the material interface. This limited adsorption of adhesion-mediating biomolecules may subsequently hinder cell attachment and spreading, resulting in reduced or even suppressed cellular adhesion [15]. In contrast, moderately hydrophilic surfaces are more likely to preserve protein conformation and promote favorable orientation, facilitating integrin binding, focal adhesion formation, and enhanced cell adhesion. Therefore, biomaterial performance depends not only on the amount of adsorbed proteins but also on the accessibility of their functional domains [9].

In addition to adsorption quantity, the orientation and conformational stability of proteins are crucial in determining cellular responses. Adhesive ECM proteins such as fibronectin, vitronectin, and laminin contain specific cell-binding domains, including the Arg–Gly–Asp (RGD) sequence, which must remain accessible for recognition by integrin receptors. Surface properties such as chemistry, charge, and wettability influence not only adsorption levels but also protein orientation and structural integrity [9].

Despite extensive research on protein behavior at solid–liquid interfaces, the fundamental mechanisms governing protein adsorption from single- and multi-component systems, as well as the associated adsorption kinetics, remain incompletely understood. In particular, the influence of surface properties on competitive protein adsorption and conformational changes continues to require systematic investigation [16].

1.4. Mechanotransduction

Mechanotransduction is the process by which cells convert mechanical stimuli into biochemical signals [17]. Over the past decades, research has identified numerous mechanosensitive components involved in this process, including stretch-activated ion channels, caveolae, integrin- and cadherin-mediated adhesion complexes, growth factor receptors, myosin motors, the cytoskeleton, the nucleus, and ECM components [18]. Rather than functioning independently, these elements operate as interconnected systems that transmit and integrate mechanical signals across multiple length scales. Such hierarchical organization enables the distribution and concentration of mechanical forces onto specific mechanotransductive elements, thereby coordinating cellular responses essential for mechanosensation, embryonic development, tissue homeostasis, and physiological regulation [19].

Mechanical forces are now recognized as key regulators of embryonic development, cellular differentiation, normal tissue function, and the progression of numerous pathological conditions [20]. Consequently, considerable attention has been devoted to understanding how cells detect and respond to changes in their physical microenvironment. Among the various mechanosensitive structures identified, integrin- and cadherin-mediated adhesion complexes play a central role because they not only transmit mechanical forces but also initiate intracellular signaling pathways that regulate diverse cellular functions [21].

Integrins are transmembrane receptors that mediate cell adhesion to the ECM and serve as primary mechanosensors of the extracellular environment. Upon ligand binding, integrins undergo clustering and activation, promoting the recruitment of cytoplasmic adaptor proteins that physically connect integrins to the actin cytoskeleton [22] [23]. This mechanical coupling enables cells to sense the stiffness and composition of the surrounding ECM while simultaneously regulating matrix remodeling through downstream signaling pathways that control the expression of ECM-related proteins. Consequently, integrin-mediated mechanotransduction plays a fundamental role in regulating cellular processes such as proliferation, migration, survival, and differentiation in response to mechanical stimuli [24].

The transmission of mechanical forces between the extracellular environment and the intracellular cytoskeleton is primarily achieved through focal adhesions (FAs), specialized multiprotein complexes assembled around activated integrins [25]. FAs are highly dynamic structures that continuously assemble, mature, and disassemble in response to mechanical and biochemical cues. During maturation, FAs progressively increase in size while undergoing extensive compositional remodeling, thereby strengthening the mechanical linkage between the ECM and the actin cytoskeleton. Beyond their structural role, FAs function as major signaling platforms that regulate cytoskeletal organization, traction force generation, and intracellular signaling pathways controlling cell migration. These structures establish a physical connection between integrin receptors bound to the ECM and the actin cytoskeleton, enabling bidirectional force transmission and signal transduction. In addition to mediating cell–ECM interactions, cells also transmit forces to neighboring cells through specialized cell–cell adhesion complexes, both of which contribute to maintaining tissue integrity and coordinating cellular responses to mechanical stimuli [7]. These processes are essential for numerous physiological and pathological events, including embryonic development, wound healing, and cancer metastasis. Depending on their size (approximately 0.1–10 μm^2), molecular

composition, and stage of maturation, FAs are commonly classified as nascent adhesions, focal complexes, or mature focal adhesions (**Figure 3**) [26].

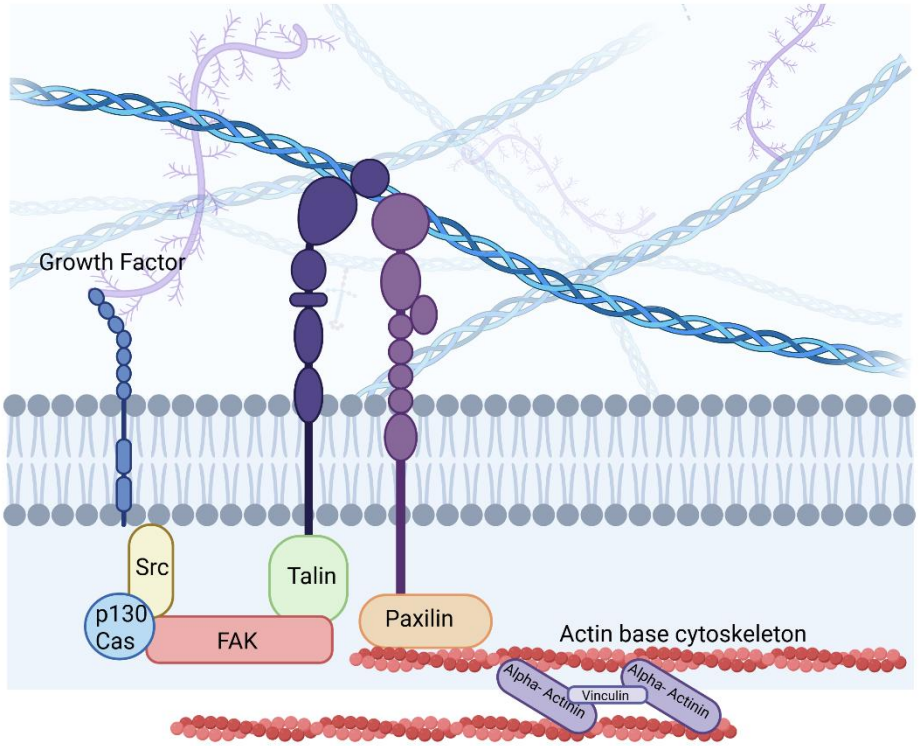


Figure 3. Schematic illustration of focal adhesion composition. Focal adhesions are dynamic multiprotein complexes assembled at the plasma membrane that serve as critical sites for cell–extracellular matrix interactions. These structures mediate bidirectional signal transduction between the extracellular environment and the intracellular cytoskeleton, thereby regulating key cellular processes including adhesion, migration, proliferation, and differentiation (adapted from reprinted with permission from [27] and recreated in BioRender).

1.5. Cell signaling after adhesion

Cells express a diverse array of cell-surface adhesion receptors that not only serve as mechanical interfaces connecting cells to the ECM and neighboring cells but also function as signaling mediators that regulate key cellular processes, including survival, proliferation, migration, and differentiation. Under normal physiological conditions, most adherent cells require attachment to the ECM to maintain viability and undergo apoptosis upon loss of adhesion, emphasizing the fundamental role of adhesion-mediated signaling in cell survival [28].

Dynamic interactions between cells and the ECM, as well as between neighboring cells, provide continuous biochemical and mechanical signals that regulate cellular behavior. These adhesive interactions form the basis of anchorage-dependent growth and influence numerous intracellular signaling pathways involved in cell cycle progression and cell fate determination. Recent studies [29] have demonstrated that integrins and other cell adhesion molecules (CAMs) regulate not only the early signaling events initiated by soluble growth factors but also downstream pathways controlling proliferation and survival. These functions largely depend on the ability of CAMs to assemble highly organized signaling complexes that coordinate efficient intracellular signal transduction [30].

Among the major classes of cell adhesion molecules, integrins and cadherins function cooperatively to regulate both cell adhesion and intracellular signaling [31]. Cadherins mediate calcium-dependent homophilic cell–cell adhesion and are mechanically linked to the actin cytoskeleton through a protein complex composed of β-catenin, α-catenin, and vinculin. Beyond their structural role, cadherins also regulate intracellular signaling by controlling the availability of cytoplasmic β-catenin. Within the canonical Wnt signaling pathway, inhibition of the APC/GSK-3β destruction complex prevents β-catenin degradation, allowing its accumulation in the cytoplasm and subsequent translocation into the nucleus [32]. Nuclear β-catenin associates with transcription factors such as LEF-1 to regulate the expression of genes involved in cell proliferation and differentiation. Furthermore, β-catenin activity is also influenced by integrin-linked kinase (ILK), highlighting the functional crosstalk between integrin-mediated adhesion signaling and the Wnt/β-catenin pathway.

In addition to their interaction with cadherins, integrins cooperate with other adhesion receptors, including syndecan-4, to regulate cell spreading and focal adhesion maturation on fibronectin substrates [33]. Upon ligand binding, integrins recruit numerous focal adhesion

proteins, including talin, focal adhesion kinase (FAK), paxillin, Src, α-actinin, vinculin, and p130Cas, which assemble into signaling complexes at the cytoplasmic tail of β1-integrins. Simultaneously, syndecan-4 binds to the heparan sulfate-binding domains of fibronectin and activates signaling pathways involving protein kinase C (PKC) and Rho family GTPases. The coordinated activation of these pathways promotes cytoskeletal organization, focal adhesion maturation, and stable cell adhesion, illustrating the functional integration of multiple adhesion receptors in regulating cellular responses to the extracellular environment (**Figure 4**) [30].

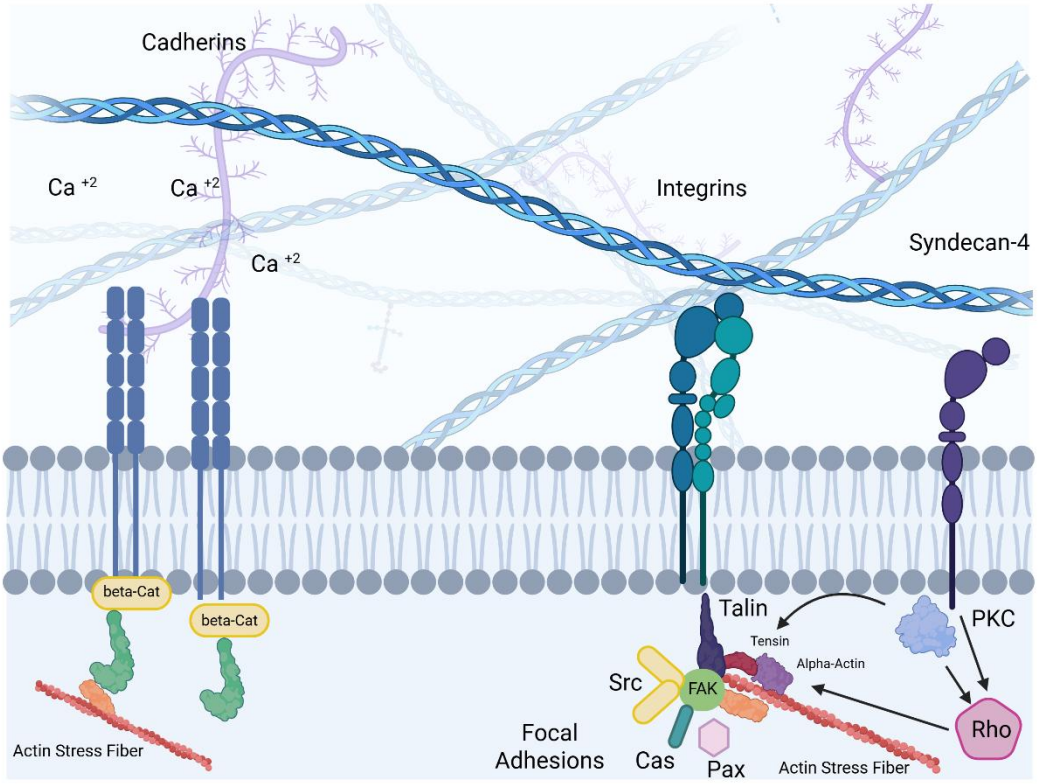


Figure 4. Crosstalk and synergistic interactions among cell adhesion molecules contributing to the coordinated regulation of cell–cell and cell–extracellular matrix adhesion (adapted and reprinted with permission from [27]and re-created in BioRender).

1.6. Physicochemical factors affecting cellular responses

From a materials engineering perspective, the properties of biomaterial surfaces including topographical features [34], mechanical stiffness [35], surface functional groups [36], and interfacial free energy, can significantly influence underlying biochemical processes. Moreover, commonly employed surface modification techniques and chemical functionalization strategies can further modulate biomaterial–cell interactions [37].

1.6.1. Surface chemistry

The chemical composition of biomaterial surfaces is a crucial factor governing interactions at the biointerface, influencing the adsorption of biological molecules and the subsequent responses of cells and tissues to implanted materials [38]. In recent years, the development of multifunctional bioactive surfaces has become a central topic in biomedical engineering. Through surface modification strategies, it is possible to tailor material interfaces to exhibit a range of desired properties, such as improved cell adhesion and proliferation, as well as antibacterial and anti-inflammatory activity. Various aspects of cell adhesion, differentiation, proliferation, and migration are strongly influenced by the chemical composition of the surface [39], provided by introducing specific biochemical components onto material surfaces, thereby enabling targeted biological responses and enhanced interaction with the surrounding biological environment [40].

Common functional groups employed to modify the surface chemistry of biomaterials include $–CH_3$, $–NH_2$, –COOH, –OH, –CO–, and $–CO_3^{2–}$ [41]. A wide range of techniques has been developed to alter the surface properties of bulk materials. These include plasma and ultraviolet (UV) treatments, self-assembled monolayers (SAMs), layer-by-layer (LbL) assembly, polymer brush fabrication through both "grafting to" and "grafting from" approaches, thin-film deposition *via* vapor-phase reactions, as well as chemical vapor deposition (CVD)-based methods such as plasma-enhanced CVD (PECVD), initiated CVD (iCVD), and photoinitiated CVD (piCVD). would it be correlating with effect of surface chemistry on cell behavior. By modifying surface chemistry, these approaches regulate key interfacial properties such as surface energy, charge, and functional group availability, which ultimately govern protein adsorption and downstream cell adhesion, proliferation, and differentiation [42].

In a study by Liu et al. [43] investigated the influence of surface chemistry on the behavior of human adipose-derived stem cells (hASCs). To systematically vary surface chemical

functionality, self-assembled monolayers of alkanethiolates on gold substrates were used as a model system, enabling the presentation of distinct terminal groups such as hydroxyl (–OH), carboxyl (–COOH), amine ($–NH_2$), phenyl, thiol (–SH), bromine (–Br), and methyl ($–CH_3$). Initial observations showed that hASC morphology and focal adhesion organization varied significantly depending on the underlying surface chemistry. The results further demonstrated that amine-terminated surfaces promoted osteogenic differentiation, whereas phenyl- and thiol-functionalized surfaces favored chondrogenic differentiation, as evidenced by elevated expression of type II collagen and aggrecan. In contrast, bromine-terminated surfaces enhanced adipogenic differentiation, indicated by increased expression of PPARγ and aP2. Overall, these findings emphasize the strong regulatory role of surface chemistry in directing stem cell fate and highlight chemical surface modification as a promising strategy for designing biomaterials for tissue engineering and regenerative medicine applications [43].

In another study, Harding et al. [44] demonstrated that plasma polymer gradients can be used to investigate the subtle effects of surface chemistry on embryonic stem cell behavior and to explore the underlying mechanisms governing these responses. By varying the plasma polymerization time, the properties of the resulting gradient could be readily controlled. To evaluate the suitability of these surfaces for screening cell–material interactions, the response of mouse embryonic stem cells was examined and compared across substrates prepared with different deposition times. A strong relationship was observed between surface chemistry and cellular responses, including adhesion, colony size, and maintenance of stem cell marker expression. Notably, both cell attachment and colony formation varied markedly across gradients generated under different plasma deposition conditions. The deposition time was found to influence the thickness of the plasma polymer layer and the spatial distribution of surface functional groups, while the overall range of plasma-generated chemical species remained unchanged [44]. In such systems, it is generally assumed that surface properties influence the adsorption of protein components from the surrounding culture medium, and that the resulting changes in cellular behavior arise from a complex interplay between the solid substrate and the protein-containing liquid phase in contact with it. In this study, cellular responses observed along the gradient appear to be governed primarily by variations in the thickness of the deposited film, which in turn affect the adsorption of adhesion-promoting serum proteins from the culture medium [45].

1.6.2. Surface roughness

Surface roughness is a key physicochemical property of biomaterials that describes the microscopic texture and irregularities of a material surface. It is commonly quantified using roughness parameters such as the R_a or S_a. Surface roughness can be tailored using techniques including mechanical blasting, acid etching, electropolishing, nanoparticle deposition, electrospinning, and micro-/nanofabrication methods. Modifying surface roughness influences protein adsorption, cell attachment, proliferation, and differentiation by altering the available surface area and the physical cues presented to cells [37]. Chung et al. [46] demonstrated that introducing nanoscale roughness (10–100 nm) onto polyurethane surfaces significantly enhanced the adhesion, proliferation, and metabolic activity of human umbilical vein endothelial cells (HUVECs) when compared with a smooth surface. The roughest surfaces exhibited the highest cell density, highlighting the important role of nanoscale roughness in regulating cell–material interactions and supporting tissue engineering applications.

1.6.3. Surface topography

Surface topography refers to the geometric and morphological features of a material surface, including its spatial arrangement and structural organization. Based on the directional distribution of these features, surface topography can generally be classified as isotropic, exhibiting similar characteristics in all directions, or anisotropic, displaying preferential orientation or direction-dependent characteristics [47]. Nanotopography refers to the controlled modification of surfaces to generate nanoscale features, including nanopores, nanotubes, nanodots, nanoroughness, nanogrooves, and hierarchical micro/nanostructures [48]. These engineered architectures can mimic specific features of the ECM, providing physical cues that influence cellular behavior.

Despite extensive research, the molecular mechanisms through which cells sense and respond to surface topography remain incompletely understood. Nevertheless, current evidence indicates that two interconnected processes: mechanotransduction mediated by the cytoskeleton and integrin-dependent signaling play central roles in governing these responses [49].

Schulte et al. [50] investigated whether surface topography alone could regulate cellular behavior on an inherently nonadhesive biomaterial without the need for additional chemical functionalization. The selected model material consisted of a hydrogel fabricated from star-

shaped poly(ethylene glycol) macromonomers. While smooth hydrogel surfaces exhibited minimal cell adhesion, the introduction of microstructured topographies promoted the attachment and spreading of L929 mouse fibroblasts. Cells aligned along micropatterned grooves and, depending on the feature dimensions, either bridged or occupied the grooves. Topographical features smaller than or comparable to cell dimensions (<10 μm) facilitated the formation of stable focal adhesions, as evidenced by vinculin and actin accumulation. On micropillar arrays, fibroblasts spread across the tops of the pillars while partially enveloping the structures. These findings demonstrate that surface topography alone can significantly enhance cell adhesion on otherwise nonadhesive materials, likely through effects on initial protein adsorption and consequently cell adhesion.

1.6.4. Surface wettability

Among the various surface properties that regulate cell–material interactions, wettability plays particularly important roles by affecting the adsorption of proteins from the surrounding biological environment and the subsequent attachment of cells [51] [52]. In general, surfaces can be classified as hydrophilic (low contact angle) or hydrophobic (high contact angle) [53]. Highly hydrophobic surfaces tend to adsorb larger amounts of proteins; however, the adsorbed proteins may undergo conformational changes that mask cell-binding domains and reduce their biological functionality. Consequently, cell attachment and spreading may be impaired despite extensive protein adsorption. On the other hand, extremely hydrophilic surfaces can limit protein adsorption due to the formation of a strongly bound hydration layer, which may also reduce cell adhesion [54].

The relationship between wettability and cell adhesion is therefore complex and often exhibits an optimum range rather than a simple linear trend. Numerous studies have reported enhanced cellular responses on surfaces with water contact angles between 40° and 70°, although the optimal value depends on the cell type, material composition, and surface chemistry [55]. Surfaces with moderate hydrophilicity promote the adsorption of extracellular matrix proteins while preserving their native conformation and bioactivity [10]. As a result, cells can effectively recognize adhesion sites through integrin receptors, leading to enhanced spreading, proliferation, and cytoskeletal organization [56].

1.6.5. Surface charge

Electrostatic potential arises from the redistribution of ions and charged species at the interface between two distinct phases, resulting in the development of an interfacial charge layer. This charge separation generates an electrical potential difference across the interface, which influences electrostatic interactions between the material surface and the surrounding biological environment [6] [57]. Consequently, the surface charge of a biomaterial significantly influences the initial interactions between the material and biological molecules [6, 58]. Surface charge refers to the quantity and distribution of electrical charges present at a material surface, whereas surface potential describes the electrical potential generated by these charges at the solid–liquid interface [59] [60].

Since most cell membranes possess an overall negative charge due to the presence of phospholipids and glycoproteins, electrostatic interactions between cells and the substrate can affect cell attachment [61]. Positively charged surfaces generally promote stronger cell adhesion by attracting negatively charged proteins and cellular components. This enhanced adsorption of adhesion-mediating proteins, such as fibronectin, vitronectin, and laminin, facilitates the formation of focal adhesions and strengthens cell–substrate interactions [52] [62]. Conversely, negatively charged surfaces may exhibit reduced direct electrostatic attraction toward cells. However, cell adhesion on negatively charged substrates is not solely determined by charge polarity but also depends on the type, orientation, and conformation of adsorbed proteins. In some cases, negatively charged surfaces can support effective cell attachment when they promote favorable protein adsorption and maintain the biological activity of adhesion ligands [51].

Surface charge also affects the organization of the electrical double layer at the material–liquid interface, influencing ion distribution and local cellular microenvironments. These factors can alter cell signaling pathways and ultimately impact cellular responses. Therefore, optimizing surface charge is essential for improving the biocompatibility and biological performance of biomaterials [9]. For instance, Chang et al. [63] studied, the influence of surface potential on epithelial cell behavior using human embryonic kidney (HEK293T) cells and human hepatocellular carcinoma (HepG2) cells. Binary SAM-modified gold substrates were employed to generate a series of surfaces with comparable mechanical and chemical properties while systematically varying surface potential, enabling isolation of electrostatic effects on cellular responses. The results indicated that epithelial cell adhesion density increased with increasing surface potential, exhibiting a trend similar to that observed in fibroblasts, although with more

pronounced variation. In contrast, cell proliferation rates in both epithelial cell types appeared to be independent of surface potential. Moreover, epithelial cells did not exhibit noticeable morphological changes across different surface potentials, whereas fibroblasts showed clear morphology-dependent responses under the same conditions.

Surface charge and wettability are closely interconnected and often act synergistically to regulate cell behavior. Modifications that alter surface chemistry frequently affect both properties simultaneously. These changes influence the adsorption, orientation, and biological activity of proteins at the biomaterial interface, which ultimately determine the extent of cell attachment and spreading. A surface possessing suitable wettability and an appropriate charge density can enhance protein-mediated cell adhesion, promote focal adhesion formation, and improve overall cellular performance. Consequently, controlling both surface charge and wettability has become a common strategy in the design of biomaterials for tissue engineering, regenerative medicine, and implant applications. For instance, Guo et al. [64] developed a two-dimensional surface modification strategy to independently control surface charge and wettability while minimizing the influence of other parameters, such as surface roughness. This was achieved by adjusting the polyion charge density during layer-by-layer assembly and modifying the chemical structure of the polymer side chains. The resulting surfaces exhibited isoelectric points between 5 and 9 and water contact angles ranging from 35° to 70°. Using this platform, the effects of surface charge and wettability on protein adsorption and NIH/3T3 fibroblast adhesion were evaluated. Both parameters influenced protein adsorption and cell attachment, with positively charged, moderately hydrophilic surfaces promoting the greatest cell adhesion, whereas negatively charged, hydrophobic surfaces showed the lowest adhesion. These findings demonstrate the combined importance of surface charge and wettability in regulating biomaterial–cell interactions.

Apart from wettability, the surface charge of biomaterials is governed by multiple interconnected factors, including chemical composition, microstructural organization, surface topography, mechanical characteristics, and surface free energy. Although significant progress has been made in understanding these effects, the mechanisms by which surface charge regulates cellular responses remain incompletely understood [65]. Several challenges continue to limit progress in this area, including the lack of standardized approaches for measuring and reporting zeta potential, variability in the assessment of charge magnitude and stability over time, and limited integration of electrochemical principles into experimental design and data interpretation. Therefore, a more comprehensive understanding of electrical charge effects in

biomaterial–tissue interactions is crucial for the rational design of implant surfaces with improved biological performance [58]. **Figure 5** shows a schematic illustration of how tailoring physicochemical properties can modulate the cell adhesion and consequently improve tissue engineering.

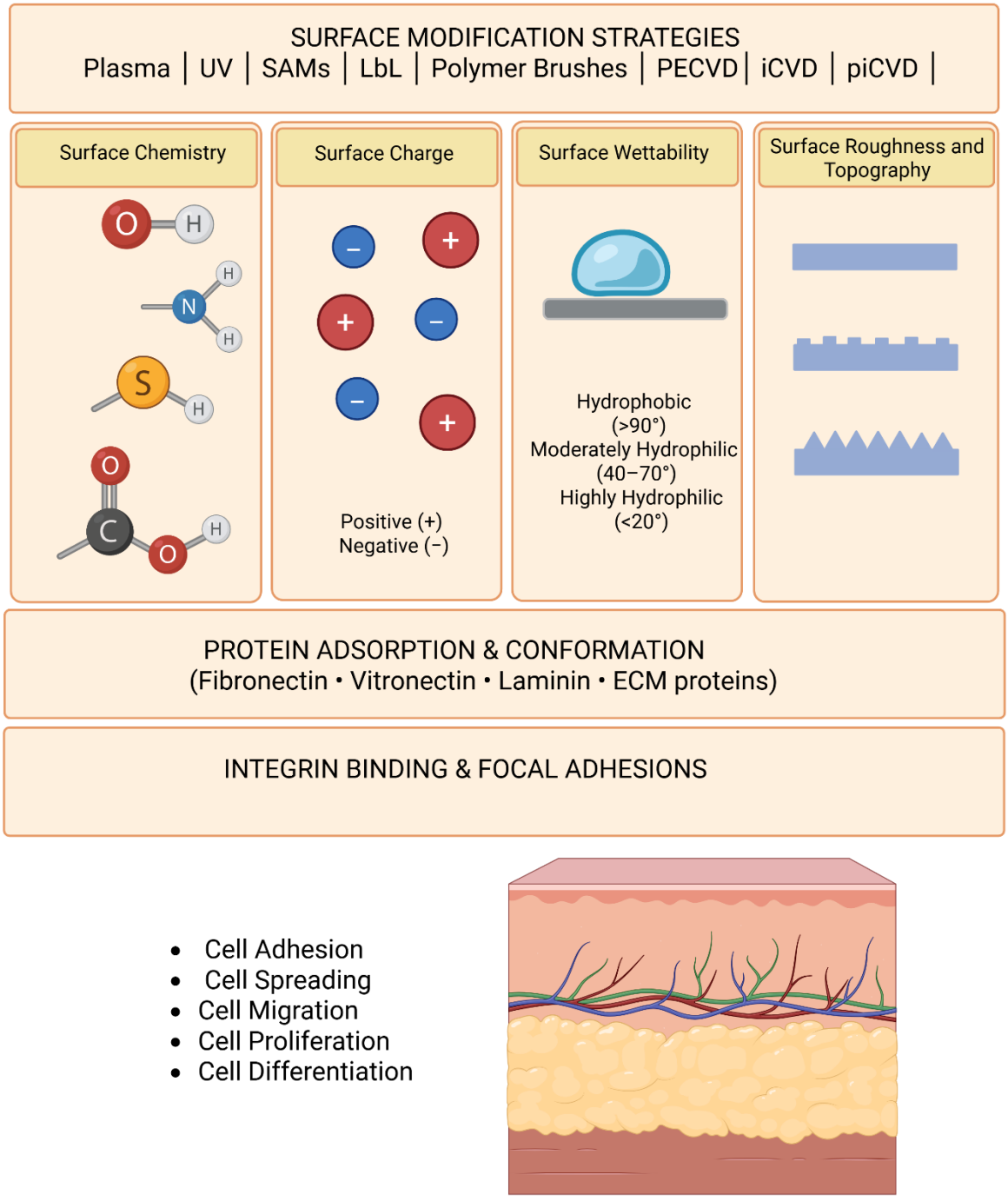


Figure 5. Schematic illustration of the modulation of cellular responses through surface modification. Created in BioRender.

1.6.6. Electroactive properties

It is well known that cells exhibit both active and passive electrical characteristics [66]. The active component is primarily represented by the transmembrane potential, typically ranging from approximately −90 mV to −10 mV, which is sustained by ionic gradients established through membrane transport mechanisms such as the Na^+/K^+-ATPase pump. In contrast, the passive surface potential is generated by the distribution of negatively charged membrane constituents, including phosphatidylserine and various membrane-associated proteins [67] [68]. Unlike the transmembrane potential, this passive electrostatic property can persist even after cell death. Consequently, it is understandable that cell adhesion depends also on the electrical and electrochemical properties of the substrate.

Electroactive biomaterials have gained significant attention due to their ability to serve not only as structural scaffolds but also as regulators of cellular activity, particularly in electrically responsive tissues [69] [70]. These materials can influence various biological processes, including cell migration, proliferation, differentiation, neural signaling, muscle contraction, embryonic development, and tissue repair. The design of electroactive biomaterials is largely inspired by endogenous bioelectricity and piezoelectricity, enabling the recreation of dynamic electrical cues present in native tissues. Through controlled electrical stimulation, these materials can modulate cellular responses and promote regeneration [71].

Recent advances have demonstrated the potential of electroactive biomaterials in directing stem cell fate and enhancing tissue repair, particularly in nerve, bone, and cardiac tissue engineering [70]. For instance, Barrejon et al. [72] investigated a covalent surface-functionalization strategy to improve the integration of Poly(3,4-ethylenedioxythiophene) PEDOT with carbon microfibers. Aminophenyl-EDOT derivatives enabled effective covalent modification of the carbon surface and subsequent PEDOT electropolymerization; however, their incorporation adversely affected charge-transfer characteristics. In contrast, the azido-functionalized derivative, EDOT-Ph-N_3, provided efficient carbon surface modification while preserving favorable electrochemical properties, exhibiting greater resistance to PEDOT delamination under mechanical stress and after implantation in neural tissue. Furthermore, these modified microfibers demonstrated favorable biological integration within the spinal cord, with minimal tissue damage and cellular reactivity.

Despite encouraging progress, further research is required to optimize material properties and stimulation strategies for successful clinical translation. The ability to reproduce key features

of the natural tissue microenvironment remains crucial for the future development of electroactive biomaterials [73].

1.7. Surface engineering strategies for modulating cell adhesion

Surface engineering approaches for modulating cell adhesion encompass a broad range of strategies that extend beyond purely chemical surface functionalization [74]. In addition to controlling surface chemistry, these methods integrate structural, electrical, and bioactive cues to better replicate the complexity of native biological environments. Approaches such as surface nanostructurization, electrodeposition, and electrospinning, collectively enable more advanced regulation of cell–material interactions. By combining topographical, physicochemical, and biochemical modifications, these approaches provide versatile platforms for influencing cellular adhesion and subsequent biological responses in a controlled manner.

1.7.1. Surface nanostructurization

The surface properties of metallic biomaterials play a crucial role in determining their interaction with biological systems [75]. Although metals such as titanium, stainless steel, cobalt–chromium alloys, and magnesium-based materials possess favorable mechanical properties and are widely used in biomedical implants, their biological performance is largely governed by the characteristics of their surface layer [76]. Therefore, considerable research efforts have been devoted to the development of micro- and nanoscale surface architectures to improve biological responses, including protein adsorption, cell adhesion, proliferation, differentiation, and tissue integration [77].

In particular, nanoscale surface modifications have been shown to regulate cell morphology, cytoskeletal organization, focal adhesion formation, and intracellular signaling pathways by altering the interaction between cells and the underlying material surface [78]. Consequently, nanostructured metallic surfaces have emerged as promising platforms for improving the biological performance of implants used in orthopedics, dentistry, cardiovascular applications, and neural interfaces [79].

For instance, Sjöström et al. [80] fabricated well-defined TiO_2 nanopillar arrays with controllable dimensions ranging from 15 to 100 nm using a through-mask anodization approach. The influence of nanopillar geometry on the early adhesion and spreading behavior

of MG63 osteoblast-like cells was subsequently investigated. Increasing the nanopillar height from 15 to 100 nm resulted in a progressive reduction in cell spreading and promoted a more pronounced elongated cellular morphology. High-resolution analysis of the cell–substrate interface using focused ion beam/scanning electron microscopy demonstrated that the taller nanopillars limited the ability of MG63 cells to conform to the underlying surface architecture, resulting in the formation of interfacial gaps between the cells and the titanium substrate. These findings indicate that nanoscale feature dimensions strongly influence cell–surface interactions and suggest that relatively small surface features, particularly those below approximately 20 nm, may provide more favorable conditions for early osteoblast attachment and spreading.

Titanium is a transition metal known for its outstanding corrosion resistance, high strength-to-weight ratio, and excellent biocompatibility making it a material of choice in biomedical applications. Due to the optimal combination of mechanical, chemical, and biological properties, Ti-based materials are among the most desirable biomaterials, successfully applied in dentistry, orthopedics, and traumatology. Despite these advantages, ongoing research seeks to further enhance cellular response to Ti to improve its performance in clinical applications, and one of the most promising directions is through surface structurization. Commonly recognized and investigated methods for achieving surface modification of Ti include acid etching, grit blasting, mechanical roughening, plasma spraying, anodization or laser milling [81]. However, most of those techniques provide either pore-like or pillar-like short-range organized surface features. In contrast, anodization followed by chemical etching may lead to creating nanoscale features that are uniform all over the prepared samples [82, 83]. It is well known fact that anodization is considered as a highly reproducible process as processing parameters such as applied voltage, electrolyte composition, temperature and cell dimensions are well-controlled [84] [85].

1.7.2. Bioactive coatings

Over the past decades, a wide range of implantable devices based on different material classes has been developed to enhance clinical outcomes and improve patients' quality of life. Traditionally, the selection of implant materials was primarily guided by bulk properties, particularly mechanical performance, as well as general biological response [86]. In this context, relatively inert materials were often preferred in order to minimize foreign body reactions and reduce the risk of implant rejection [87]. A critical aspect of successful

implantation is the proper integration of the device with the surrounding host tissue. Therefore, the development of biomedical implants has evolved from the use of conventional bulk materials to more advanced systems incorporating bioactive surface coatings able to prevent chronic inflammation, excessive fibrous capsule formation, or implant-associated infections [88] [89].

For instance, Xu and Yamamoto [90] reported that uniform, nonporous amorphous poly(L-lactide) (PLLA) coatings exhibited stronger adhesion to magnesium substrates compared with semi-crystalline poly(ε-caprolactone) (PCL) layers. These polymers were investigated as protective coatings to reduce magnesium corrosion and improve cytocompatibility, and both materials supported satisfactory adhesion and proliferation of SaOS-2 cells. Kunjukunju et al. [91] developed multilayer coatings composed of alginate and poly(L-lysine) (PLL) using a layer-by-layer (LbL) assembly approach on alkaline- and fluoride-pretreated AZ31 magnesium alloys. These systems were designed for controlled delivery of growth factors and biomolecules, and subsequent functionalization with fibronectin further improved cellular bioactivity.

In conclusion, bioactive coatings have emerged as a key strategy to enhance the biological performance of biomedical implants by improving tissue integration and guiding cellular responses at the implant–tissue interface. Compared with traditional bulk materials, these surface-engineered systems enable more precise control over biofunctionality while maintaining the required mechanical support of the underlying substrate. Studies involving polymer-based and multilayer coating systems demonstrate their potential to improve adhesion, corrosion resistance, and cellular compatibility. However, achieving a fully optimized coating that ensures long-term stability, controlled bioactivity, and reliable integration *in vivo* remains a significant challenge, highlighting the need for continued research in this field.

1.7.3. Electrodeposition

One of the most successful approaches to the formation of bioactive coatings on the surface of metallic biomaterials is electrodepositon, which is an electrochemical surface modification technique that enables the formation of material coatings through the controlled reduction or oxidation of species at an electrode interface under an applied electrical potential. This versatile approach can be applied to a broad range of materials, including metals, alloys [92], semiconductors [93], metal oxides [94], nanostructured materials, and electrically conductive

polymers [95]. The characteristics of the deposited layers, including their composition, morphology, and microstructure, are strongly influenced by both the nature of the underlying substrate and the electrochemical conditions employed during the deposition process. In particular, parameters such as electrolyte composition, solvent properties, applied potential, current density, and deposition time play crucial roles in determining the final properties of the coating [96].

Surface modification using conducting polymers (CPs) has attracted considerable attention as an effective strategy for enhancing electrode performance and tissue integration. Among the various CPs investigated, poly(3,4-ethylenedioxythiophene) (PEDOT) [97] and polypyrrole (PPy) [98] [99] are the most extensively studied. The electrical properties of these materials originate from their conjugated molecular backbone, which contains alternating single and double bonds that facilitate charge transport. Although CPs are generally classified as semiconducting materials, their conductivity can be significantly enhanced through oxidation (p-type doping) or reduction (n-type doping), enabling conductivity values approaching those of metallic conductors [98].

An important advantage of CPs is the possibility of tailoring their physicochemical characteristics by adjusting both their oxidation state and dopant composition. Such modifications influence not only electrical conductivity and charge transport behavior but also surface morphology, volumetric changes, and biological interactions [100]. In neural engineering applications, CPs offer additional benefits compared with conventional rigid electrode materials. Due to their relatively soft and compliant nature, they can better match the mechanical properties of neural tissue, thereby reducing tissue damage caused by electrode micromotion and minimizing glial scar formation around implanted devices [97]. These characteristics have established CPs as promising materials for the development of advanced neural interfaces [101] [102]. Moreover, their biocompatibility and ability to interact with electrically responsive tissues, including neural, muscular, epithelial, and connective tissues, further support their use in a broad range of bioelectronic and tissue engineering applications [103] [104]. For instance, Ferreira et al. [105] developed composite materials based on polycaprolactone (PCL), poly(lactic-co-glycolic acid) (PLGA), and polypyrrole (PPy). The resulting constructs exhibited favorable biocompatibility, porous morphology, and hydrophilic surface characteristics. Incorporation of PPy imparted electrical conductivity of approximately 2.0×10^{-1} S cm^{-1}, while maintaining thermal stability and a degradation profile suitable for peripheral nerve regeneration applications.

Among conducting polymers, PEDOT has emerged as one of the most widely utilized materials because of its favorable electrical conductivity (typically ranging from 1 to 200 S cm^{-1}), excellent biocompatibility, and long-term electrochemical stability under *in vivo* conditions [106] [107] [108]. Nevertheless, PEDOT coatings, particularly those based on PEDOT doped with poly(styrene sulfonate) (PEDOT:PSS), often exhibit relatively dense and non-porous morphologies, which can restrict tissue infiltration and integration. Certain studies have reported adverse cellular responses associated with its polymerization process. For example, Chen et al. [109] observed immediate membrane damage in both primary neural cells and PC12 cells following the *in situ* polymerization of EDOT in their vicinity. To overcome these limitations, researchers have developed various strategies, including the fabrication of PEDOT nanostructures [97] and the application of lithographic patterning techniques [110]. These approaches have been shown to decrease electrode impedance, enhance polymer adhesion to substrates, improve neural cell attachment, and stimulate neurite extension. Furthermore, considerable research efforts have been directed toward identifying alternative electroactive materials capable of providing improved biological performance while maintaining desirable electrical characteristics.

Another CP with the potential applicability in biomedical engineering is polyaniline (PANI). Previous studies have shown that PANI can support neuronal adhesion, proliferation, and differentiation while simultaneously enhancing the mechanical performance of electrode coatings [111] [112]. In addition, nanostructured PANI coatings increase the effective surface area of electrodes, leading to reduced electrical resistance, enhanced signal transmission efficiency, and increased capacitance [113]. The regenerative potential of PANI-containing systems has also been demonstrated *in vivo*. For instance, Xu et al. [114] successfully employed cellulose–PANI composite conduits for the repair of rat sciatic nerve defects measuring 5 mm. Furthermore, the implanted conduits maintained structural stability for at least three months without significant degradation [114] [115]. Despite these advantages, the conductivity of PANI is highly dependent on environmental pH and is typically maximized under acidic conditions. This pH sensitivity presents a significant challenge for its application in physiological environments, where near-neutral pH conditions prevail [116] [117, 118].

Although CPs represent a versatile class of materials for neural interface, each polymer possesses inherent limitations, including restricted porosity, potential cytotoxic effects associated with polymerization [119] [116], or environmental sensitivity of electrical conductivity [120]. Consequently, ongoing research is focused on developing novel conducting

polymer systems and composites that combine optimal electrical performance with enhanced biological compatibility and long-term stability for tissue engineering applications.

1.7.4. Electrospinning

Electrospinning is a versatile fabrication technique for producing micro- and nanofibrous polymeric matrices with a high surface-area-to-volume ratio, interconnected porous architecture, and tunable fiber morphology. These structural characteristics make electrospun scaffolds highly attractive for biomedical applications, including tissue engineering, drug delivery, wound healing, biosensing, and regenerative medicine [121].

Electrospun fibrous scaffolds have emerged as one of the most extensively explored biomaterial platforms owing to their ability to mimic the fibrous architecture of the native ECM [122]. Unlike autologous grafts, which are associated with donor-site morbidity and limited tissue availability, or allogeneic grafts, which may elicit immune responses, electrospun fibers represent a flexible and attractive alternative for neural tissue engineering applications [123]. These fibrous systems can be tailored to serve as carriers for therapeutic molecules or designed to provide biochemical and physical cues that influence neural stem cell behavior and differentiation [123].

To modulate cell-material interaction, several studies have employed electrospun fibers. For example, Muñoz-González et al. [124] investigated conductive poly(ε-caprolactone)-polypyrrole (PCL–PPy) nanofibers produced through a sequential fabrication process. In this approach, electrospun PCL fibers were first generated and subsequently coated with PPy by immersing the fibers in a solution containing pyrrole monomers and an oxidizing agent, promoting in situ oxidative polymerization on the fiber surface. The incorporation of PPy significantly enhanced the mechanical performance of the resulting scaffolds, with the optimized formulations demonstrating increased tensile strength and Young's modulus compared with pristine PCL nanofibers. Furthermore, PPy modification substantially altered the surface characteristics of the scaffolds by improving their wettability, transforming the initially hydrophobic PCL matrix into a more hydrophilic platform favorable for tissue engineering applications. Biological evaluation using MTT assays with L929 fibroblasts and Alamar Blue assays with bone marrow-derived mesenchymal stem cells (bmMSCs) confirmed the absence of cytotoxic effects and demonstrated enhanced cellular metabolic activity, indicating that the conductive scaffolds could support cell viability and functional activity.

Overall, the study highlighted that the controlled integration of PPy into electrospun PCL matrices provides a promising strategy for developing conductive biomaterial scaffolds with improved mechanical, physicochemical, and biological properties for regenerative medicine applications [124].

In another study an improved hydrophilicity was achieved *via* electrospinning for enhanced cell attachment and proliferation [125]. The surface wettability of electrospun PCL fiber mats was enhanced through co-electrospinning with poly(vinyl alcohol) (PVA) using a dual-spinneret electrospinning technique. Water contact angle measurements demonstrated a significant increase in the hydrophilicity of the resulting PCL/PVA composite mats. To evaluate their biological performance, *in vitro* cell culture experiments were conducted using human prostate epithelial cells (HPECs), comparing cell attachment on pure PCL mats with that on the modified PCL/PVA scaffolds. Microscopic observations obtained from scanning electron microscopy, field-emission scanning electron microscopy, and optical microscopy revealed enhanced cell adhesion and proliferation on the PCL/PVA mats compared with the hydrophobic PCL counterparts [125].

Although synthetic polymer-based electrospun fibers are particularly attractive due to their reproducible fabrication, structural homogeneity, and tunable properties [63], many synthetic polymers possess surface characteristics that are not inherently favorable for cell attachment and subsequent cellular activities [126]. Consequently, optimizing biomaterial surfaces has become a critical aspect of scaffold design, as cellular responses such as adhesion, proliferation, and morphology are strongly influenced by surface-related properties [127]. Parameters including wettability [128], surface charge [129], chemical functionality, and topographical roughness [130] have all been shown to regulate cell–material interactions and ultimately affect tissue regeneration outcomes.

1.8. Biomedical applications

Cell–material interactions play a fundamental role in determining the success of biomaterials used in tissue engineering and regenerative medicine, as they regulate essential cellular processes including adhesion, spreading, proliferation, migration, and differentiation [131]. Therefore, understanding and tailoring cell adhesion through controlled modification of surface properties is essential for the development of effective biomaterial platforms across a wide range of biomedical applications. Although these principles are applicable to various fields of

regenerative medicine, this thesis focuses specifically on their role in neural tissue engineering, where precise regulation of cell–material interactions is particularly challenging due to the complex biological environment and limited regenerative capacity of neural tissues [132].

The scope of this thesis encompasses three interconnected areas within neural biomedical applications: neural tissue engineering, where biomaterial surfaces are engineered to support neural cell adhesion and regeneration [133]; neural stimulation, where optimization of the cell–electrode interface is critical for stable and functional neural interfaces [134]; and cranial implant applications, where controlling cellular responses at the implant–tissue interface is important for promoting favorable integration while minimizing undesirable fibrotic adhesion [135]. Through the design of electroactive, chemical, and topographical surface modifications, this thesis aims to elucidate how tailored physicochemical cues can regulate cell adhesion and improve the biological performance of neural-related biomaterials.

1.8.1. Neural tissue engineering

Injuries affecting the nervous system that involve disruption of axonal bundles have profound clinical, social, and economic consequences. The spontaneous regeneration of damaged or degenerated axonal tracts is generally limited, as it depends on a complex interplay of multiple inhibitory and permissive factors [136]. Axonal regeneration within the central nervous system (CNS) is particularly constrained following conditions such as traumatic brain injury (TBI), stroke, spinal cord injury (SCI), and other disorders associated with axonal damage. In contrast, axons of the peripheral nervous system (PNS) retain a certain regenerative capacity, allowing partial functional recovery when injury spans relatively short distances [137]. In the CNS, regenerative failure is attributed both to the intrinsically low growth capacity of mature neurons and to the presence of an inhibitory extracellular environment [138].

Currently, conventional clinical approaches offer limited effective treatments for severe nervous system injuries, with symptom management often representing the primary therapeutic option. To overcome these limitations and restore functional neuronal connectivity, tissue engineering strategies increasingly employ biocompatible three-dimensional biomaterials, together with cells and bioactive molecules, to reconstruct damaged neural tissue while preserving native anatomical organization and function [139]. Both natural and synthetic biomaterials have demonstrated promising outcomes in neural tissue engineering, including

promotion of neurite extension, differentiation of human neural stem cells, and bridging of nerve gaps [140].

Nerve regeneration is a highly complex biological process. In the PNS, limited injuries may undergo spontaneous regeneration; however, larger nerve defects typically require surgical intervention, most commonly using autologous nerve grafts obtained from other sites of the body [141]. In contrast, SCI presents a significantly greater challenge due to the presence of multiple inhibitory factors that restrict regenerative processes [142]. At present, no fully effective strategy exists to achieve complete functional recovery following spinal cord damage. As a result, bioengineering approaches for the PNS primarily focus on developing alternatives to autologous nerve grafts, whereas strategies for SCI aim to establish a more permissive environment that can support axonal regeneration.

Chedly et al. [143] developed a chitosan-based biomaterial for SCI repair in the form of a fragmented physical hydrogel suspension (Chitosan-FPHS), composed solely of chitosan and water, with carefully controlled physicochemical parameters including the degree of acetylation, polymer concentration, and fragment size. Following implantation into a rat bilateral dorsal hemisection SCI model, Chitosan-FPHS promoted extensive tissue remodeling by supporting the restoration of neural tissue architecture and vascularization while reducing the formation of dense fibrotic glial scars. The scaffold facilitated a more permissive lesion environment, characterized by the directional organization of astrocytic processes toward the injury site, which enabled axonal extension into and beyond the damaged region. Regenerating axons exhibited myelination or ensheathment by endogenous Schwann cells that migrated into the lesion area and showed prolonged survival. Furthermore, the chitosan-based hydrogel influenced the local inflammatory response, suggesting an additional role in modulating the regenerative microenvironment. These structural and biological improvements were accompanied by sustained recovery of locomotor function, highlighting Chitosan-FPHS as a promising biomaterial platform for SCI repair and as a potential substrate for integration with complementary regenerative strategies.

In another study Namhongsa et al. [144] developed three-dimensional electrospun nerve guidance scaffolds by integrating 3D printing and electrospinning technologies to improve the structural and biological performance of nerve regeneration platforms. Poly(L-lactide-co-ε-caprolactone) (PLCL) and poly(L-lactide-co-glycolide) (PLGA) were utilized as scaffold materials, generating hierarchical architectures containing both micro- and nanoscale features

suitable for nerve guidance conduits (NGCs). To further enhance the biological and electroactive properties of the scaffolds, PPy was deposited onto the polymeric fibers. The resulting PLCL-3D/E and PLGA-3D/E scaffolds exhibited average pore sizes of 289 ± 79 nm and 287 ± 95 nm, respectively, providing a favorable porous structure for neural regeneration. PPy incorporation significantly improved the surface hydrophilicity, electrical conductivity, and cytocompatibility of both scaffold systems compared with the unmodified counterparts. Moreover, the conductive properties of PLCL-3D/E/PPy and PLGA-3D/E/PPy scaffolds were maintained over extended periods, with conductivities of 12.40 ± 0.12 S cm^{-1} and 10.50 ± 0.08 S cm^{-1} sustained for up to 15 and 9 weeks, respectively, demonstrating their potential to support electroactive neural environments. Biological evaluation using L929 fibroblasts and Schwann cells revealed enhanced cell viability, proliferation, and attachment, particularly for the PLGA-3D/E/PPy scaffolds [144].

While a wide range of biomaterials has been proposed for tissue engineering and SCI, a comprehensive understanding of how physicochemical surface properties can improve cell adhesion and optimize scaffold performance is still lacking. An effective scaffold for SCI repair should provide a supportive microenvironment that promotes neural regeneration while regulating the responses of surrounding non-neuronal cells. Although fibroblast activation has traditionally been associated with excessive ECM deposition and fibrotic scar formation following injury, recent studies have demonstrated that fibroblasts also contribute to tissue repair by supporting extracellular matrix organization, secreting growth factors and cytokines, and modulating immune responses [145]. Therefore, the development of biomaterials capable of regulating fibroblast adhesion and activity, while simultaneously supporting neural outgrowth and limiting detrimental gliosis, may represent a promising approach for improving spinal cord repair strategies [146].

1.8.2. Neural stimulation

An increased incidence of neurological disorders is arising due to the aging population. A spectrum of conditions including epilepsy, Parkinson's disease, Alzheimer's disease, chronic pain, and depression necessitates diverse therapeutic approaches, with electrical stimulation emerging as a powerful option. Electrotherapy stands as an established method for neuromodulation through the stimulation or inhibition of neural firing in discrete regions of the brain through electrode delivered electrical pulses [147].

The long-term effectiveness of electrical stimulation therapies depends largely on the establishment and maintenance of a stable interface between the electrode surface and the surrounding neural tissue. Sustained integration at the tissue–electrode interface is essential for ensuring efficient signal transmission, minimizing performance degradation, and preserving therapeutic efficacy over extended implantation periods [148]. Several studies have demonstrated that engineering neural electrode surfaces with nanostructured conductive materials can significantly enhance device performance. Such modifications increase the effective electroactive surface area, thereby improving the sensitivity and efficiency of both neural recording and electrical stimulation, while enabling high-resolution spatiotemporal control of neural interfaces [97].

Consequently, Seyedkhani et al. [149] developed a conductive polymer-based coating composed of polydopamine-modified poly(3,4-ethylenedioxythiophene) (PEDOT-PDA) deposited onto titanium nitride electrodes for neural interface applications. The TiN substrates, fabricated as approximately 150 nm thick films using physical vapor deposition, were subsequently functionalized through rapid galvanostatic electrochemical co-polymerization to generate PEDOT and PEDOT-PDA coatings. Morphological characterization using FESEM demonstrated that PDA incorporation resulted in a dense and compact coating structure, contributing to improved mechanical integrity and charge transport properties. AFM analysis further revealed an increase in surface roughness following PEDOT-based modification, providing additional surface features favorable for cellular interactions. Electrochemical characterization showed that PEDOT-PDA-coated electrodes exhibited significantly reduced impedance (0.27 Ω) when compared with conventional gold electrodes (4.7 Ω), indicating enhanced charge transfer capability through mixed ionic–electronic conduction mechanisms. Furthermore, all fabricated coatings demonstrated excellent biocompatibility, maintaining cell viability above 85%, while PEDOT-PDA surfaces promoted improved cellular attachment and spreading, characterized by extensive filopodia formation and interaction with the conductive interface. These findings highlight the potential of PDA-functionalized PEDOT coatings for improving both electrochemical performance and biological integration of neural electrode interfaces [149].

Long-term efficacy of therapeutic electrical stimulation relies on the ability of neural electrodes to provide stable and efficient charge transfer at the electrode–tissue interface. However, maintaining this interface remains challenging due to the significant mechanical disparity between conventional rigid metallic electrodes and the soft, dynamic nature of neural tissue.

This biomechanical incompatibility can trigger the formation of perielectrode fibrotic encapsulation, which increases interfacial impedance, disrupts effective charge transmission, and ultimately compromises stimulation performance over time. Consequently, there is a growing need to optimize the physicochemical properties of electroactive surfaces to improve cellular behavior, as controlling the cell-surface interactions is critical for the development of stable and high-performance neural interfaces.

1.8.3. Skull implants

Cranioplasty is a well-established neurosurgical intervention aimed at reconstructing cranial defects in order to restore the integrity of the skull vault and provide adequate protection for the brain. Beyond its protective function, the procedure has been reported to contribute to improved vestibular balance, thereby reducing the risk of falls [150], alleviation of the trephined syndrome [151], and enhancement of aesthetic outcomes [152]. It is most commonly performed following decompressive craniectomy, once patients have recovered from the acute phase of treatment and are considered clinically stable. The timing of cranioplasty is generally determined based on both neurological and surgical stabilization [153], and the procedure offers important functional and cosmetic benefits for patients with skull defects [154].

Despite significant advances in surgical techniques and materials, cranioplasty remains associated with a range of complications. These include resorption of autologous bone flaps, postoperative infection, and intracranial hemorrhage [155]. In addition, surgical dissection between the musculocutaneous flap and the *dura mater* can be technically challenging, particularly in the presence of dense adhesions or insufficient tissue separation, which may prolong operative time [156]. Improper handling of these tissue layers can result in serious complications such as cortical hemorrhage, cerebrospinal fluid (CSF) leakage, epidural bleeding, and injury to the temporalis muscle [156]. A common consequence of decompressive craniectomy is the formation of dural adhesions, characterized by fibrotic scar tissue development between the dura and surrounding structures [157]. These adhesions can significantly complicate subsequent cranioplasty procedures by increasing surgical difficulty, prolonging operative duration, and elevating the risk of dural and cerebral injury. Moreover, longer intervals between craniectomy and cranioplasty have been associated with more pronounced adhesion formation, further increasing surgical complexity. For this reason, the use

of anti-adhesion barriers has been proposed as a strategy to facilitate safer and more efficient dissection during secondary reconstruction procedures [158].

However, currently available dural substitutes are not free from limitations. A systematic review by Azab et al. [159], which included 22 studies and 570 patients across multiple clinical centers, reported an overall postoperative complication rate of 20.5% following cranioplasty. The most common complications included epidural or subdural fluid accumulation (8.4%), surgical site infection (8.1%), dural tears (2.0%), cortical injury (1.2%), temporalis muscle damage (0.4%), and dural calcification (0.4%).

Among anti-adhesion materials used in cranial surgery, expanded polytetrafluoroethylene (ePTFE) dural substitutes (Preclude® Dura Substitute, W.L. Gore & Associates Inc.) [160] and silicone elastomer sheets (SILASTIC® Sheeting, Dow Corning Corporation) [157] are widely applied. While these materials are effective in limiting post-surgical tissue adhesion, their non-degradable nature raises clinical concerns. In particular, persistent implants may contribute to an increased risk of infection [161] [162], and cases of CSF leakage have also been reported [161] [163]. Such leakage may occur due to collagen deposition around suture sites, where removal of sutures can disrupt the newly formed tissue and reopen puncture pathways [158]. Pierson et al. [164], in a retrospective analysis of 39 patients treated with ePTFE membranes, reported a 25% complication rate, including infection, fluid accumulation, hematoma formation, reoperation, and seizures. Similarly, silicone-based implants have been associated with adverse outcomes such as cyst formation, infection, implant extrusion, and displacement [165].

Titanium is one of the most commonly used materials in cranioplasty due to its excellent biocompatibility, chemical stability, corrosion resistance, and minimal inflammatory response [166]. It also exhibits favorable mechanical properties, including high strength, formability, and a relatively low risk of infection, making it a widely preferred metallic implant material [167]. Clinical studies have shown that titanium-based implants can reduce complications such as hematoma formation, poor implant fit, and the need for revision surgery [168]. Titanium mesh systems, in particular, have demonstrated low infection rates and effective restoration of cranial contour and structural continuity, as reported in small case series [169]. Nevertheless, unmodified titanium surfaces may not optimally support biological integration. Without appropriate surface treatments such as mechanical polishing, sandblasting, acid etching, or

electrochemical anodization, titanium surfaces may promote excessive cellular adhesion or suboptimal tissue response, potentially affecting implant performance [169].

Consequently, current strategies are moving beyond the development of mechanically suitable cranial implants toward the rational engineering of titanium surface properties to achieve controlled cellular responses, minimize undesirable fibrotic adhesion, and promote favorable implant–tissue integration. As a result, current research efforts are increasingly focused on developing surface modification strategies that impart anti-adhesive properties to titanium implants, or alternatively, on designing new biomaterials that can replace conventional titanium-based systems in cranial reconstruction.

1.9. Hypothesis and objectives

In my PhD thesis, I hypothesized that cellular adhesion and cell–material interactions can be effectively regulated through specific surface engineering approaches including nanoscale topographical modification, bioactive surface functionalization, and electroactive material integration. I hypothesized by tailoring biomaterial interfaces, it is possible to direct cellular responses and improve the performance of biomaterials for tissue engineering, neural interfaces, and regenerative medicine applications (**Figure 6**).

Accordingly, I aimed for the following research objectives:

1- To investigate the influence of nanoscale surface topography on cellular adhesion behavior through the fabrication of nano-dimpled titanium surfaces and evaluation of their effects on fibroblast, neuronal, and astrocytic responses.
2- To examine the ability of bioactive polymeric coatings to selectively modulate cellular adhesion and simultaneously enhance the bioactivity and mineralization potential of titanium-based biomaterials intended for cranioplasty applications.
3- To develop electroactive conducting polymer coatings for neural electrodes and evaluate their effects on electrochemical performance, neural cell adhesion, and neurite outgrowth at the electrode–tissue interface.
4- To improve the cellular adhesion properties of nonconductive electrospun polymeric scaffolds through incorporation of conducting polymers and to assess how electroactive modification influences cellular attachment, spreading, and focal adhesion formation. .
5- To characterize the physicochemical, morphological, and electrochemical properties of the engineered biomaterial surfaces using surface analytical, microscopic, and electrochemical techniques.

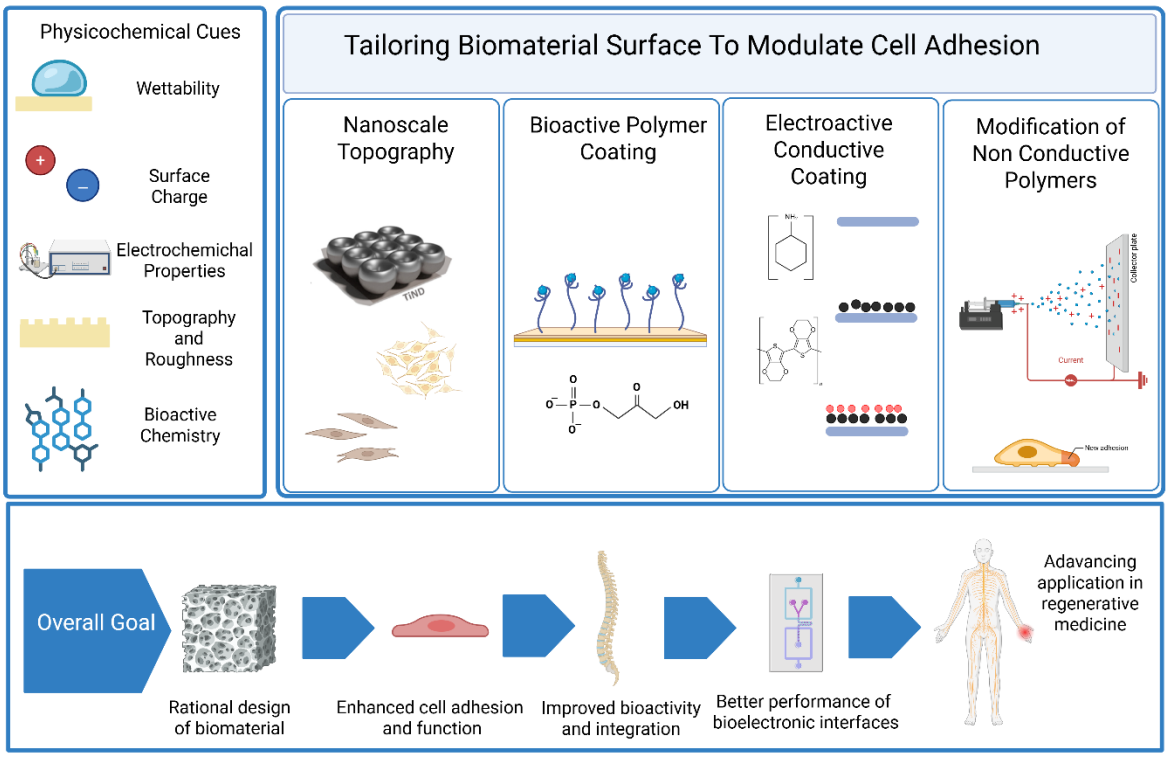


Figure 6. Schematic illustration of aim and objectives of the thesis. Created in BioRender.

Chapter 2

2. Materials and methods

2.1. Chemicals

All chemicals used in this study were of analytical grade and were used in accordance with occupational health and safety regulations.

Glycerol ethoxylate (average M_n~1000 g mol^{-1}), acetic anhydride ($(CH_3CO)_2O$), acetic acid (CH_3COOH), poly(vinyl alcohol) (PVA) $[CH_2CH(OH)]_n$ (molecular weight of 30 000-70 000 g mol^{-1}), 3,4-ethylenedioxythiophene (EDOT) ($C_2H_4O_2C_4H_2S$), polycaprolactone (PCL) $[C_6H_{10}O_2]_n$ (M_n = 80 000 g mol^{-1}) were purchased from Sigma Aldrich. Chloroform ($CHCl_3$), dimethylformamide (DMF, C_3H_7NO) were purchased from CHEMPUR. Aniline ($C_6H_5NH_2$), sulfuric acid (H_2SO_4), pyrrole (C_4H_4NH), iron(III) chloride hexahydrate ($FeCl_3 \cdot 6H_2O$), ethanol (C_2H_6O), acetone (C_3H_6O), sucrose ($C_{12}H_{22}O_{11}$), sodium hydroxide (NaOH) were purchased from Acros Organics. Glutaraldehyde (GA, $C_5H_8O_2$) and dimethyl sulfoxide (DMSO, $(CH_3)_2SO$, >99,7%), were purchased from Fisher BioReagents. Deionized water (DW, Millipore quality) was produced from Hydrolab water purification systems, Poland, with the conductivity of the 0.055 μS cm^{-1}.

2.2. Cells

SH-SY5Y neuroblastoma cell line (CRL-2266, ATCC), normal human dermal fibroblasts (NHDF, ATCC), U87 glioblastoma cell line (ATCC), and human osteosarcoma U2OS cell line (ATCC) were used for *in vitro* biological assays. A mixed neural population was also extracted from the ventral mesencephalon of E14 rat embryos obtained by laparotomy from time-mated female Sprague–Dawley rats according to the previously published protocol [170].

2.3. Biological reagents

Dulbecco's Modified Eagle Medium/Nutrient Mixture F-12 (DMEM/F12), fetal bovine serum (FBS), penicillin-streptomycin (PS), trypsin-EDTA (Merck), phosphate-buffered saline (PBS) were purchased from Merck. Alamar blue reagent, Hanks' balanced salt solution modified with sodium bicarbonate, Alexa Fluor 488-conjugated goat anti-rabbit IgG (H+L) (ab150081) and rhodamine-conjugated phalloidin (R415) were purchased from Thermo Fisher Scientific. Rabbit monoclonal antibody against paxillin (Y113, Abcam) was purchased from Abcam, Cambridge, United Kingdom.

2.4. Consumables

Titanium (Ti) foil and Ti-6Al-4V discs (Sigma-Aldrich) were used as substrates for surface modification. Platinum mesh or Thermanox coverslips (Electron Microscopy Sciences, Hatfield, PA, USA) working electrode, Ag/AgCl (3 M KCl) (EDAQ, Sydney, Australia) reference electrode, and a Pt-coated titanium rod (EDAQ, Sydney, Australia) were employed for electrochemical measurements.

2.5. Laboratory equipment

The list of laboratory equipment that was used in this work include: Multiwell plate reader (Biologix, Shandong, China), field emission scanning electron microscope (FESEM, FEI Quanta FEG250), scanning electron microscope (SEM, Phenom ProX, Thermo Fisher Scientific, Waltham, MA, USA), atomic force microscope (AFM, Nanosurf EasyScan 2), FV3000 laser confocal microscope equipped with a UPLSAPO 40XS objective lens (Olympus, Tokyo, Japan), optical microscope (JuLI™ FL, NanoEnTek), Fourier-transform infrared spectrometer (IR PerkinElmer Spectrum Two with UATR diamond accessory, Waltham, MA, USA), ultraviolet–visible spectrophotometer (GenovaBio), goniometer (OCA15, Dataphysik, Filderstadt, Germany), scratch tester (open platform equipped with a CSM Micro-Combi-Tester), multi-well plate reader SYNERGY4 (BioTek Instruments, New York, NY, USA), incubator (Heracell™ 150i, Thermo Fisher Scientific), PalmSens EmSTAT3 potentiostat, Raman spectrometer (Renishaw InVia instrument equipped with 532 nm and 830 nm excitation laser), sputter coater (Q150R Quorum Technologies, Lewes, UK), zeta potential analyzer (Electrokinetic analyzer, SurPASS 3, Anton Paar GmbH, Graz, Austria), stirrer (AREX-6 DIGITL, VELP Scientifica, Usmate Velate, Italy), voltage source (Genvolt 7000 series, Shropshire, UK) X-ray photoelectron spectrometer (AXIS SUPRA+XPS spectrometer equipped with an Al Kα X-ray source).

2.6. Software and programmes

The software used in this work include: ImageJ software (National Institutes of Health, USA), 3D Roughness Reconstructions software integrated with SEM (Phenom ProSuite, Thermo Fisher Scientific, USA), JuLI™ FL software (NanoEnTek, South Korea) and CasaXPS software (Casa Software Ltd., Teignmouth, UK).

2.7. Surface modification approaches

2.7.1. Topographical modification of Ti surface

Nanotopographic modification of titanium was performed at the Centre of Plasma and Laser Engineering, Institute of Fluid-Flow Machinery Polish Academy of Sciences, Gdańsk, Poland. Titanium foil specimens measuring 2 × 3 cm were sequentially cleaned by ultrasonication in acetone, ethanol, and deionized water for 10 min in each medium prior to anodization. The fabrication of TiO_2 nanotubes was carried out using a two-step electrochemical anodization procedure, with chemical etching applied following each anodization cycle. The anodization experiments were performed in a two-electrode configuration consisting of a titanium working electrode (anode) and a platinum mesh counter electrode (cathode). The electrodes were arranged parallel to one another with an interelectrode spacing of 2 cm inside a cylindrical glass reactor equipped with a thermostatic jacket to maintain the electrolyte temperature at 23 °C. The electrolyte solution contained 0.27 M NH_4F dissolved in a mixture of ethylene glycol (99 vol%) and deionized water (1 vol%).

A constant potential of 40 V was applied throughout both anodization stages. The initial anodization step was conducted for 2 h, followed by a second anodization lasting 6 h. After each anodization stage, the former TiO_2 nanotube layer was removed by immersing the samples overnight in a 0.5% oxalic acid solution. This etching treatment generated titanium nanodimple (TiND) structures on the substrate surface. Finally, the resulting uniformly nanodimpled titanium substrates were rinsed thoroughly with deionized water and dried prior to further use.

2.7.2. Fabrication of PEDOT and PANI-based coatings

Conducting polymer coatings were fabricated by electrochemical polymerization using a three-electrode electrochemical setup connected to a portable PalmSens EmSTAT3 potentiostat. The Pt-coated Thermanox coverslip served as the working electrode, while an Ag/AgCl electrode filled with 3 M KCl and a Pt-coated titanium rod were used as the reference and counter electrodes, respectively.

Electropolymerization of PANI was carried out by cyclic voltammetry (CV) in an electrolyte containing 20 mM aniline and 1 M H_2SO_4. The polymerization process consisted of 20 CV cycles performed at a scan rate of 100 $mV \cdot s^{-1}$ within a potential window ranging from −0.5 to 1.0 V *vs.* Ag/AgCl.

Subsequently, a PEDOT layer was electrodeposited on top of the previously prepared PANI-coated electrodes using the same cyclic voltammetry approach. For this purpose, the electrolyte solution consisted of 10 mM EDOT and 1 M H_2SO_4. Electrodeposition was conducted over 20 CV cycles at a scan rate of 100 $mV \cdot s^{-1}$ in the potential range from −0.5 to 1.0 V *vs.* Ag/AgCl.

2.7.3. Preparation of PEG-DBB

Betulin and betulin disuccinate were provided by the researchers from the Department of Organic Chemistry, Faculty of Pharmacy, Poznan University of Medical Sciences. In the first step the purity of the Betulin was verified by nuclear magnetic resonance (NMR) spectroscopy and melting point determination. Betulin disuccinate was synthesized following a previously reported method [171], resulting in a white amorphous powder.

The PEG-DBB polyanhydride copolymer was prepared by dr Daria Niewolik (Department of Physical Chemistry and Technology of Polymers, Silesian University of Technology) *via* melt polycondensation of betulin disuccinate with a tricarboxylic poly(ethylene glycol) (PEG) derivative, according to the procedure described earlier [171]. Melt polycondensation using acetic anhydride was selected because it provides a straightforward route for polyanhydride synthesis while minimizing the need for extensive purification steps [172].

Briefly, betulin disuccinate (3 g) and PEG (2 g) were reacted in 50 mL of acetic anhydride under nitrogen atmosphere at a reagent-to-solvent ratio of 1:10 (w/v). The reaction mixture was refluxed for 40 min to obtain the prepolymer intermediate. Subsequently, excess acetic anhydride together with the acetic acid generated during the reaction was removed under reduced pressure. The resulting diacylated betulin disuccinate/PEG-COOH prepolymer was then subjected to polycondensation at 150 °C for 2 h under vacuum (0.1 mm Hg) with continuous stirring in a nitrogen atmosphere.

The resulting PEG-DBB copolymer was isolated as a solid amorphous material with a yield exceeding 90% and stored under frozen conditions until further use. Detailed physicochemical characterization of the copolymer has been reported previously [171]. The molecular weight determined by multi-angle light scattering (MALS) analysis was M_n = 9 900 $g \cdot mol^{-1}$ and M_w = 22 800 $g \cdot mol^{-1}$.

2.7.4. Preparation of nanofibers via electrospinning

A solution containing 8 wt.% PVA was prepared in deionized water. Electrospinning was carried out at an applied voltage of 20 kV, with a tip-to-collector distance of 7 cm, while the collector surface was covered with aluminum foil. The solution flow rate was adjusted at 0.5 $mL \cdot min^{-1}$, and the ambient temperature during electrospinning was kept at 25 °C. For fabrication of fibers containing PEG-DBB, two separate solutions were prepared: an aqueous PVA solution (8 wt.%) and a PEG-DBB solution (0.01 wt.%) dissolved in dimethyl sulfoxide (DMSO). Afterwards, 9 mL of the PVA solution was blended with 1 mL of the PEG-DBB solution and mixed thoroughly until a uniform solution was obtained. The prepared mixture was subsequently electrospun using the same processing parameters as described previously. In the proof-of-concept experiments, Ti-6Al-4V substrates (10 mm in diameter and 3 mm in thickness) were mounted directly onto the collector prior to electrospinning. Fiber deposition onto the metallic substrates was then conducted under identical electrospinning conditions. Before coating, the discs were chemical cleaning with isopropyl alcohol and mechanical roughening by sandblasting was performed on the surface.

To create PPy-modified PCL fibers, a 10 mL electrospinning solution was prepared by dissolving 10 wt.% PCL in a solvent of a mixture of chloroform and DMF in a 9:1 (v/v) ratio. The solution was magnetically stirred for 12 h at room temperature until a homogeneous, clear solution was obtained. For *in situ* formation of conducting polymer within the PCL matrix, pyrrole monomer (100 µL for PCL-1PPy and 300 µL for PCL-3PPy) was added to 10 mL of the PCL solution while maintaining the polymer concentration at 10 wt.%. The resulting mixture was further stirred for 12 h at room temperature to ensure uniform dispersion of the pyrrole monomer. Subsequently, 200 µL of ferric chloride hexahydrate ($FeCl_3 \cdot 6H_2O$) solution (0.5 M in DMF, Acros Organics) was introduced to initiate chemical oxidative polymerization of pyrrole. The reaction mixture was continuously stirred for 48 h at room temperature, during which the solution gradually changed from transparent to a greenish-black color, confirming the formation of PPy (**Figure 7**).

Finally, all prepared solutions were electrospun using a 10 mL syringe equipped with a 510 µm (G25) needle in ambient conditions (room temperature and natural humidity). A voltage of 20 kV was applied, with a 13 cm tip-to-collector distance and a flow rate of 1 $mL \cdot h^{-1}$ (**Figure 7**) [173].

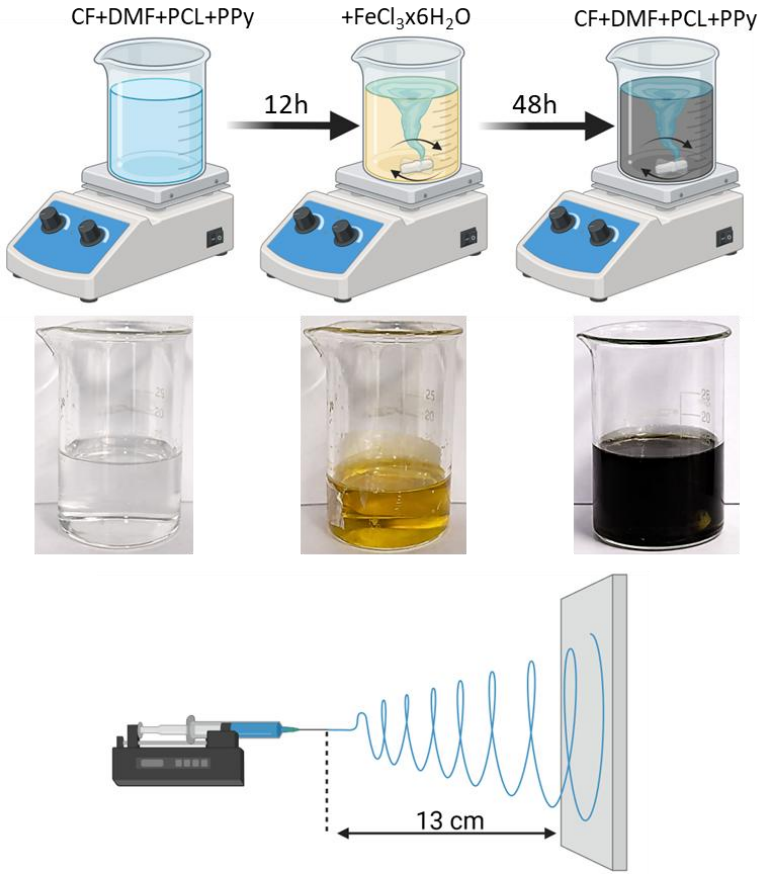


Figure 7. Schematic illustration of preparing the electrospinning solution and electrospinning. Created in BioRender.

2.8. Surface characterization

2.8.1. Morphological characterisation

SEM was used to investigate the surface morphology of the fabricated samples. Prior to imaging, all samples were sputter-coated with a 5 nm gold layer to improve surface conductivity. SEM images were acquired at accelerating voltages in the range of 10–15 kV. Morphological characterization of Ti nanodimpled (TiND) substrates was additionally performed using a FESEM equipped with an ET secondary electron detector. The microscope was operated at an accelerating voltage of 20 kV. AFM was used to analyze the surface topography at the nanoscale. Surface roughness and topography were characterized by the arithmetical mean height (S_a) and the root mean square height (S_q), which describe the average

surface height deviation and the root mean square of the surface height distribution relative to the mean plane, respectively.

The fiber fraction within the electrospun mats was quantified using digital image analysis. SEM micrographs were processed in ImageJ by thresholding to distinguish fiber regions from the background. The fiber fraction was then determined as the ratio of the projected area occupied by fibers to the total image area.

Porosity of the electrospun scaffolds was determined using a combined gravimetric–geometric approach. Rectangular samples were cut, and their mass, thickness, and area were measured experimentally. The apparent density (d_{app}) of the scaffold was calculated using Equation (1):

$$d_{app} = \frac{m_s}{t_s \times A_s} \quad (1)$$

where $m_s$is the mass of the scaffold (mg), $t_s$is the thickness of the scaffold (cm), and $A_s$is the surface area of the scaffold (cm^2).

The porosity was subsequently calculated using Equation (2):

$$p = \frac{1 - d_{app}}{d_{PCL}} \quad (2)$$

where d_{PCL}represents the bulk density of poly(ε-caprolactone) ($mg\ cm^{-3}$).

The scaffold thickness (t_s) was calculated based on the average maximum height (R_z) obtained from 3D Roughness Reconstruction software coupled with SEM analysis. The parameter R_z corresponds to the mean peak-to-valley height of the surface profile and was used as an approximation of scaffold thickness.

Surface roughness was evaluated in terms of the arithmetic average roughness (R_a), calculated using 3D Roughness Reconstruction software integrated with SEM-derived topographical data.

2.8.2. Chemical characterization

Chemical characterization of the materials was performed using Raman spectroscopy and Fourier transform infrared spectroscopy. FTIR spectra were collected over the range of 400–4000 cm^{-1} with a spectral resolution of 4 cm^{-1} and 16 scans per sample. To detect hydroxyapatite (HA), Raman spectroscopy was operated with 532 nm diode laser line and using 100× objective, and to detect the constitutes of the electroactive layers the laser was changed to 830 nm.

Surface chemical composition and elemental states of the samples were analyzed using XPS.

Surface wettability was evaluated by WCA measurements. A 4 μL droplet of deionized water was carefully deposited onto the sample surface at room temperature. Each measurement was repeated at least three times to ensure reproducibility.

Zeta potential measurements were performed based on the streaming potential method. Samples were mounted in a cylindrical measuring cell designed for porous materials. Prior to analysis, samples were equilibrated by flushing with 0.01 M KCl solution. Measurements were conducted at pH values of 5.8, 7.4, and 9.0, with pH adjustment achieved by gradual addition of 0.05 M NaOH. Each measurement was repeated four times for statistical reliability. The permeability index during electrolyte flow was maintained in the range of approximately 80–110.

2.8.3. Mechanical characterization

The adhesion strength of bioactive coatings deposited on titanium substrates was evaluated using a scratch test. A Rockwell diamond indenter was used to generate scratches under progressively increasing normal load. The critical load (L_c) was defined as the minimum load at which coating delamination from the substrate was observed. This value was determined based on changes in friction force, friction coefficient, and optical microscopy observations integrated within the testing system.

The scratch test was conducted under the following conditions: the normal load was increased from 0.03 N to 30 N at a loading rate of 10 $N \cdot min^{-1}$, with a constant scratching speed of 1 $mm \cdot min^{-1}$ and a total scratch length of 3 mm.

2.8.4. Electrochemical characterization

The electrochemical behavior of PANI, PEDOT, and PANI–PEDOT composite coatings was chracterized using Electrochemical Impedance Spectroscopy (EIS) and CV in a conventional three-electrode configuration. A bare Pt foil or modified Pt-coated Thermanox coverslip served as the working electrode, an Ag/AgCl electrode (3 M KCl) was used as the reference. Moreover, a Pt-coated titanium rod was used as the auxiliary electrode. EIS measurements were carried out in PBS over a frequency range from 100 kHz to 0.1 Hz, with an AC amplitude of 100 mV (*vs*. Ag/AgCl), and a DC potential of 0 V (*vs*. Ag/AgCl). The CSC of the electrodes was determined from CV curves. CSC was calculated according to Equation (3) [174]:

$$CSC = \frac{1}{Sv}\int_{E1}^{E2} I(E)dE \qquad (3)$$

In this equation, v represents the scan rate (V s^{-1}), S denotes the electrode's geometric area (cm^2), and I stands for the current (A). $\int_{E1}^{E2} I(E)dE$ signifies the total voltammetric charge derived from integrating the positive (anodic) and negative (cathodic) sweeps within a CV curve. This integration spans between E_1 and E_2, the cutoff potentials recorded in the CV measurements (V).

In addition, both CV and EIS measurements were performed under varying pH conditions ranging from pH 1 to pH 7. These solutions were prepared by gradual dilution of 1 M H_2SO_4 with PBS, enabling evaluation of the pH-dependent electrochemical stability and performance of the coatings.

2.8.5. Hydrolytic degradation

Samples were incubated in phosphate-buffered saline (PBS, pH 7.4) at 37 °C for a period of 14 days to evaluate their degradation behavior under physiological conditions. After incubation, the samples were rinsed and subsequently analyzed using SEM and FTIR to assess morphological and chemical changes induced by degradation.

The mass loss was quantified gravimetrically, and the percentage weight loss was calculated using Equation (4):

$$\text{Weight loss (\%)} = \frac{W_1 - W_2}{W_1} \times 100\% \qquad (4)$$

where W_1 is the initial dry mass of the sample prior to incubation, and W_2 is the dry mass measured after the degradation period.

2.8.6. Bioactivity of the coatings

To assess the *in vitro* bioactivity and potential to form hydroxyapatite (HA), samples were immersed in simulated body fluid (SBF) with a physiological pH of 7.40. The SBF was prepared based on Hanks' balanced salt solution modified with sodium bicarbonate, supplemented with 0.185 g· L^{-1} $CaCl_2 \cdot 2H_2O$ and 0.09767 g· L^{-1} $MgSO_4$. The ratio of sample surface area to SBF volume was maintained at approximately 0.1 $cm^2 \cdot mL^{-1}$ [175].

The samples were incubated in SBF for 21 days at 37 °C. During the incubation period, the medium was refreshed every 48 h to maintain concentration stability. After 3 weeks, the specimens were removed from the solution, rinsed thoroughly with distilled water, and dried under clean bench conditions. Post-incubation characterization was performed using scanning SEM, Raman spectroscopy, and energy-dispersive X-ray spectroscopy (EDS) to evaluate the formation of calcium phosphate deposits. Point EDS measurements were performed at an accelerating voltage of 15 kV with a collection time of 60 s. To ensure statistical reliability and representativeness, spectra were acquired in triplicate from three different regions of each sample surface.

Surface coverage of the formed hydroxyapatite layer was quantified from SEM micrographs using ImageJ software through image thresholding and area fraction analysis. The thickness of the HA layer was estimated indirectly based on the mean roughness depth (R_z) derived from surface topography analysis. Raman spectroscopy was performed to confirm the presence and structural characteristics of HA.

2.8.7. Biological characterization

In vitro biological evaluation of the fabricated materials was performed through adhesion, morphology, and cell viability assays cell lines such as SH-SY5Y neuroblastoma cells (CRL-2266, ATCC), normal human dermal fibroblasts (NHDF, ATCC), U2OS osteosarcoma cells (ATCC), and U87 cell lines (ATCC).

Cells were cultured in DMEM/F12, Merck, supplemented with 10% FBS and 1% penicillin/streptomycin. Cultivation was carried out at 37 °C under humidified conditions (80% relative humidity) and 5% CO_2 in a Heracell™ 150i incubator. For routine passaging, cells were detached using 0.25% trypsin–EDTA, followed by neutralization with twice the volume of complete culture medium.

Cell viability was assessed using the Alamar Blue assay. SH-SY5Y, NHDF, U87, and U2OS cells were seeded on the samples and cultured for 48 h. Subsequently, Alamar Blue reagent was added to each well (the volume ratio of the Alamar blue to culture medium was 1:10) and incubated for 3 h. Fluorescence/absorbance was then measured using a Synergy™ 4 microplate reader, and cell viability was calculated accordingly.

Cell adhesion and spreading were evaluated by optical microscopy after 48 h of culture using a JuLI™ FL imaging system. Cell confluency was quantified using the built-in JuLI FL software based on captured phase-contrast images.

For detailed morphological analysis, cells were seeded at a density of 2×10^4 cells per well in 48-well plates containing 500 µL of culture medium and incubated for 48 h. After incubation, samples were fixed using 3% glutaraldehyde (500 µL per well) and stored at 4 °C for 24 h. A graded ethanol dehydration series (10%, 30%, 50%, 70%, 80%, 95%, and 99%) was subsequently performed, with 10 min incubation in each concentration, followed by air drying at room temperature for 24 h. Prior to SEM imaging, samples were sputter-coated with a 5 nm gold layer. SEM images were analyzed using ImageJ software to quantify cell morphology parameters, including cell area, circularity, fractal dimension, and the number of cellular protrusions.

For immunofluorescence analysis of focal adhesion formation and cytoskeletal organization, NHDF and SH-SY5Y cells were seeded at a density of 2×10^4 cells per well onto the samples and cultured for 48 h. After incubation, cells were fixed with 4% PFA containing 1% sucrose for 15 min at room temperature and washed with PBS. Permeabilization was performed using a HEPES-based buffer containing 0.5% Triton X-100 at 4 °C for 5 min. The buffer composition included sucrose (10.3 g), NaCl (0.292 g), $MgCl_2$ (0.06 g), and HEPES (0.476 g), adjusted to pH 7.2. Non-specific binding sites were blocked by incubation with 1% BSA in PBS for 5 min at 37 °C. Samples were then incubated with a primary rabbit monoclonal anti-paxillin (Y113, Abcam, Cambridge, UK) antibody diluted 1:100–1:200 in PBS-BSA (100 µL per sample) for 2 h at 37 °C. After washing three times with 0.05% Tween 20 in PBS, samples were incubated for 1 h with secondary antibodies, including Alexa Fluor 488-conjugated goat anti-rabbit IgG (ab150081, Thermo Fisher Scientific, Waltham, MA, USA) and rhodamine-conjugated phalloidin (R415, Thermo Fisher Scientific, Waltham, MA, USA) (both diluted 1:100–1:200 in PBS-BSA; 300 µL per sample), to visualize focal adhesion sites and F-actin, respectively.

Following staining, samples were protected from light and mounted using a coverslip with SlowFade™ Gold antifade mounting medium (S36937, Thermo Fisher Scientific, Waltham, MA, USA). Fluorescence imaging was performed using an FV3000 laser scanning confocal microscope (Olympus) equipped with a UPLSAPO 40× objective. Sequential scanning was used to minimize spectral overlap. Channel settings were as follows: DAPI (405 nm excitation, 430–470 nm emission), rhodamine-phalloidin (561 nm excitation, 570–670 nm emission), and Alexa Fluor 488 (488 nm excitation, 500–600 nm emission). Images were acquired at a resolution of 1024 × 1024 pixels using a Galvano scanner (1-way mode) with a scan speed of 2.0 µs/pixel. The confocal aperture was set to automatic, and acquisition parameters were optimized in live mode to avoid signal saturation. Final images were saved in LSM/OIR format and processed using FIJI/ImageJ software.

For electroactive samples based on conducting polymers mixed population of neural cells was isolated from the ventral mesencephalon (VM) of embryonic day 14 (E14) Sprague–Dawley rat embryos obtained from time-mated pregnant females via laparotomy. The dissection and isolation procedure followed a previously described protocol [170]. All animal work was conducted in accordance with European Union Directive 2010/63/EU on the protection of animals used for scientific purposes and ARRIVE guidelines and was approved by the Health Products Regulatory Authority (AE19125/I179) and the University of Galway Research Ethics Committee.

The isolated VM-derived cells were seeded onto conducting polymer-coated Thermanox coverslips and cultured for 3, 7, and 14 days *in vitro*. At each time point, samples were fixed and processed for indirect double immunofluorescence staining. Neuronal populations were identified using a rabbit anti-β-tubulin III primary antibody followed by Alexa Fluor 594-conjugated goat anti-rabbit IgG (H+L), while astrocytes were labeled using a mouse anti-GFAP primary antibody with detection via Alexa Fluor 488-conjugated goat anti-mouse IgG/IgA/IgM (H+L). Imaging was carried out using an Olympus Fluoview 1000 confocal laser scanning microscope at 60× magnification with a resolution of 1024 × 1024 pixels (aspect ratio 1:1).

For quantitative assessment of cell distribution, nuclei corresponding to neuronal and astrocytic cells were counted within predefined regions of interest measuring 100 µm × 100 µm across at least five randomly selected images per sample.

Neurite extension was evaluated using a stereological method, with total neurite length (L) calculated using Equation (5) [176]:

$$L = \frac{nT\pi}{2} \qquad (5)$$

where L represents the total neurite length (μm), n is the number of neurite intersections with the grid lines, and T is the spacing between grid lines (μm).

After 14 days in culture, focal adhesion structures were analyzed using a similar immunofluorescence approach.

2.9. Statistical analysis

All experimental conditions were performed in minimum triplicate biological replicates. Statistical analysis was conducted using one-way analysis of variance (ANOVA) and Student's t-test, with significance defined as $p < 0.05$. Data are presented as mean values ± standard deviation.

Chapter 3

3. Results and Discussion

3.1. Influence of surface topography on cell adhesion behaviour

3.1.1. Aims and objectives

The aim of this study was to investigate the modulation of cell adhesion on metallic implants, using titanium as a model substrate, through the application of topographical surface modifications, with the goal of designing an implantable scaffold suitable for the treatment of spinal cord injuries (**Figure 8**).

Specific objectives of this study involved:

1- To fabricate and characterize topographically modified titanium surfaces using anodization and chemical etching techniques to generate uniformly distributed Ti nanostructures.

2- To evaluate the influence of surface topography on cellular behaviour, including cell attachment, morphology, spreading, and focal adhesion formation.

3- To compare the responses of different cell types, including normal human dermal fibroblasts (NHDF), human astrocytes (U87), and human neuroblastoma cells (SH-SY5Y), toward the developed surface modifications.

4- To establish correlations between surface topographical properties and biological performance to identify surface engineering strategies suitable for biomedical applications.

5- To develop an implantable scaffold for spinal cord injury treatment, designed to bridge lesion sites within the spinal cord.

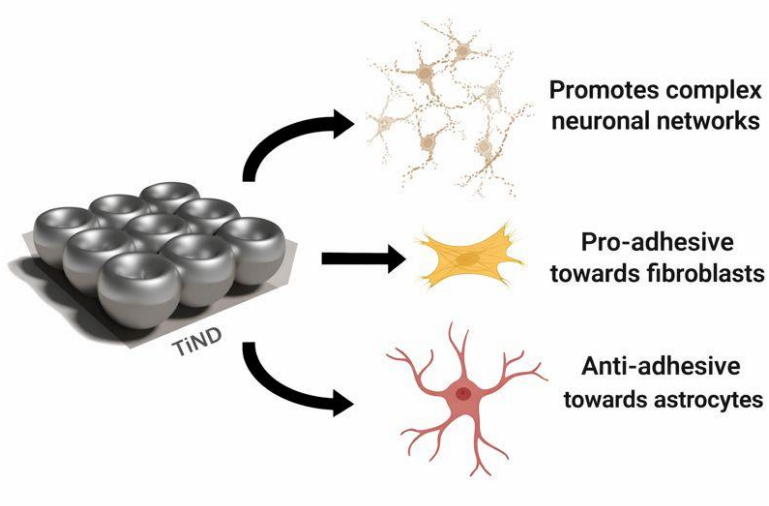


Figure 8. Schematic illustration of how surface topography influence adhesion behaviour of SH-SY5Y, U87 and NHDF cells.

3.1.2. Fabrication and surface characterization of TiND

Figure 9A illustrates the preparation route of the electrode material fabricated in this study. The process involved electrochemical anodization followed by chemical etching, which resulted in the formation of uniformly distributed Ti nanodimples (TiND) corresponding to the inverted geometry of the bottom region of titania nanotubes. SEM analysis revealed that the produced nanodimples possessed an average diameter of approximately 85 ± 3 nm (**Figure 9B**) [82, 177]. Nanotopographical features have been already shown to influence the adsorption, conformation, and spatial distribution of extracellular matrix proteins, thereby regulating integrin engagement and focal adhesion assembly [178]. Particularly, topographical features smaller than or comparable to the dimensions of individual cells (<10 μm) promoted the formation of stable focal adhesions, as indicated by the accumulation of vinculin and actin [50]. Therefore, with the average size of 85 ± 3 nm, nanodimples present of the surface of TiND were supposed to be able to affect cellular behavior.

The surface topography and roughness of TiND substrates were further characterized using AFM (**Figure 9C**). Analysis of a 5 × 5 μm scanned area demonstrated that untreated Ti surfaces exhibited relatively high roughness values, with S_q and S_a values of 60 nm and 48 nm, respectively. In comparison, the TiND surfaces displayed markedly lower roughness parameters, with S_q reduced to 10 nm and S_a to 8 nm. These findings indicate that the introduction of nanodimples significantly decreased surface height variations and generated a more homogeneous nanoscale topography. Overall, the nano dimpled modification reduced both the root mean square roughness and the average surface roughness by nearly six-fold compared with bare titanium surfaces.

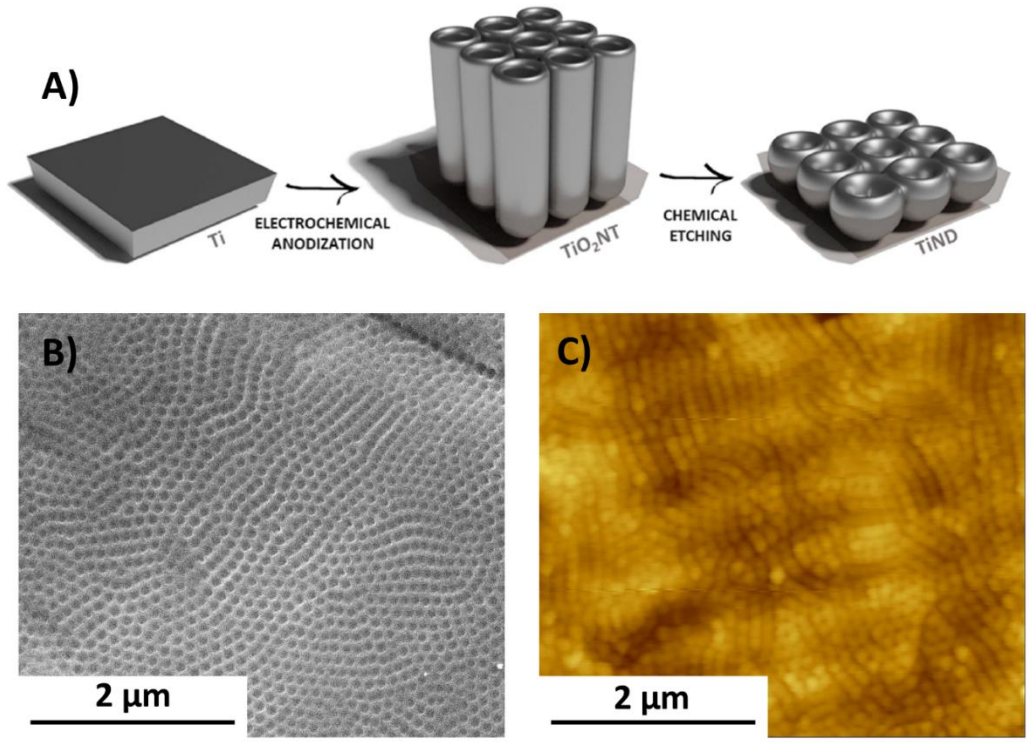


Figure 9. Schematic illustration of the fabrication process of Ti nanodimple structures (A), together with representative SEM (B) and AFM (C) images depicting the resulting surface morphology and topographical features.

To investigate whether the electrochemical anodization and subsequent chemical etching processes altered the surface chemical composition of titanium, XPS analysis was performed on both untreated titanium (bare Ti) and TiND surfaces. The survey spectra of bare Ti (**Figure 10A**) and TiND (**Figure 10B**) exhibited similar elemental compositions, with signals corresponding to Ti, O, C, N, and Na detected on both surfaces. However, after TiND fabrication, an additional fluorine signal was observed, which can be attributed to residual electrolyte species originating from the chemical etching step. Furthermore, differences in the relative intensity of the titanium-related peaks indicated changes in the chemical state distribution of titanium following surface nanostructurization.

High-resolution Ti 2p spectra of bare Ti (**Figure 10C**) were deconvoluted into three characteristic components assigned to metallic titanium Ti(0) (453.72 eV), Ti(II) (455.02 eV), and Ti(IV) (458.94 eV), corresponding to Ti, TiO, and TiO_2 species, respectively [179] [180]. Additional Ti $2p_{1/2}$ peaks associated with Ti(0) and Ti(IV) were identified at 459.85 eV and 463.59 eV, respectively. Quantitative analysis based on the Ti $2p_{3/2}$ peak fitting revealed that

Ti(IV) was the dominant oxidation state on the untreated titanium surface (47.62%), followed by Ti(II) (26.35%) and Ti(0) (26.03%).

In comparison, the Ti 2p spectrum of the TiND surface (**Figure 10D**) exhibited four distinct components, assigned to Ti(0) at 453.70 eV, Ti(II) at 454.41 eV, Ti(III) at 457.60 eV, and Ti(IV) at 458.97 eV [179, 180]. The corresponding Ti $2p_{1/2}$ peaks were detected at 459.40 eV, 461.14 eV, 463.50 eV, and 464.80 eV for Ti(0), Ti(II), Ti(III), and Ti(IV), respectively. The relative contribution of each titanium oxidation state was calculated from the Ti $2p_{3/2}$ peak areas, revealing an increased proportion of oxidized titanium species after nanostructurization, with Ti(IV), Ti(III), Ti(0), and Ti(II) accounting for 57.59%, 27.90%, 7.27%, and 7.24%, respectively.

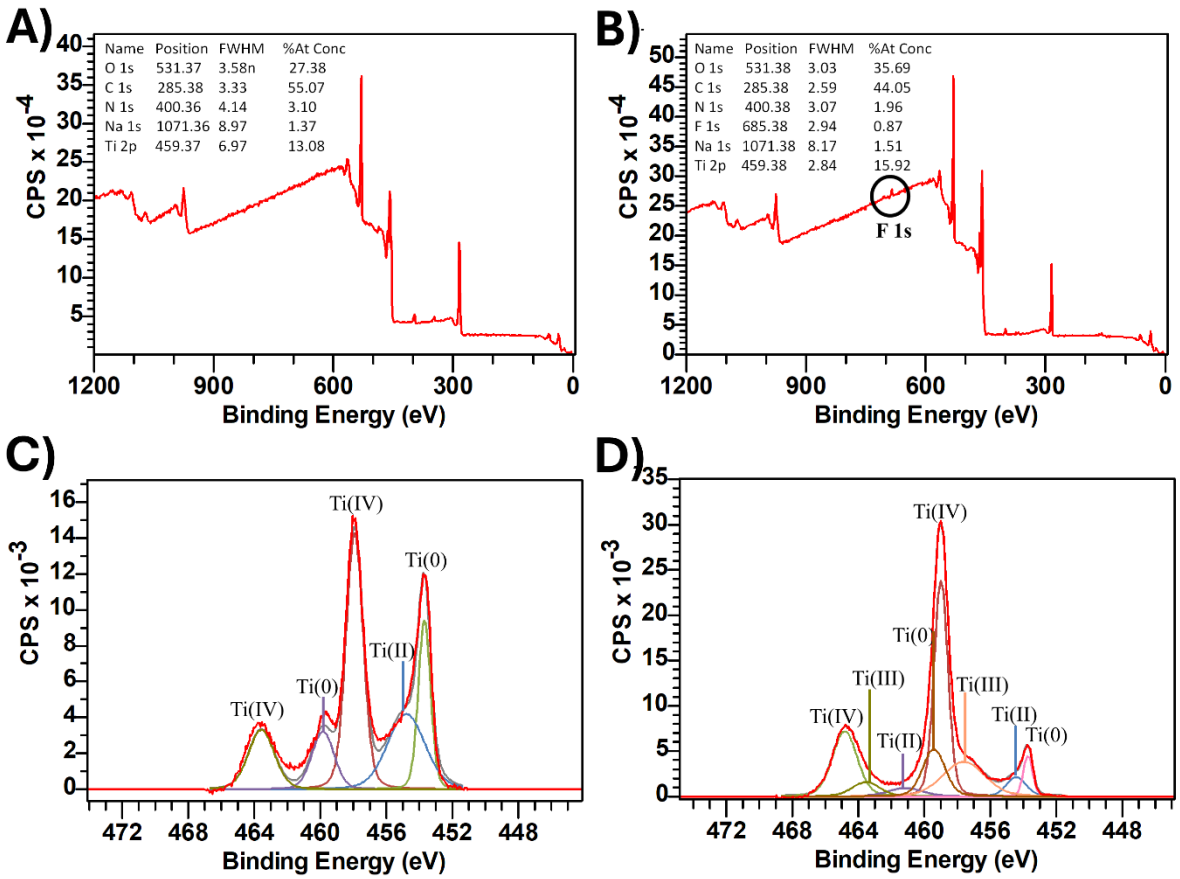


Figure 10. XPS survey spectra of bare Ti (A) and TiND (B), the latter containing a circle indicating F 1s signal, as well as Ti 2p region spectra of bare Ti (C) and TiND (D) showing the deconvoluted peaks.

Although this surface modification approach did not induce significant changes in wettability, with both untreated and modified titanium maintaining a moderately hydrophilic character (~56°), it resulted in notable alterations in surface chemical composition and titanium oxidation

states. XPS analysis revealed the incorporation of fluorine species, most likely originating from residual electrolyte components during the etching process, together with a redistribution of titanium oxide species. While the untreated Ti surface was mainly composed of metallic titanium and stable titanium oxide phases, including TiO and TiO_2, the nanostructurization process increased the proportion of oxidized titanium species and promoted the formation of Ti(III)-containing states [181].

The presence of a stable titanium oxide layer is a key factor contributing to the excellent biological performance of titanium-based biomaterials. Due to its strong affinity for oxygen, titanium spontaneously forms a passive oxide film that protects the underlying metal from corrosion and limits the release of potentially harmful metallic ions into the surrounding biological environment. Furthermore, titanium oxide surfaces provide favorable physicochemical conditions for protein adsorption and subsequent cellular attachment, thereby supporting implant integration. Therefore, the increased fraction of oxidized species observed after TiND fabrication may contribute to the improved biological interactions of the nanostructured titanium surface by providing a more chemically active and cell-supportive interface.

3.1.3. Biocompatibility of unmodified and modified Ti surfaces

The biocompatibility of bare Ti and TiND substrates was assessed using three different cell models, including NHDF, SH-SY5Y, and U87 cells, following 48 h of incubation (**Figure 11**). The obtained results demonstrated that nanostructurization of the titanium surface did not negatively affect cellular viability, as no statistically significant differences were observed between bare Ti and TiND for any of the investigated cell types. Both titanium substrates exhibited excellent cytocompatibility, with NHDF and SH-SY5Y cells displaying viability levels comparable to the tissue culture plastic (TCP) control, reaching values close to 100%. Interestingly, U87 cells cultured on both bare Ti and TiND surfaces exhibited a slight but statistically significant increase in viability compared with the TCP control. This observation suggests that titanium-based substrates may provide a more favorable microenvironment for U87 astrocytic cell survival and metabolic activity compared with conventional culture plastic. Overall, these findings confirm that the fabrication of nanoscale surface features on titanium does not compromise biocompatibility and provides a suitable platform for further investigation of cell–surface interactions.

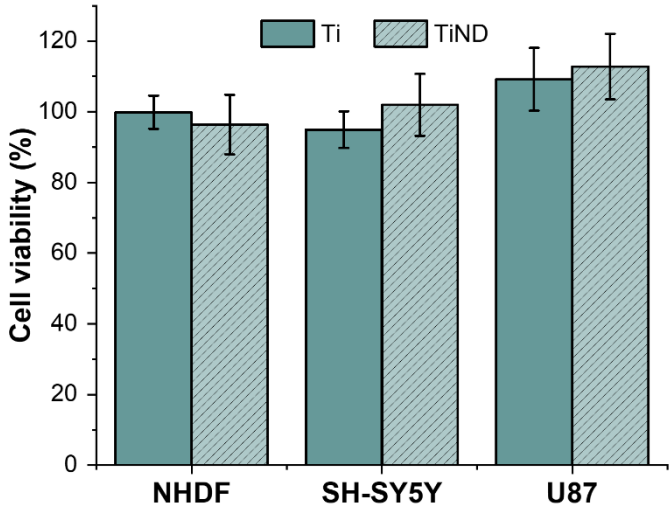


Figure 11. Cell viability percentage of NHDF, SH-SY5Y and U87 cells cultured on the surface of Ti and TiND relative to the control (TCP); $p \geq 0.05$.

3.1.4. Effect of nanodimples on cell morphology

The influence of nanodimpled surfaces on fibroblast adhesion and morphology was evaluated using SEM combined with morphometric analysis (**Figure 12A–D**). NHDF cells cultured on pristine Ti surfaces formed a uniform cellular layer and exhibited a characteristic spindle-like morphology (**Figure 12A**). In contrast, cells grown on TiND substrates appeared less elongated and displayed a more spread morphology (**Figure 12B**).

Quantitative morphometric analysis further confirmed these observations. NHDF cells cultured on TiND surfaces showed a larger average cell area (1732 ± 643 μm²) compared with cells cultured on untreated Ti surfaces (1353 ± 481 μm²) (**Figure 12C**). In addition, the circularity index of cells on TiND substrates (0.46 ± 0.18) was higher than that observed for cells on pristine Ti (0.33 ± 0.10) (**Figure 12D**), indicating a transition toward a more rounded and extensively spread cellular phenotype. These findings suggest that the nanodimpled topography significantly influences fibroblast morphology and cell–surface interactions.

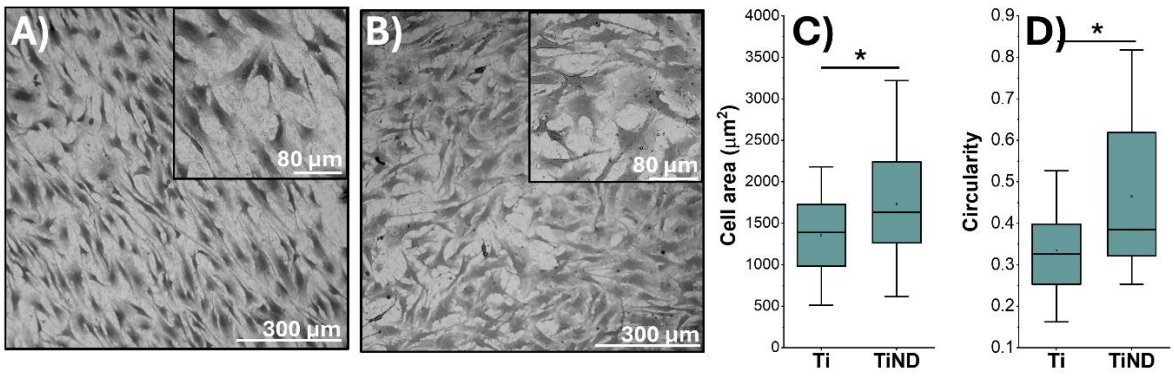


Figure 12. Morphology of NHDF cells grown on pristine Ti and TiND surfaces. Representative SEM images of cells cultured on pristine Ti (A) and TiND (B) are shown. Cell area (C) and circularity index (D), calculated from SEM micrographs, were used to assess differences in cell spreading and shape between the two substrates; * = $p < 0.05$. The box represents the interquartile range (25^{th}–75^{th} percentiles), the central line indicates the median, the square denotes the mean, while whiskers extend to the 5^{th} and 95^{th} percentiles.

Fibroblasts, as major constituents of connective tissue, are highly adherent cells capable of attaching to and spreading across a wide range of substrates. Their adhesion characteristics are closely reflected in their morphology. Under physiological conditions, fibroblasts typically exhibit a spindle-shaped morphology; however, upon activation and enhanced adhesion, they undergo cytoskeletal reorganization accompanied by the formation of prominent actin stress fibers [182]. The observed increase in cell spreading area and circularity index for NHDF cultured on TiND surfaces is therefore indicative of enhanced cell–substrate affinity and stronger adhesive interactions.

These findings are consistent with previous studies demonstrating that surface nanotopography plays a critical role in regulating fibroblast adhesion. Depending on feature geometry and size, topographical cues can either promote cellular entry into surface depressions or facilitate bridging across nanostructures, thereby directly influencing cell behavior [183]. Kolind et al. [184] reported that inter-pillar spacing, rather than pillar geometry, is a key determinant of cell proliferation, emphasizing the importance of nanoscale spacing parameters in cell–material interactions. Similarly, studies on crater-like nanopatterns [185] have shown that smaller feature dimensions (e.g., 500 nm diameter, 45 nm depth) do not inhibit cell adhesion, whereas

larger pitches (e.g., 1000 nm diameter, 350 nm depth) can induce non-adherent regions, further confirming the regulatory role of nanotopographical design on fibroblast behavior.

Human neuroblastoma SH-SY5Y cells were also studied using SEM. It was observed that, they formed a continuous layer on pristine Ti surfaces (**Figure 13A**). However, when cultured on TiND substrates, the cellular network appeared visually more homogeneous and densely organized (**Figure 13B**). To quantitatively assess these observations, SEM images were analyzed using fractal analysis, with particular focus on the fractal dimension (FD) as an indicator of morphological complexity (**Figure 13C**). In neuronal systems, higher FD values are generally associated with increased neurite branching and network connectivity [186]. Although the mean FD values obtained for cells cultured on pristine Ti (1.608 ± 0.093) and TiND surfaces (1.576 ± 0.032) were comparable, notable differences were observed in the variability of the measurements. Specifically, the relatively large standard deviation observed on pristine Ti (±0.093) suggests a heterogeneous and poorly regulated cellular organization, indicative of a surface that does not consistently support defined neuronal patterning. In contrast, the lower variability on TiND substrates (±0.032) indicates a more uniform and reproducible cellular response. This suggests that nanodimpled topography promotes more consistent neuronal adhesion and network formation, leading to well-defined morphological organization despite similar average FD values.

Neuronal-like SH-SY5Y cells were also strongly influenced by the presence of nanodimpled topography, which promoted the formation of more organized and homogeneous cellular networks. Previous studies have similarly demonstrated that SH-SY5Y cell morphology and differentiation are highly sensitive to nanoscale surface features such as topography, geometry, and material composition. For example, cells cultured on silver-coated nanolines exhibited pronounced morphological changes, with enhanced neuronal branching observed on 180 nm-wide patterns, whereas wider features (500 nm) failed to induce branching [187]. In addition, it has been shown that groove-based topographies can promote differentiation of SH-SY5Y cells toward an N-type neuronal phenotype within 48 h, even in the absence of exogenous differentiation factors [188]. Such substrates induce elongated and polarized neurite outgrowth with increased neurite length compared to flat surfaces, suggesting that topographical cues alone can direct neuronal maturation and potentially suppress proliferation of undifferentiated cancer-like phenotypes.

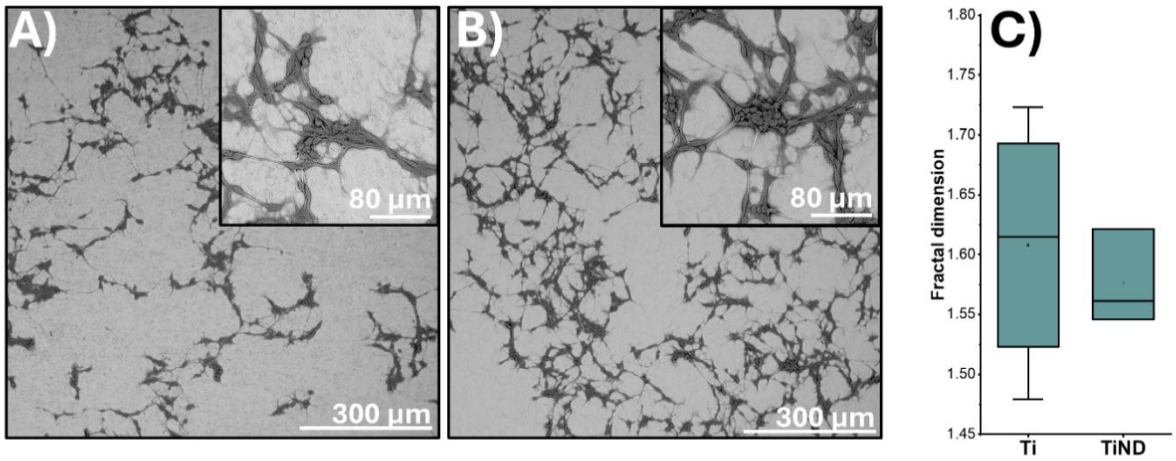


Figure 13. Morphological assessment of SH-SY5Y cells cultured on pristine titanium and titanium nanodimple (TiND) surfaces. Representative SEM images of cells on pristine Ti (A) and TiND (B) are shown. The corresponding fractal dimension values (C), derived from SEM image analysis, were used to evaluate the complexity of cellular morphology on the different substrates; $p \geq 0.05$. The box represents the interquartile range (25^{th}–75^{th} percentiles), the central line indicates the median, the square denotes the mean, while whiskers extend to the 5^{th} and 95^{th} percentiles.

SEM analysis of U87 astrocytic cells cultured on pristine Ti (**Figure 14A**) and TiND surfaces (**Figure 14B**) demonstrated clear differences in cellular morphology, particularly with respect to the number of cellular protrusions (**Figure 14C**). Cells grown on pristine Ti exhibited a higher number of protrusive structures per cell, whereas those cultured on TiND displayed a noticeably reduced protrusive activity. Quantitative analysis confirmed this trend, with U87 cells on TiND showing a significantly lower number of protrusions per cell (8.15 ± 2.25) compared with cells on pristine Ti (13.61 ± 5.55). This reduction in cellular protrusiveness suggests that the nanodimpled surface exerts an inhibitory effect on astrocyte adhesion dynamics and may suppress migratory behavior [189].

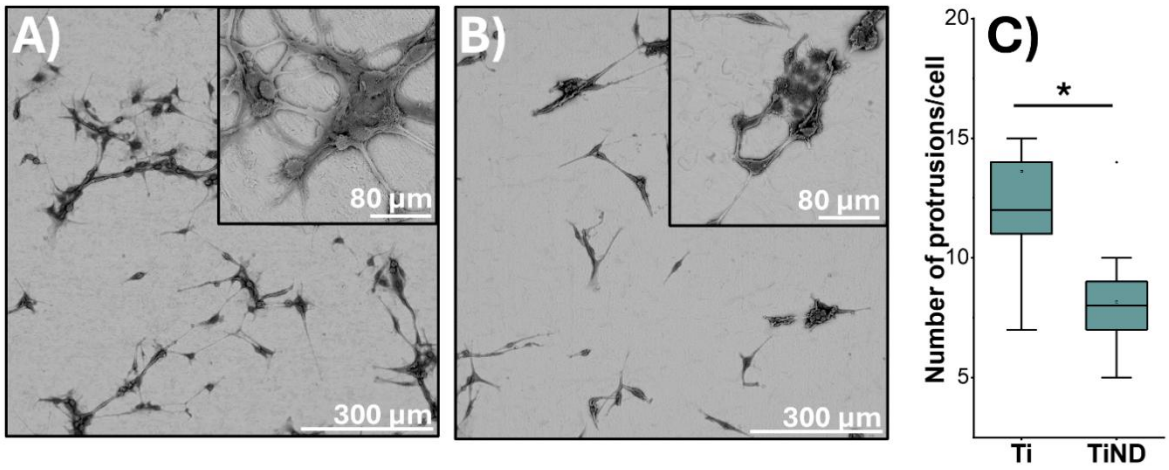


Figure 14. Morphological characterization of U87 cells cultured on pristine titanium and titanium nanodimple (TiND) surfaces. Representative SEM images of cells on pristine Ti (A) and TiND (B) are shown. Quantitative analysis of the number of cellular protrusions per cell (C) was performed based on SEM micrographs; * = $p < 0.05$. The box represents the interquartile range (25^{th}–75^{th} percentiles), the central line indicates the median, the square denotes the mean, while whiskers extend to the 5^{th} and 95^{th} percentiles.

Astrocytes, represented here by U87 cells, are glial cells characterized by their migratory and highly dynamic behavior, enabling them to respond to physiological and pathological cues within the central nervous system. Their functions include structural and metabolic support of neurons, as well as regulation of synaptic activity [190]. Astrocyte migration is a multistep process involving membrane protrusion formation, adhesion to the extracellular environment, and generation of traction forces through cytoskeletal rearrangement. In the present study, TiND surfaces reduced the number of protrusions per cell, indicating an anti-adhesive and anti-migratory effect. This behavior may be beneficial in limiting excessive astrocytic activation and reducing the risk of gliosis formation [189].

Comparable findings have been reported by Vallejo-Giraldo et al. [110], who demonstrated that PEDOT:PSS-coated microelectrodes functionalized with ordered micropit arrays (with diameter of 0.82 ± 0.07 µm and interpit spacing of 2.28 ± 0.06 µm) reduced astrocyte adhesion in mixed primary cultures. This effect was accompanied by altered cellular morphology, decreased focal adhesion formation, and downregulation of pro-inflammatory signaling molecules [110]. Collectively, such results suggest that topographical modification can be used

to modulate glial responses, potentially reducing glial scarring and improving the performance and long-term stability of neural interfaces.

3.1.5. Effect of nanodimples on focal adhesion formation

Cell adhesion is primarily governed by cell–substrate interactions mediated through integrin signaling pathways. In adherent cell types, including astrocytes and fibroblasts, focal adhesion formation is tightly regulated by integrin clustering and downstream signaling cascades, in which the FAK–paxillin axis plays a central role in controlling cell spreading, morphology, and migration [191]. Given that the most pronounced topography-dependent effects were observed in NHDF cells based on SEM analysis, these cells were selected for focal adhesion analysis.

Fluorescence microscopy images of NHDF cells cultured on the control substrate (**Figure 15A**), pristine Ti (**Figure 15B**), and TiND surfaces (**Figure 15C**) show immunostaining of the focal adhesion protein paxillin. Distinct differences in the distribution and abundance of paxillin-positive puncta were observed across the tested surfaces. Quantitative analysis of discrete paxillin-containing focal adhesion structures (**Figure 15D**) demonstrated a pronounced influence of surface nanostructuring on focal adhesion formation. Cells cultured on TiND exhibited a higher number of focal adhesions per cell (3.5 ± 2.4 FA/cell) compared with those grown on pristine Ti (1.5 ± 0.9 FA/cell) and the control substrate (1.6 ± 0.6 FA/cell). These results indicate that the nanodimpled Ti surface significantly enhances focal adhesion assembly, suggesting improved cell–material interactions at the nanoscale.

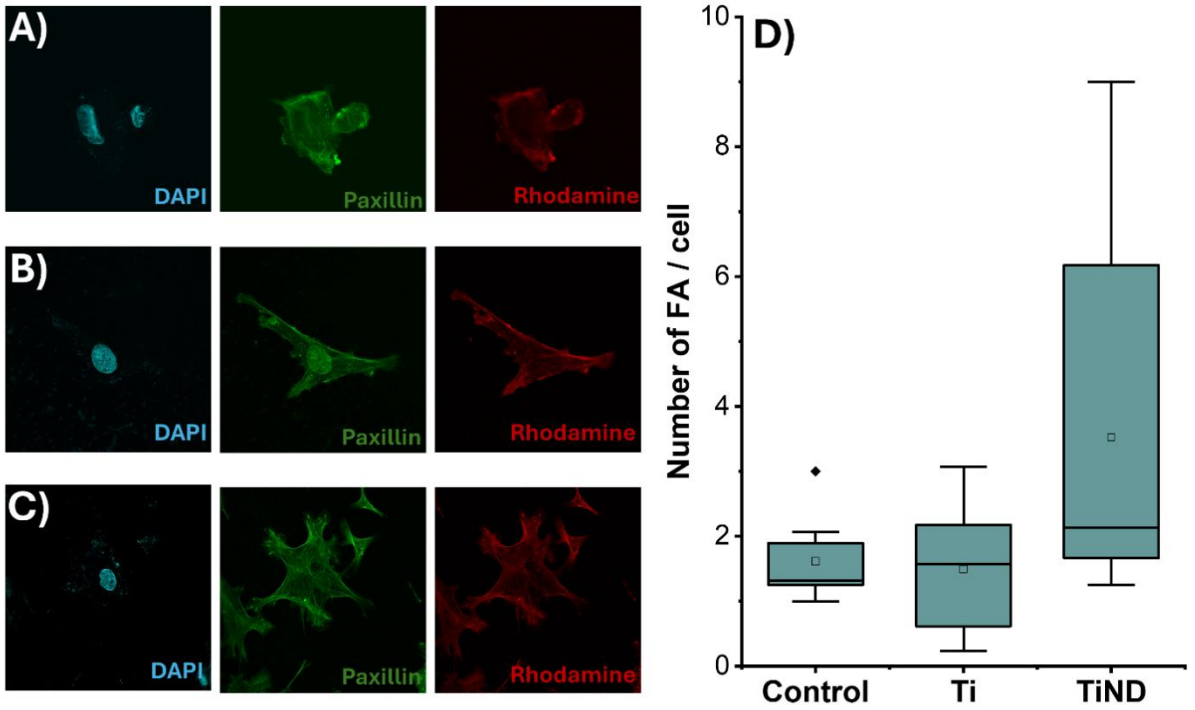


Figure 15. Fluorescence microscopy images of NHDF cells cultured on a control surface (A), pristine titanium (B), and titanium nanodimple (TiND) surfaces (C). F-actin was stained in red to visualize the cytoskeleton, focal adhesions were labeled with anti-paxillin in green, and nuclei were counterstained with DAPI in blue. The average number of focal adhesions per cell on each substrate, quantified from fluorescence images, is presented in (D); $p \geq 0.05$. The box represents the interquartile range (25^{th}–75^{th} percentiles), the central line indicates the median, the square denotes the mean, while whiskers extend to the 5^{th} and 95^{th} percentiles.

The increased number of paxillin-positive FAs observed on TiND surfaces correlates with enhanced cell spreading and morphology changes, confirming that nanodimpled topography promotes stronger and more stable cell adhesion. The selective adhesion behavior induced by TiND surfaces may offer significant potential for tissue engineering applications where cell-specific responses are required. The simultaneous promotion of fibroblast adhesion and spreading, enhancement of neuronal network organization, and reduction of astrocytic protrusive activity suggest that such surfaces could be particularly advantageous for neural interface and spinal cord regeneration strategies. In spinal cord injury, glial scar formation is driven by complex interactions between resident CNS cells and infiltrating peripheral immune cells, including fibroblasts and macrophages [192]. Following injury, activated astrocytes and microglia accumulate at the lesion site and release pro-inflammatory mediators that inhibit

axonal regeneration, while extracellular matrix components such as chondroitin sulfate proteoglycans further contribute to growth inhibition.

In parallel, infiltrating macrophages recruit perivascular fibroblasts that contribute to the formation of the fibrotic scar component [193]. Within the first week post-injury, this region becomes densely cellular, and by approximately two weeks, a well-defined interface forms between fibrotic and glial compartments [193]. Importantly, recent evidence suggests that fibroblasts are not solely detrimental, but also play regulatory roles in modulating neuroinflammation and supporting tissue repair [194]. Their beneficial functions include extracellular matrix production, secretion of growth factors and cytokines, and participation in immune cell signaling pathways [195]. Accordingly, biomaterials supporting controlled fibroblast adhesion may still be considered advantageous for neural tissue regeneration.

3.1.6. Perspectives and limitations

Titanium and its alloys are already widely used in spinal surgical applications as structural implants for stabilizing the spine and protecting neural tissues [196]. Their favorable mechanical properties, including high toughness, moderate elastic modulus, and excellent biocompatibility, make them suitable for biomedical use. Additionally, titanium's ductile behavior reduces the risk of brittle fracture and improves implant safety by minimizing fragmentation under mechanical stress [197].

In vitro biological evaluation in this study demonstrated that TiND surfaces promoted the adhesion of NHDF, resulting in enhanced cell spreading, increased circularity, and greater focal adhesion formation compared with the control surface. SH-SY5Y neuroblastoma cells cultured on TiND also formed denser and more interconnected neurite networks, indicating improved neuronal organization. Conversely, U87 astrocytes exhibited reduced adhesion and migratory behavior on the nanotextured surfaces, suggesting that the engineered nanotopography may selectively modulate cell-specific responses. Such differential regulation of fibroblasts, neuronal cells, and astrocytes highlights the potential of TiND surfaces as a promising platform for neural interfaces, particularly in applications related to spinal cord injury repair.

While immortalized cell lines provide a reproducible and suitable model for proof-of-concept investigations, they cannot fully reproduce the complexity of the native central nervous system, including the morphology, functional phenotype, inflammatory signaling, and dynamic cell–

cell interactions characteristic of primary neural cells. Consequently, future studies should validate these findings using primary neurons and astrocytes, more physiologically relevant three-dimensional or organotypic *in vitro* models, and ultimately appropriate *in vivo* spinal cord injury models to determine the translational potential of nanotopographically modified titanium electrodes. Furthermore, investigating a wider range of culture durations together with additional nano-dimple geometries would provide deeper insight into the temporal and topography-dependent mechanisms governing cellular responses to these engineered surfaces.

Given its established clinical relevance in spinal applications [196] [198] [199], the ability to tailor cell adhesion via surface modification strategies such as electrochemical anodization followed by chemical etching represents a promising approach for expanding the functionality of titanium-based biomaterials in regenerative medicine.

3.1.7. Conclusions

This study demonstrated that titanium surfaces featuring nano-dimpled structures, produced through a combination of electrochemical anodization and chemical etching, provide a highly uniform and controlled surface morphology capable of influencing cell–material interactions. Compared with untreated titanium, the TiND surfaces exhibited lower surface roughness, indicating the successful generation of a consistent nanoscale topography. Biological evaluation *in vitro* revealed improved adhesion of normal human dermal fibroblasts on TiND surfaces, accompanied by greater spreading, increased circularity, and enhanced focal adhesion development. Furthermore, SH-SY5Y neuroblastoma cells formed more extensive and homogeneous neuronal networks on the modified surfaces. Conversely, U87 astrocytes displayed diminished adhesion and migratory behavior, suggesting a selective inhibitory effect toward this cell type. Collectively, these results highlight the potential of nano-engineered titanium electrodes to direct cell-specific responses, supporting their application in central nervous system therapies, particularly in strategies aimed at spinal cord injury repair.

3.2. Effect of bioactive coatings on cell adhesion

3.2.1. Aim and objectives

The aim of this study was to develop a bioactive polymeric coating for metallic skull implants designed to mitigate brain scar formation during cranial reconstruction procedures (**Figure 16**). The coating was based on PVA incorporated with a polyanhydride derived from betulin disuccinate and tricarboxylic poly(ethylene glycol) (PEG-DBB).

Specific objectives included:

1- To fabricate a bioactive polymer coating based on PVA functionalized with PEG-DBB derived from betulin disuccinate and tricarboxylic PEG derivatives.
2- To optimize the processing and deposition of the coating, including its application onto titanium substrates as a clinically relevant proof-of-concept material.
3- To characterize the physicochemical and morphological properties of the developed PVA/PEG-DBB system, including surface structure and material uniformity.
4- To evaluate the cytocompatibility of the coating using representative cell lines, including neuroblastoma, fibroblast, and osteosarcoma cells.
5- To assess the influence of betulin-based functionalization on cell adhesion behaviour, with emphasis on its bioactive and anti-adhesive effects.
6- To investigate the potential of the coating to regulate cell–material interactions in the context of preventing brain scarring and improving implant integration.
7- To demonstrate the feasibility of the coating for cranial reconstruction applications, supporting its potential translation into regenerative medicine and biomedical implant technologies.

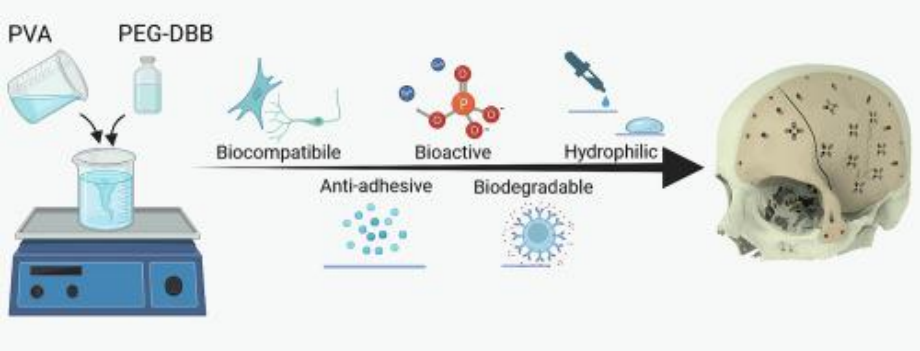


Figure 16. Schematic illustration of fabrication process to create an anti-adhesive polymeric coating for prevention of brain scarring during cranial reconstruction. Reprinted with permission from [135].

3.2.2. Formation of PVA-based electrospun fibers

PVA is a synthetic, water-soluble polymer widely recognized for its biocompatibility, non-toxicity, biodegradability, and ease of processing. A notable advantage of PVA is its compatibility with aqueous systems, which enables environmentally benign fabrication routes. Electrospinning of PVA allows the formation of nanoscale fibrous architectures with broad applicability in drug delivery, tissue engineering, and filtration technologies. The use of water as a solvent further enhances its suitability for biomedical applications by eliminating the need for toxic organic solvents [200].

Electrospinning is a versatile and effective method for producing fibrous coatings with controllable structural characteristics. By carefully adjusting the electrospinning parameters, it is possible to generate micro- and nanofibers with relatively uniform diameters and lengths that can organize into porous scaffolds or coatings. PVA fibers with diameters ranging from 52 to 232 nm were obtained, exhibiting an average diameter of 131 ± 40 nm (**Figure 17A**), which corresponds to values commonly reported for electrospun PVA fibers prepared from aqueous solutions [201]. After incorporating 10 vol.% DMSO and PEG-DBB, the fiber diameter increased substantially, yielding fibers between 120 and 485 nm with an average diameter of 256 ± 88 nm (**Figure 17B**), together with a broader size distribution.

Several factors may explain the observed increase in fiber diameter. Betulin possesses lipophilic and hydrophobic characteristics and exhibits limited solubility in polar solvents [202] [203]. Consequently, its incorporation can modify the surface tension of the spinning solution, thereby affecting fiber morphology and dimensions [204]. In addition, DMSO itself likely contributed to the increase in fiber diameter. Gupta et al. [205] investigated the electrospinning behavior of PVA in water/DMSO solvent systems and reported that increasing the DMSO content from 0 to 30% resulted in thicker fibers. Although both water and DMSO are suitable solvents for PVA, DMSO promotes a more extended conformation of PVA chains compared with pure water. In mixed solvent systems, interactions between water and DMSO are stronger than those between the solvents and the polymer chains. As the DMSO concentration rises, greater polymer chain entanglement occurs, increasing solution viscosity and relaxation time, which ultimately leads to the formation of fibers with larger diameters.

Fiber diameter is considered one of the key material parameters influencing cellular responses to biomaterials. Pelipenko et al. [206] examined how nanofiber diameter affects cell behavior *in vitro* to determine fiber dimensions favorable for tissue regeneration. In their work,

electrospun PVA fibers with diameters between 69 and 1116 nm were produced by modifying polymer concentration and environmental humidity. Keratinocytes demonstrated the highest metabolic activity on fibers with an average diameter of approximately 305 nm, whereas the lowest activity was detected on fibers with diameters of 69 nm. Conversely, when fiber diameter increased to 1116 nm, cell proliferation declined, likely because thicker fibers less closely resembled the architecture of the native ECM, whose structural components are typically within the 260–410 nm range [207]. Fibroblasts also showed significantly lower proliferation on fibers with diameters of 69 and 161 nm. This variation in cellular response may be associated with the greater degree of fibroblast differentiation and their comparatively slower metabolism. Furthermore, changes in fiber diameter can influence mechanical properties, which in turn affect cellular activity. Fibers with smaller diameters are generally stiffer, and enhanced stiffness has been associated with improved cell proliferation for fibers below 1000 nm [208] . In the present study, both pure PVA and PVA/PEG-DBB fibers exhibited diameters below 500 nm. Notably, the dimensions of the PVA/PEG-DBB fibers were comparable to those of natural ECM components, suggesting their suitability for supporting cell adhesion and proliferation.

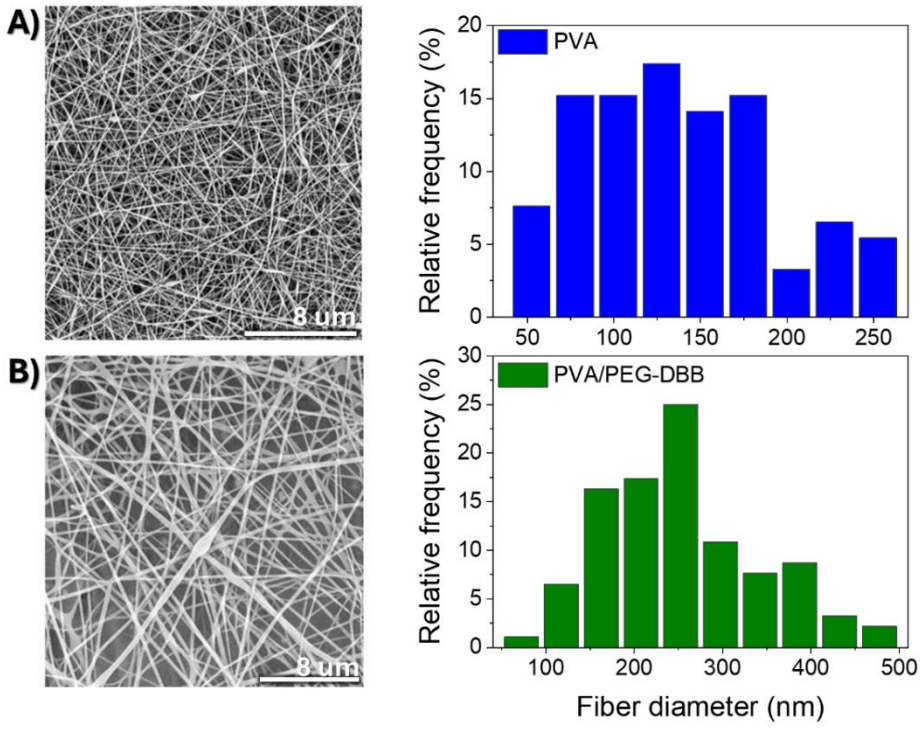


Figure 17. Representative FE-SEM micrographs and corresponding histograms showing the diameter distributions of electrospun PVA fibers (n = 95) (A) and PVA/PEG-DBB fibers (n = 91) (B). Reprinted with permission from [135].

3.2.3. Chemical analysis of PVA-based electrospun fibers

The FTIR spectra of PVA, PEG-DBB, and PVA/PEG-DBB fibers are presented in **Figure 18A**. In the spectrum of PVA, the characteristic absorption bands corresponding to hydroxyl and residual acetate groups are clearly visible. The broad peak centered at 3318 cm^{-1} is assigned to O–H stretching vibrations, while the band at 2940 cm^{-1} corresponds to C–H stretching vibrations of alkyl groups. In addition, the absorption bands observed between 1733 and 1091 cm^{-1} are related to C=O and C–O stretching vibrations, respectively [209]. For PEG-DBB, the FTIR spectrum exhibits characteristic peaks associated with carbonyl groups. The absorption bands at 1818 cm^{-1} and 1730 cm^{-1} are attributed to the C=O stretching vibrations of anhydride and ester groups, respectively [210]. Furthermore, the peak at 2914 cm^{-1} is related to alkyl group vibrations originating from both PEG and DBB components (**Figure 18C**). The FTIR spectrum of PVA/PEG-DBB fibers retained the main characteristic bands of PVA, including the O–H stretching band at 3292 cm^{-1}, the C–H stretching vibration of alkyl groups at 2948 cm^{-1}, the C–O stretching vibration at 1086 cm^{-1}, and the C=O stretching vibration of residual acetate groups at 1712 cm^{-1}. A slight shift in the O–H stretching band between pure PVA and PVA/PEG-DBB fibers suggests the possibility of intermolecular interactions between the two polymeric components. Notably, distinct absorption bands characteristic of PEG-DBB were not clearly detected in the spectrum of PVA/PEG-DBB fibers. This observation may indicate that PEG-DBB was incorporated within the PVA fibers in the form of a core–shell structure. Since PVA is hydrophilic whereas PEG-DBB exhibits more hydrophobic behavior, the combination of these polymers may induce phase separation during electrospinning [171], potentially leading to the formation of core–shell-like fibers in which PVA forms the outer layer surrounding a PEG-DBB-rich core. To verify this assumption, both PVA and PVA/PEG-DBB fibers were dissolved in deionized water and analyzed using UV–Vis spectroscopy (**Figure 18B**). The UV–Vis spectrum of PVA/PEG-DBB displayed a characteristic absorption peak at 210 nm, corresponding to the maximum absorption of betulin [211] [212]. This result confirms the presence of PEG-DBB within the fibers and further supports the proposed core–shell morphology of the PVA/PEG-DBB system.

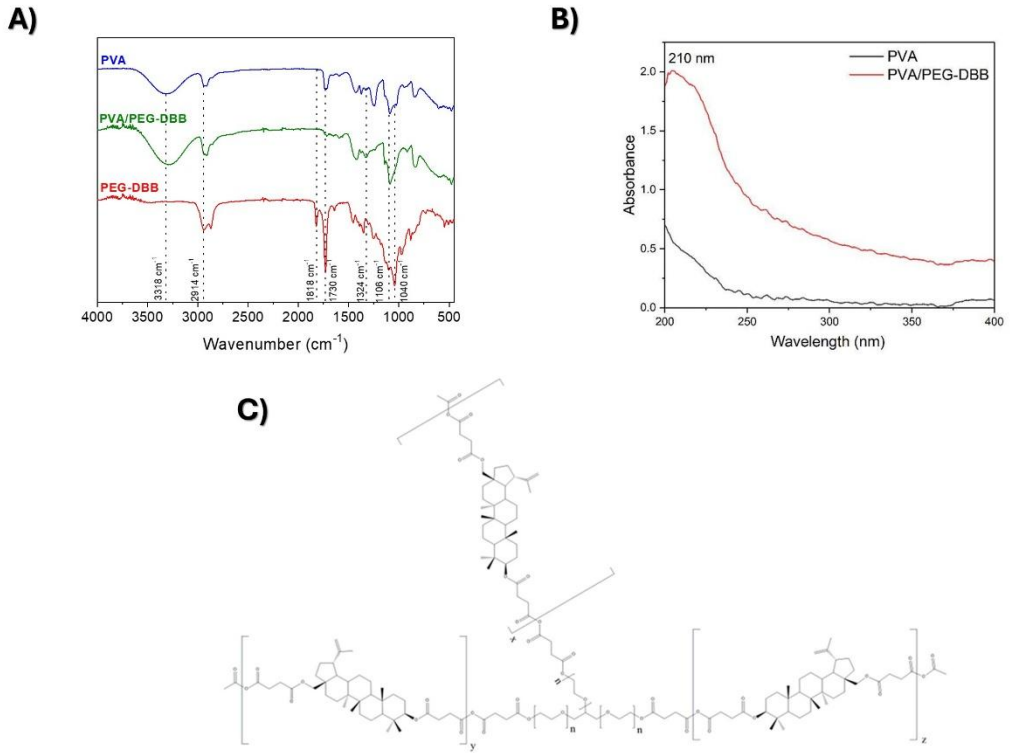


Figure 18. FTIR spectra of PVA, PEG-DBB, and the PVA/PEG-DBB composite (A), UV–Vis spectra of solutions prepared by dissolving PVA and PVA/PEG-DBB in deionized water (B), indicating successful incorporation of PEG-DBB through the characteristic absorption band at 210 nm. And the molecular structure of PEG-DBB (C). Reprinted with permission from [135].

3.2.4. Cell viability

The biocompatibility of the fabricated materials was assessed using NHDF, SH-SY5Y, and U2OS cell lines cultured on PVA fibers, PVA/PEG-DBB fibers, and glass control substrates for 48 h. For NHDF fibroblasts (**Figure 19A**), the highest cell viability was observed on pure PVA fibers, reaching 116.5 ± 7.9%. Similar findings have previously been reported, where fibroblasts cultured on PVA-based materials demonstrated enhanced viability compared with standard control surfaces [213]. In the present study, the highly hydrophilic character of the coating and its partial dissolution in the culture environment may have contributed to macromolecular crowding effects, thereby creating conditions more closely resembling the *in vivo* extracellular environment [214].

The incorporation of PEG-DBB reduced NHDF viability to 91.3 ± 5.5%; however, according to ISO 10993 standards, materials exhibiting cell viability above 85% are still regarded as

biocompatible. The slight reduction in viability may be associated with the biological activity of betulin derivatives. Małaczewska et al. [215] demonstrated that mitochondria are particularly sensitive to betulin exposure, while other cellular functions remain less affected. Their results showed a significant decline in fibroblast viability after 24 h at betulin concentrations of 1.95 μg mL^{-1} or higher. Likewise, Pfarr et al. [216] reported decreased mitochondrial activity in melanoma cell lines exposed to betulin concentrations as low as 15 μM, suggesting inhibition of proliferation rather than direct induction of cell death. Comparable observations were described by Lin et al. [217], who found that betulin concentrations up to 5.12 μg mL^{-1} did not compromise membrane integrity in porcine chondrocytes, despite influencing cellular metabolism.

In contrast, SH-SY5Y neuroblastoma cells exhibited the highest viability on PVA/PEG-DBB fibers, reaching 104.1 ± 5.3%, whereas cells cultured on pure PVA fibers showed lower viability (90.3 ± 6.3%). SH-SY5Y cells are commonly used as an *in vitro* neuronal model in their undifferentiated state [218]. The improved viability observed in the presence of PEG-DBB may be related to the biological activity of DBB, which has been shown to reduce superoxide radical formation, decrease caspase-3/7 activity, and stabilize mitochondrial membrane permeability [219]. Jiang et al. [220] demonstrated that betulinic acid enhanced SH-SY5Y viability and alleviated ischemia/reperfusion injury through modulation of pathways involving HIF-1α, AMPK, PPARα, PGC-1α, and NF-κB. Furthermore, previous investigations have highlighted the neuroprotective potential of betulin derivatives. Pandey et al. [221] reported that pretreatment with betulinic acid restored cellular redox balance by reducing reactive oxygen species and malondialdehyde levels while simultaneously increasing antioxidant defense mechanisms, including glutathione production and the activity of superoxide dismutase and catalase enzymes.

For the U2OS osteosarcoma cell line (**Figure 19A**), no statistically significant differences in viability were observed among the tested substrates. Cell viability remained comparable for the glass control (104.0 ± 4.2%), PVA fibers (105.1 ± 3.9%), and PVA/PEG-DBB fibers (102.3 ± 3.6%).

Electrospun PVA materials have previously been applied successfully in bone tissue engineering applications [222, 223] and the present findings indicate that the addition of PEG-DBB does not negatively affect their cytocompatibility toward bone-related cells. Although direct comparative analyses of NHDF, SH-SY5Y, and U2OS cells under identical

mitochondrial-targeting conditions remain limited, the observed differences in viability may be explained by variations in metabolic activity, adhesion behavior, and mitochondrial sensitivity among these cell types. Fibroblasts generally possess high metabolic reserves and may therefore respond more sensitively to disturbances in mitochondrial function, particularly under suboptimal adhesion conditions. In contrast, neuron-like SH-SY5Y cells depend more strongly on oxidative metabolism and may benefit more substantially from compounds that stabilize mitochondrial function. Consequently, the mitochondrial protective effects associated with DBB, such as reduced reactive oxygen species production and stabilization of membrane potential, may preferentially enhance SH-SY5Y viability, whereas fibroblasts may exhibit a slight reduction in metabolic activity or adhesion efficiency in response to the same modification.

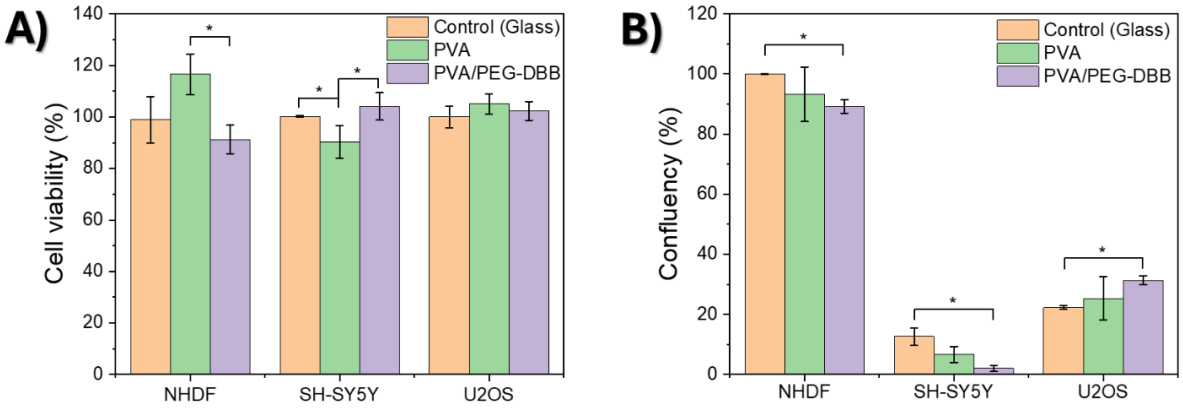


Figure 19. Cell viability (Alamar Blue assay) of NHDF, SH-SY5Y, and U2OS cells on PVA and PVA/PEG-DBB fibers (A), and cell confluency after 48 h of culture (B); *p < 0.05. Reprinted with permission from [135].

3.2.5. Cell adhesion

Cell adhesion was investigated by culturing NHDF, SH-SY5Y, and U2OS cells on PVA fibers, PVA/PEG-DBB fibers, and glass control surfaces for 48 h. Following incubation, cell confluency was determined as the percentage of the substrate surface covered by cells (**Figure 19B**).

NHDF fibroblasts, which are strongly adherent cells, nearly completely covered the glass control surface, reaching a confluency of 99.9 ± 0.1%. The introduction of electrospun coatings reduced fibroblast attachment, with confluency values decreasing to 93.2 ± 9.1% on PVA fibers

and 89.2 ± 2.2% on PVA/PEG-DBB fibers. A similar trend was observed for SH-SY5Y neuroblastoma cells. Although these cells already displayed relatively low attachment to the glass control surface, with a confluency of 12.6 ± 2.9%, the presence of PVA and PVA/PEG-DBB coatings further decreased cell coverage to 6.6 ± 2.7% and 2.0 ± 1.1%, respectively. These findings indicate that the electrospun coatings exhibit anti-adhesive properties toward both fibroblast and neuroblastoma cell lines. Despite the lower number of attached cells on coated substrates compared with the glass control, the morphology of both NHDF and SH-SY5Y cells remained well developed, with no visible signs of degeneration or cellular damage.

The reduced adhesion observed on PVA-based coatings may be attributed to the highly hydrophilic nature of PVA. Hydrophilic materials generally adsorb fewer proteins and induce fewer conformational changes in adsorbed proteins compared with hydrophobic surfaces. Proteins such as albumin typically exhibit greater affinity toward hydrophobic substrates [224]. Because PVA is highly hydrophilic, adsorption of serum proteins onto its surface is limited, which likely contributes to its anti-adhesive behavior toward NHDF and SH-SY5Y cells [225]. In addition, cellular adhesion is largely mediated by integrins, which are transmembrane proteins linking the ECM to the cytoskeleton [226]. Previous studies have shown that betulin may interfere with integrin expression or function, thereby impairing the ability of cells to attach to ECM components and other surfaces [227].

In contrast to fibroblasts and neuroblastoma cells, U2OS osteosarcoma cells exhibited improved adhesion on the electrospun coatings. Cells cultured on the glass control reached a confluency of 22.3 ± 0.6%, while those grown on PVA fibers achieved 25.3 ± 7.2%. The highest confluency was observed on PVA/PEG-DBB fibers, reaching 31.3 ± 1.5%. These findings are consistent with previous reports demonstrating that betulin can promote osteogenesis *in vitro* in human osteoblast models under osteogenic conditions. Betulin has been shown to stimulate osteoblast differentiation and exert pro-osteogenic effects at low, non-cytotoxic concentrations [228]. Similarly, the structurally related compound betulinic acid has been reported to enhance osteogenic differentiation. Lo et al. [229] demonstrated that betulinic acid significantly increased alkaline phosphatase (ALP) activity and calcium nodule formation, which may contribute to its bone anabolic properties.

3.2.6. Proof-of-concept: modification of titanium surface

To investigate the potential application of PVA/PEG-DBB fibers as implant coatings, the electrospun fibers were deposited onto Ti-6Al-4V alloy discs. Among titanium-based biomaterials, Ti-6Al-4V is one of the most widely utilized alloys for biomedical applications, particularly in dental implants and orthopedic support structures due to its favorable mechanical and biological properties [230]. Although flat disc-shaped substrates were employed in this study as a proof-of-concept model, electrospinning is highly adaptable and can also be applied to complex three-dimensional and non-planar implant geometries, including custom cranial implants [231] [232].

The morphology of PVA/PEG-DBB fibers deposited on the Ti-6Al-4V surface is presented in **Figure 20A.** Compared with fibers collected on aluminum supports, a greater number of polymer beads was observed on the titanium alloy surface. Nevertheless, the obtained fibers exhibited a comparable morphology, with an average diameter of 242 ± 21 nm and a diameter distribution ranging from 105 to 446 nm (**Figure 20B**), closely corresponding to the dimensions reported previously for PVA/PEG-DBB fibers shown in **Figure 17B**.

Since surface hydrophilicity strongly influences cell-material interactions, water contact angle measurements were performed for uncoated Ti-6Al-4V, PVA-coated, and PVA/PEG-DBB-coated samples. Owing to the highly hydrophilic nature of PVA, deposition of pure PVA fibers reduced the water contact angle of Ti-6Al-4V from 61.5 ± 1.7° to complete wetting (0°). In contrast, incorporation of PEG-DBB reduced the hydrophilicity of the coating, increasing the contact angle to 49.9 ± 2.1°. This run

The adhesion strength of the coatings to the Ti-6Al-4V substrate was evaluated using a scratch test (**Figure 20C**). In this method, a Rockwell indenter was applied under progressively increasing normal force until coating failure occurred. The critical load (Lc), defined as the minimum force leading to loss of adhesion between the coating and the substrate, was determined for both coatings. The obtained Lc values ranged from 1.7 to 2.7 N for both PVA and PVA/PEG-DBB layers. Independent of coating composition, the scratches exhibited a similar damage mechanism characterized by continuous plastic perforation of the coating layer. The results demonstrate that the developed coatings possess satisfactory adhesion to the titanium substrate and outperform several other polymeric implant coatings reported in the literature, such as poly (lactic-co-glycolic acid), which exhibits a critical load of approximately 0.5 N [233].

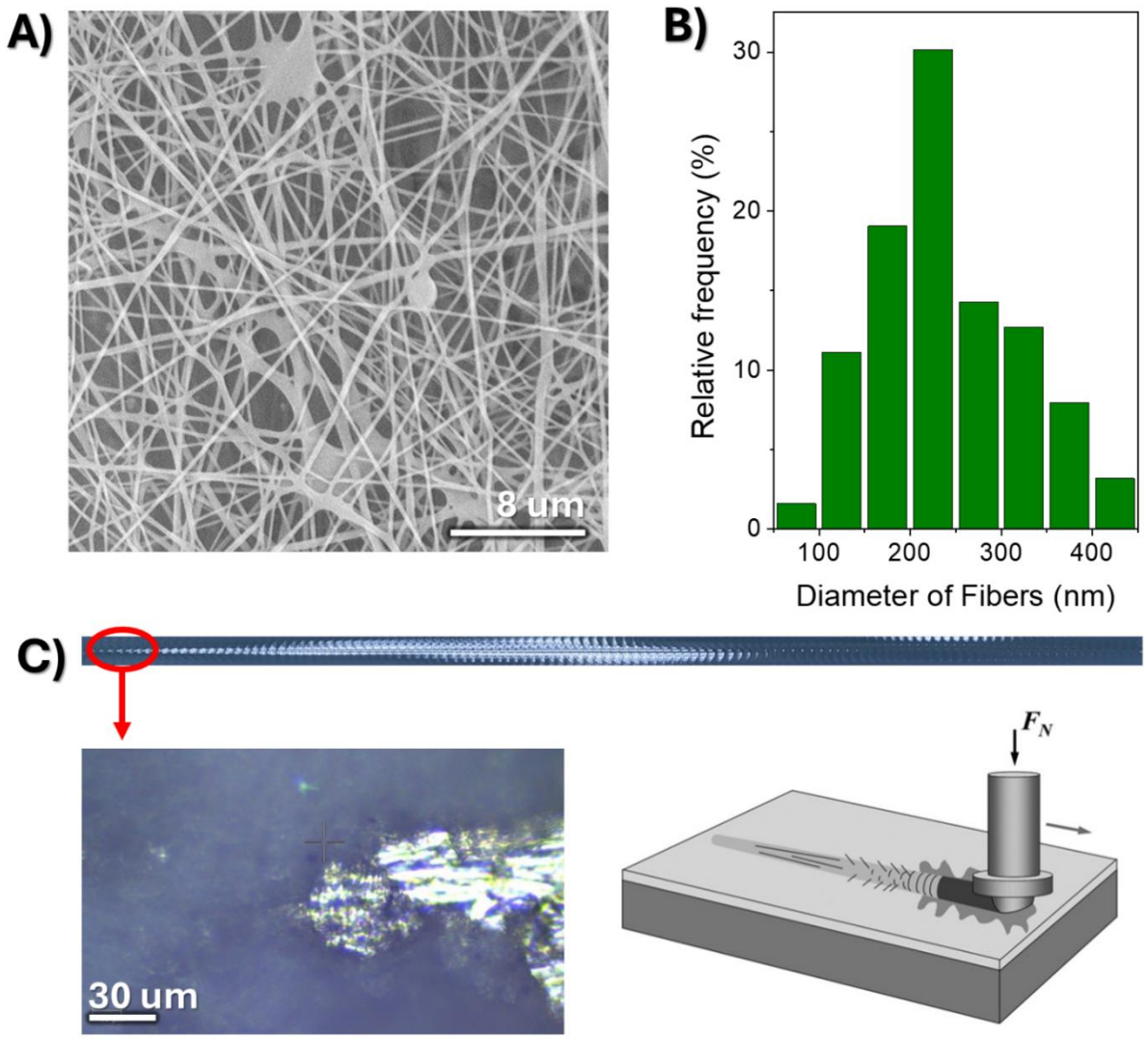


Figure 20. FE-SEM micrograph of electrospun PVA/PEG-DBB fibers on a Ti-6Al-4V substrate (A) and the corresponding histogram of fiber diameter distribution (B). (C) Schematic illustration of the scratch test used for adhesion evaluation. Reprinted with permission from [135].

3.2.7. Support in bone remodeling

Amorphous calcium phosphate is a major constituent of human bone and is well known for its excellent biodegradability, biocompatibility, and bioactivity [234]. The ability of the investigated samples to induce calcium phosphate formation was assessed by immersion in simulated body fluid (SBF) for 21 days. Surface morphology and elemental composition were analyzed using SEM and EDS on uncoated Ti-6Al-4V, PVA-coated, and PVA/PEG-DBB-coated samples after incubation (**Figure 21A–B**). Following SBF exposure, all samples

exhibited the formation of a calcium phosphate layer, covering approximately 48.1 ± 6.7% of the surface for PVA and 54.0 ± 6.5% for PVA/PEG-DBB, values comparable to the uncoated Ti-6Al-4V control (50.7 ± 1.8%). Spherical calcium phosphate deposits were observed across all surfaces (**Figure 21A**) [235] . The thickness of the formed layer was similar for the Ti-6Al-4V control (10.4 ± 0.8 μm) and PVA/PEG-DBB-coated samples (11.7 ± 1.3 μm), whereas a significantly thinner layer was detected on PVA-coated surfaces (7.4 ± 1.1 μm).

EDS analysis (**Figure 21B**) confirmed the presence of calcium (Ca) and phosphorus (P) on all post-immersion surfaces. The calculated Ca/P atomic ratios were 1.74 for PVA/PEG-DBB and 1.82 for PVA-coated samples. These values exceed the stoichiometric ratio of hydroxyapatite (1.67), suggesting the coexistence of additional calcium-rich phases, such as calcium carbonate [236]. In contrast, the Ti-6Al-4V control exhibited a Ca/P ratio of 1.54, which is close to that of β-tricalcium phosphate (1.5) [237]. The Ca/P ratio is known to strongly influence the microstructure as well as the mechanical and physicochemical properties of calcium phosphate layers. Stoichiometric hydroxyapatite (Ca/P = 1.67) typically exhibits optimal hardness and fracture toughness, whereas deviations from this ratio can alter mechanical performance due to calcium deficit.

Raman spectroscopy (**Figure 21C**) further confirmed the formation of calcium phosphate phases on all samples. The spectra showed characteristic vibrational modes of phosphate (PO_4^{3-}) tetrahedra [238]. The bands at approximately 1069 cm^{-1} and 578 cm^{-1} correspond to the asymmetric stretching and bending modes of PO_4^{3-}, respectively. Peaks at 960 cm^{-1} and 435 cm^{-1} are assigned to the symmetric P–O stretching and O–P–O bending vibrations, respectively. The presence of broad Raman features indicates a predominantly amorphous or poorly crystalline nature of the formed calcium phosphate layer [239] [240].

Overall, the *in vitro* results demonstrate that all tested materials can induce apatite formation, confirming their bioactive nature. The development of a bone-like apatite layer is essential for improving bonding between implanted materials and host bone tissue, and its rapid formation is associated with enhanced osteoconductivity and accelerated bone regeneration processes [241]. The enhanced nucleation of hydroxyapatite on the coated surfaces can be attributed to the presence of hydroxyl groups in PVA and PVA/PEG-DBB fibers. During biomimetic mineralization, hydroxyapatite formation proceeds via nucleation and growth mechanisms governed by surface functional groups such as –OH. These groups facilitate interfacial interactions through hydrogen bonding and electrostatic attraction. Initially, Ca^{2+} ions are

adsorbed onto hydroxyl-rich surfaces, creating nucleation sites that subsequently promote the accumulation and organization of phosphate ions (PO_4^{3-}), ultimately leading to apatite formation [242].

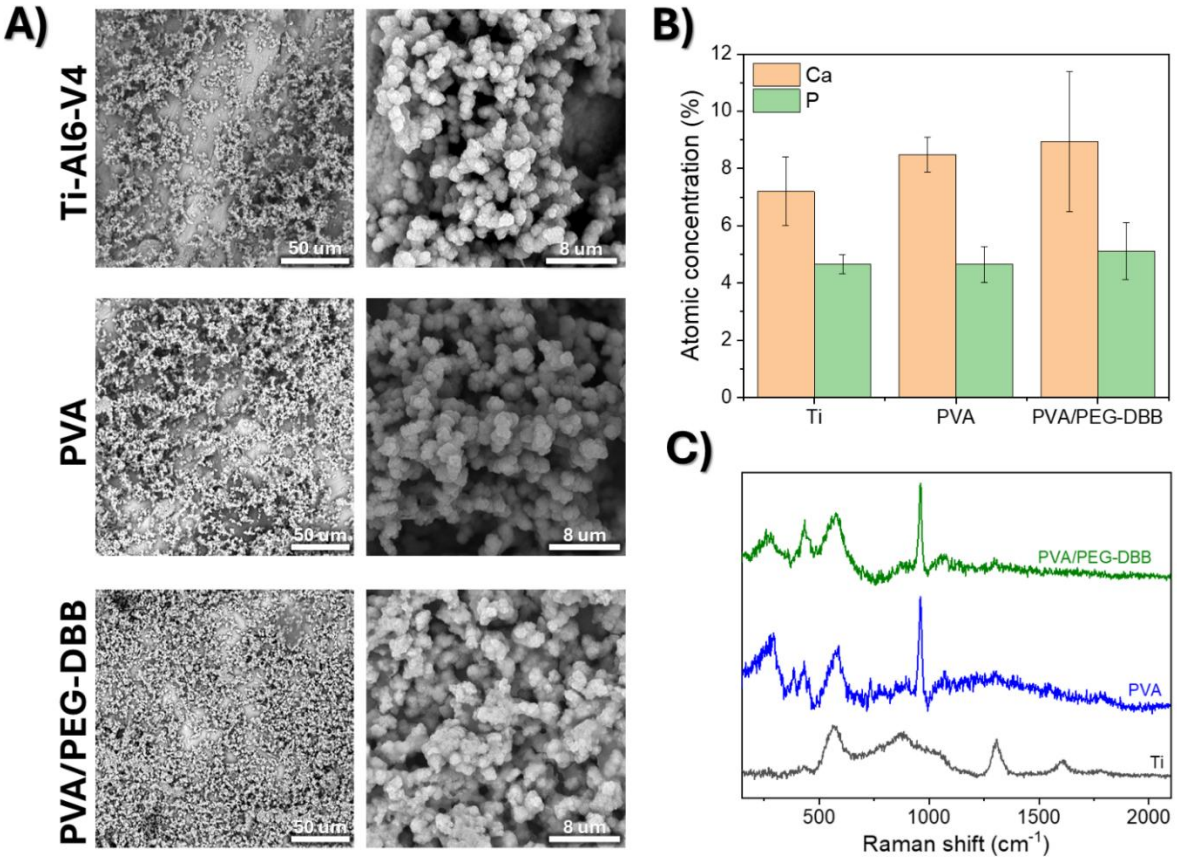


Figure 21. Surface morphology, elemental composition, and Raman spectral analysis of bare, PVA-coated, and PVA/PEG-DBB-coated Ti-6Al-4V discs after 21-day exposure to SBF, as shown in SEM micrographs (A), elemental analysis (B), and Raman spectra (C). Reprinted with permission from [135].

3.2.8. Perspectives and limitations

Cranioplasty is an established neurosurgical intervention aimed at reconstructing cranial defects to restore the integrity of the skull and re-establish protection of the brain. Beyond its protective function, the procedure may also contribute to improved vestibular balance, thereby reducing the risk of falls, alleviate symptoms associated with the syndrome of the trephined, and enhance cosmetic appearance. It is most performed in patients following craniectomy, once they have progressed beyond the acute phase of treatment and achieved medical and surgical

stability [151]. In addition to restoring cranial structure, cranioplasty offers benefits including improved aesthetic outcome and functional protection for patients with cranial defects [150].

Given that titanium mesh is associated with lower rates of graft-related infection compared with alternative materials such as PTFE and silicone sheets, the incorporation of a PVA/PEG-DBB surface modification may further enhance its clinical performance and contribute to safer cranial reconstruction procedures. In addition to preserving the favorable mechanical properties of titanium, the bioactive coating may promote improved tissue integration by supporting the adhesion and proliferation of fibroblasts while reducing excessive scar formation. These combined effects could facilitate more effective wound healing, improve long-term implant stability, and ultimately enhance clinical outcomes following cranial reconstruction.

A remaining challenge associated with PVA-based coatings is the identification of an appropriate sterilization strategy that preserves their structural integrity and biological functionality. Recent studies have indicated that ethylene oxide sterilization is more suitable than conventional methods such as steam autoclaving, gamma irradiation, or UV irradiation, as it better maintains the physicochemical properties of PVA-based materials [243]. Since the inflammatory response plays a central role in fibrotic scar formation and implant integration, future investigations should evaluate the immunomodulatory effects of the coating by assessing macrophage polarization and the expression of key inflammatory mediators, including the pro-inflammatory cytokines TNF-α, IL-1β, IL-6, and MCP-1, together with the anti-inflammatory and pro-regenerative factors IL-10 and TGF-β. Furthermore, optimization of the coating composition and fabrication process, followed by comprehensive preclinical evaluation in relevant animal models, will be essential to establish its long-term safety, biological performance, and translational potential for clinical cranial reconstruction applications.

Further optimization of the coating formulation and progression toward preclinical evaluation will be essential to establish its long-term safety and therapeutic potential prior to clinical translation.

3.2.9. Conclusion

In this chapter, I present a novel bioactive coating consisting of polymeric nanofibers incorporating betulin disuccinate and deposited onto a Ti-6Al-4V alloy substrate to address

complications commonly associated with cranioplasty procedures. Cytocompatibility assessments performed using NHDF, SH-SY5Y, and U2OS cell lines demonstrated cell viability above 90% for all tested samples, indicating the absence of cytotoxic effects. Furthermore, cell adhesion studies revealed reduced attachment of NHDF and SH-SY5Y cells, whereas adhesion of U2OS cells was promoted. The observed anti-adhesive behavior may be attributed to two primary factors: the hydrophilic nature of the coating, which limits the adsorption of adhesion-mediating proteins, and the biological activity of DBB, which appears to suppress cellular attachment. In contrast, the enhanced interaction of U2OS cells with the coating may result from the influence of PEG-DBB on alkaline phosphatase activity and calcium nodule formation, thereby supporting osteogenic processes. The coating also exhibited strong adherence to the Ti-6Al-4V substrate, suggesting adequate mechanical stability and potential applicability in load-bearing implant environments. By combining favorable biocompatibility, selective regulation of cell adhesion, and mechanical durability, the PVA/PEG-DBB coating represents a promising strategy for improving cranioplasty outcomes and reducing postoperative complications related to tissue adhesion.

3.3. Electroactive modulation of cellular adhesion

3.3.1. Aims and objectives

The aim of this part of my research was to develop PANI-based neural interfaces capable of retaining conductivity at physiological pH while interacting with neurons through both topographical and electrical cues, as demonstrated before [117, 118]. To achieve this, hybrid CP films composed of PANI and PEDOT were electrodeposited onto Pt electrode surfaces. By combining these two polymers, my aim was to create an electroactive 3D coating capable of promoting specific cellular responses, including enhanced cell adhesion and proliferation, through the combined effects of polymer chemistry and surface morphology (**Figure 22**).

Specific objectives include:

1- To fabricate bilayer CP coatings composed of PANI and PEDOT on Pt electrode surfaces using an electrodeposition technique.

2- To characterize the physicochemical properties of the developed PANI–PEDOT hybrid coatings, with particular emphasis on surface morphology, hydrophilicity, impedance, capacitance, and charge transfer capability.

3- To evaluate how the combination of PANI and PEDOT influences the structural and electrochemical performance of the resulting multilayer films compared to single-polymer systems.

4- To investigate the *in vitro* biocompatibility of the fabricated coatings using rat-derived embryonic VM neuronal cell cultures.

5- To assess the ability of the hybrid CP coatings to support neurons

6- To determine the potential of PANI–PEDOT multilayer coatings as functional neural interface materials capable of enhancing neuron–electrode interactions through combined electrical conductivity and surface topography.

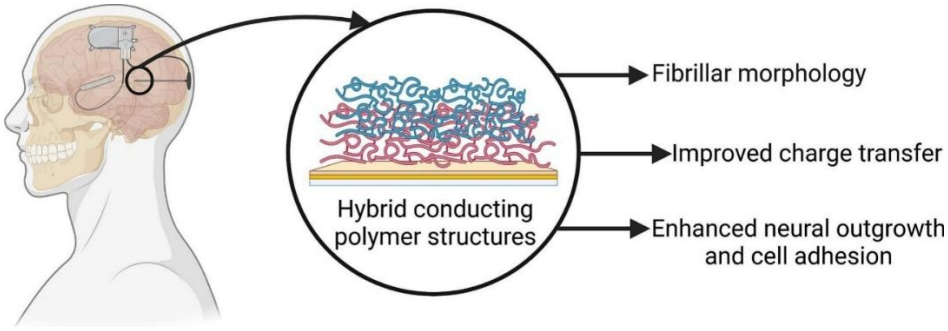


Figure 22. Schematic illustration of procedure to create hybrid conducting polymer films to promote neural outgrowth and neural-electrode integration. Reprinted with permission from [95].

3.3.2. Electrodeposition of conducting polymers

CV is a widely used and effective method for electropolymerization, as it enables controlled deposition of electroactive films while simultaneously providing real-time monitoring of the electrochemical processes occurring at the electrode surface. In this work, the electropolymerization of aniline (**Figure 23A**) was initiated at a potential of 0.9 V vs. Ag/AgCl, which is consistent with previously reported conditions for aniline polymerization in acidic media [244]. Throughout the process, three distinct redox couples (A/A′, B/B′, and C/C′) can be identified. The A/A′ system corresponds to the redox transition between the fully reduced leucoemeraldine form and the partially oxidized emeraldine state. The B/B′ peaks are associated with intermediate species formed during hydroquinone/benzoquinone redox processes, as well as related side products. The C/C′ redox pair is attributed to the conversion of the emeraldine form into the fully oxidized pernigraniline state [245].

Similarly, EDOT oxidation occurs at approximately 0.9 V vs. Ag/AgCl (**Figure 23B**), in agreement with literature reports [246]. This process begins with the formation of EDOT radical cations, which subsequently undergo coupling and dimerization reactions. These steps are stabilized through deprotonation, involving the removal of hydrogen ions. Continued coupling and deprotonation events promote the growth of conjugated oligomers and ultimately lead to the formation of PEDOT. The electrochemical signature of PEDOT is characterized by a broad redox response rather than multiple discrete peaks, reflecting its predominantly capacitive behavior [247] [248]. An increase in both anodic and cathodic currents within the potential range of −0.5 V to 0.6 V vs. Ag/AgCl indicates progressive deposition of conductive PEDOT films.

Figure 23C illustrates the cyclic voltammetry response during EDOT polymerization on a PANI-modified Pt electrode. After the initial formation of the characteristic three-redox system of PANI during the first ~20 cycles of aniline deposition, subsequent PEDOT growth modifies the electrochemical response, leading to the emergence and dominance of a broad PEDOT-related redox feature. The resulting CV profile reflects a hybrid material exhibiting mixed charge storage behavior, combining faradaic and capacitive contributions.

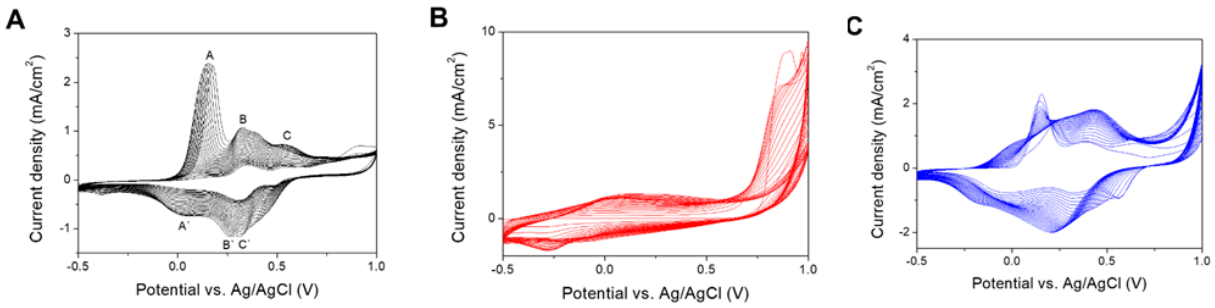


Figure 23. Cyclic voltammetric responses corresponding to the electrochemical polymerization of aniline on a bare platinum electrode (A), EDOT on a bare Pt electrode (B), and EDOT on a PANI-modified Pt electrode (C). The experiments were conducted in 1 M H_2SO_4 aqueous solution at a scan rate of 100 mV s^{-1} for 20 consecutive CV cycles. Reprinted with permission from [95].

The charge storage capacity of the resulting materials was quantified by integrating the area under the CV curves (**Figure 24A**), yielding the charge storage capacity (CSC) according to Equation (3) [174]. The calculated CSC values confirmed that PEDOT exhibits a high capacitive character (22.8 mC/cm²), whereas PANI shows a lower value (9.7 mC/cm²). The hybrid PANI–PEDOT system demonstrated an intermediate but enhanced performance (19.9 mC/cm²), indicating that incorporation of PEDOT significantly improves the charge storage ability of PANI-based coatings. This parameter is particularly important for neural interface applications, as higher CSC values are associated with improved efficiency in both neural stimulation and signal recording [148].

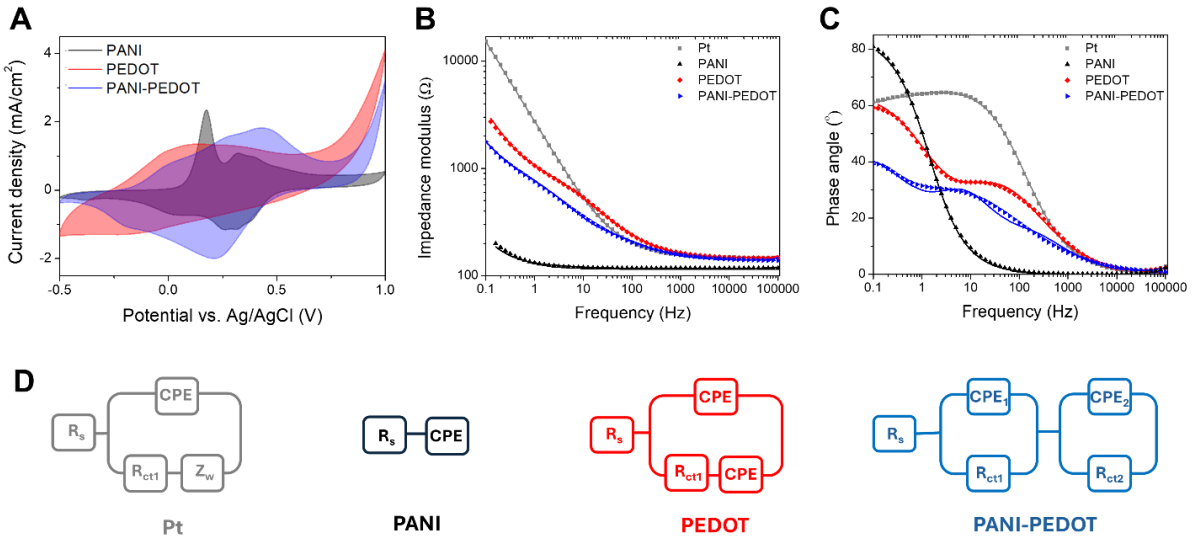


Figure 24. Electrochemical properties of PANI-, PEDOT-, and PANI–PEDOT-coated platinum electrodes. (A) Cyclic voltammograms obtained in 1 M H_2SO_4 at 100 mV s^{-1}. (B, C) Bode plots of EIS, presenting the frequency dependence of impedance magnitude and phase angle for bare and polymer-coated Pt electrodes (AC amplitude: 100 mV; DC bias: 0 V; n = 3). Experimental data and fitted curves are indicated by symbols and lines, respectively. (D) Equivalent electrical circuits used for modelling the EIS responses. Reprinted with permission from [95].

3.3.3. Electrochemical characterization

EIS is a key analytical tool for evaluating the performance of bioelectronic interfaces, as it directly reflects the efficiency of charge transfer between the electrode surface and the surrounding biological environment. Low impedance is particularly important for neural recording applications, where it contributes to an improved signal-to-noise ratio and overall device sensitivity [249].

The EIS results (**Figure 24B**) demonstrated that all investigated CP coatings effectively reduced the overall impedance of the Pt electrode, with the most pronounced reduction observed for electrodeposited PANI. In the low-frequency region (< 1 kHz), the PANI–PEDOT modified electrodes exhibited lower impedance magnitude (|Z|) compared with both bare Pt and PEDOT-coated electrodes. At 1 kHz, a frequency relevant for neural action potential detection[250], the impedance values of PANI, PEDOT, and PANI–PEDOT were comparable (~140 Ω), yet substantially lower than those reported for other CP-based systems, such as vertically aligned PEDOT nanotube arrays (5.53 kΩ at 1 kHz) [251]. This indicates

significantly improved charge-transfer efficiency, which is critical for neural interface applications. Phase angle analysis (**Figure 24C**) further revealed frequency-dependent differences among the coatings, particularly in the low-frequency range, confirming variations in capacitive behavior that are consistent with the charge storage capacity trends observed in CV measurements.

To further elucidate the electrochemical properties of the coatings, including resistive and capacitive contributions, the EIS data were fitted to equivalent circuit models using Powell and NM Sim algorithms (**Figure 24D**). The fitting showed very good agreement with the experimental data ($\chi^2 < 0.001$), validating the selected models. The equivalent circuits consisted of a solution resistance (R_s), two charge-transfer resistance components associated with the polymer layers (R_{ct1} and R_{ct2}), two constant phase elements (CPE_1 and CPE_2), and a Warburg diffusion element (Z_w). The fitted parameters, together with the experimental spectra, are presented in **Figure 24B–C**, while detailed values are summarized in **Table 1**. The solution resistance (R_s) remained nearly identical across all samples, as expected.

A marked reduction in charge-transfer resistance was observed for PEDOT (1.5 ± 0.1 kΩ) and PANI–PEDOT (1.4 ± 0.1 kΩ) compared with the bare Pt electrode (R_{ct1} = 11.5 ± 1.2 kΩ). In the case of PANI, the absence of a distinct Rct1 component indicates predominantly capacitive behavior, which is instead represented by a constant phase element (CPE). In bioelectrochemical systems, the CPE is commonly used to describe non-ideal capacitive behavior, representing a response that lies between that of an ideal capacitor and a resistor [252]. The n parameter derived from the CPE fitting provides further insight into the electrical behavior of the coatings. For PANI and PANI–PEDOT, values of n approaching unity indicate behavior close to that of an ideal capacitor. In contrast, PEDOT exhibited an n value of 0.67 ± 0.01, consistent with pseudocapacitive behavior and supporting the CV observations (**Figure 24A**). This suggests that charge storage in PEDOT is dominated by electric double-layer processes rather than purely faradaic reactions [253]. The similarity between the equivalent circuit representations of PEDOT and PANI–PEDOT indicates that the hybrid system inherits electrochemical characteristics from both components. This is further supported by the presence of two capacitive elements in the equivalent circuit of PANI–PEDOT, which reflects the contribution of both polymers within the multilayer structure on the Pt electrode surface.

Table 1. Electrochemical parameters derived from fitting impedance spectra using an equivalent circuit model, including solution resistance (R_s), charge-transfer resistance (R_{ct}), Warburg impedance (Z_w), constant phase element (CPE) parameters (P and n), and the chi-square (χ^2) value as a measure of fit quality. Reprinted with permission from [95].

	R_s [Ω]	R_{ct1} [kΩ]	R_{ct2} [kΩ]	CPE_1		CPE_2		Z_w	$\chi^2 \cdot 10^4$
				$P_1 \cdot 10^5$	n_1	$P_2 \cdot 10^5$	n_2		
Pt	147±1	11.5±1.2	-	3.1±0.1	0.802±0.001	-	-	44806±1528	1.4
PANI	118±1	-	-	110.2±0.8	0.942±0.003	-	-	-	1.8
PEDOT	144±1	1.5±0.1	-	7.7±0.1	0.670±0.002	14.8±0.4	0.767±0.005	-	3.3
PANI-PEDOT	136±2	1.4±0.1	3.71±0.03	34.9±0.9	0.981±0.009	104.4±5.9	0.948±0.031	-	6.9

Polyaniline (PANI) exhibits electrical conductivity that can vary widely, typically ranging from 10^{-9} to 100 S cm^{-1}; however, its electroactive behavior is largely restricted to acidic environments, where it exists in the protonated emeraldine salt form [102] [104]. Under neutral and alkaline conditions, PANI undergoes deprotonation and transitions into its emeraldine base form, which is electrically insulating, with conductivity decreasing to approximately 10^{-10} S cm^{-1}. This pronounced pH dependence is clearly reflected in cyclic voltammetry measurements performed at different pH values (**Figure 25A**), where a progressive suppression of redox activity is observed as pH increases, indicating a significant loss of electrochemical responsiveness. This behavior is further supported by Bode impedance analysis (**Figure 25D**), which shows a substantial increase in impedance modulus under higher pH conditions, consistent with reduced transport charge within the polymer matrix. In contrast, PEDOT maintains electroactivity under physiological pH conditions (**Figure 25B**), although its conductivity is also influenced by pH variations, as previously reported for PEDOT: PSS systems [107] (**Figure 25E**).

The PANI–PEDOT hybrid system is proposed to mitigate the limitations associated with the pH sensitivity of PANI. The increased resistance observed in the composite structure is likely related to its three-dimensional architecture, in which PANI may function as a reservoir for protons, while the PEDOT layer helps retain these protons and limits their diffusion into the surrounding medium. This structural synergy helps preserve the electroactive state of the

material even at physiological pH (~7), resulting in only a moderate reduction in both electrochemical activity **(Figure 25C)** and conductivity **(Figure 25F)** compared with acidic conditions. Importantly, the hybrid system still demonstrates markedly superior performance compared with uncoated platinum electrodes. Overall, coating PANI with PEDOT provides an effective strategy to extend the operational stability of PANI-based conducting polymers into physiologically relevant pH environments, thereby enhancing their suitability for bioelectronic and neural interface applications.

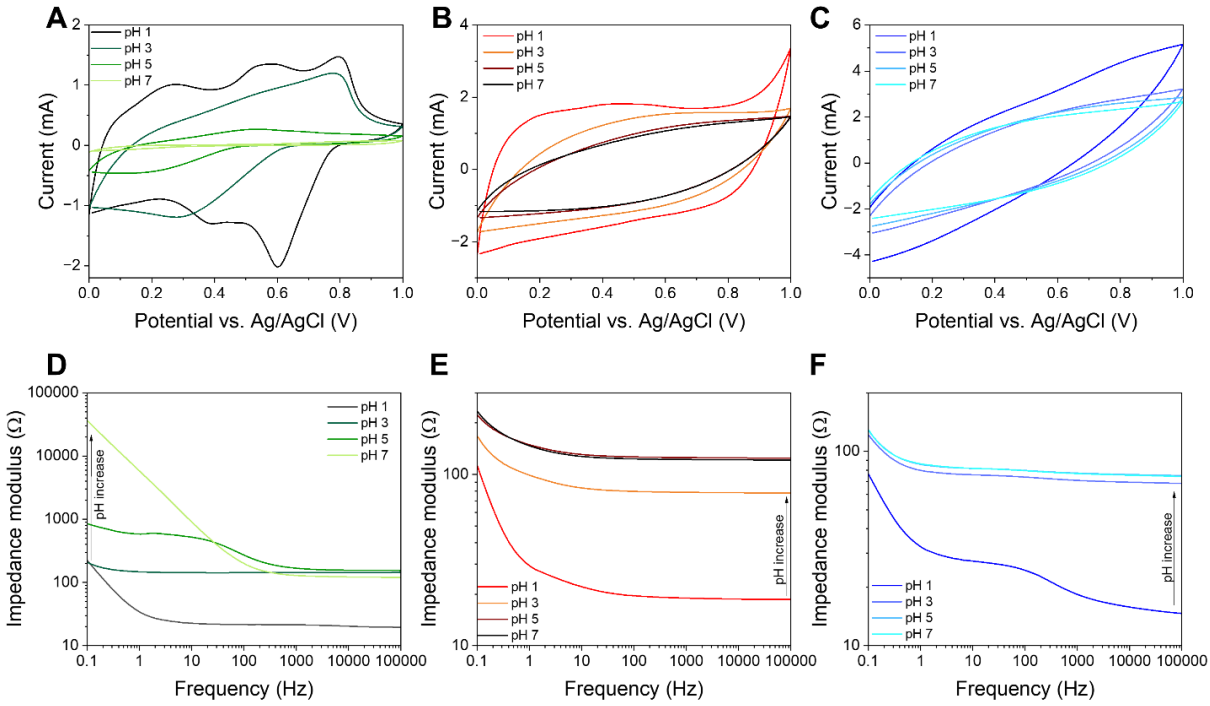


Figure 25 Electrochemical behavior of PANI-, PEDOT-, and PANI–PEDOT-modified electrodes (A–F). The coatings were synthesized in 1 M H_2SO_4 and subsequently investigated in electrolyte solutions with pH ranging from 1 to 7. Cyclic voltammetry results (A–C) were obtained at 100 mV s^{-1}, while electrochemical impedance spectroscopy (D–F) was performed at 100 mV AC amplitude and 0 V DC bias. Reprinted with permission from [95].

3.3.4. Surface characterization

Film morphology is a key parameter governing both the physical properties and the cytocompatibility of polymer coatings [254]. Electrodeposited CPs commonly exhibit a range of morphologies, including nodular, nanorod, and micro-granular structures, which are strongly

dependent on synthesis conditions such as applied potential, current density, deposition time, and polymerization kinetics.

SEM images of PANI films deposited on Pt electrodes **(Figure 26A)** reveal a well-defined nanofibrillar architecture, which can be attributed to a controlled and progressive nucleation process during electropolymerization [255]. Such fibrillar PANI coatings have been widely applied in electrochemical sensors, actuators, and energy storage systems due to their high surface area, porosity, and enhanced conductivity compared with compact or granular morphologies[256]. In the present study, the PANI nanofibers exhibited an average diameter of 115 ± 36 nm and a surface roughness of 1.87 ± 0.45 μm, which is significantly higher than that typically reported for granular PANI films (3–30 nm) [257]. Considering that neurite diameters are typically in the range of 0.2–2 μm [46], both the fibrillar dimensions and surface topography are considered suitable for supporting neuronal attachment and integration [148], while being less favorable for astrocyte colonization, which is associated with much larger cellular dimensions (~150 μm) [258].

SEM micrographs of electrodeposited PEDOT films **(Figure 26B)** show a characteristic cauliflower-like morphology. Although the deposition appears relatively uniform overall, localized aggregated domains can be observed, likely originating from nucleation around surface defects [106]. During the initial stages of polymer growth, chain elongation and globule formation occur concurrently on the electrode surface. With continued application of the oxidative potential, these globular structures grow and merge, eventually forming a continuous polymer layer. Prolonged polymerization leads to the formation of secondary globular aggregates, contributing to a surface roughness of 1.30 ± 0.52 μm. It has been previously reported that smoother and flatter surfaces may preferentially support astrocyte adhesion over neuronal attachment, potentially promoting glial scar formation that can negatively affect neural interface performance [110].

The electrodeposition of PEDOT onto pre-formed PANI fibrillar structures results in a hybrid morphology that combines the advantageous features of both polymers. As shown in **Figure 26C**, the resulting PANI–PEDOT coating retains the underlying fibrillar PANI network while being partially covered by PEDOT globular deposits. This produces a heterogeneous and relatively rough surface with a measured roughness of 1.97 ± 0.55 μm [259].

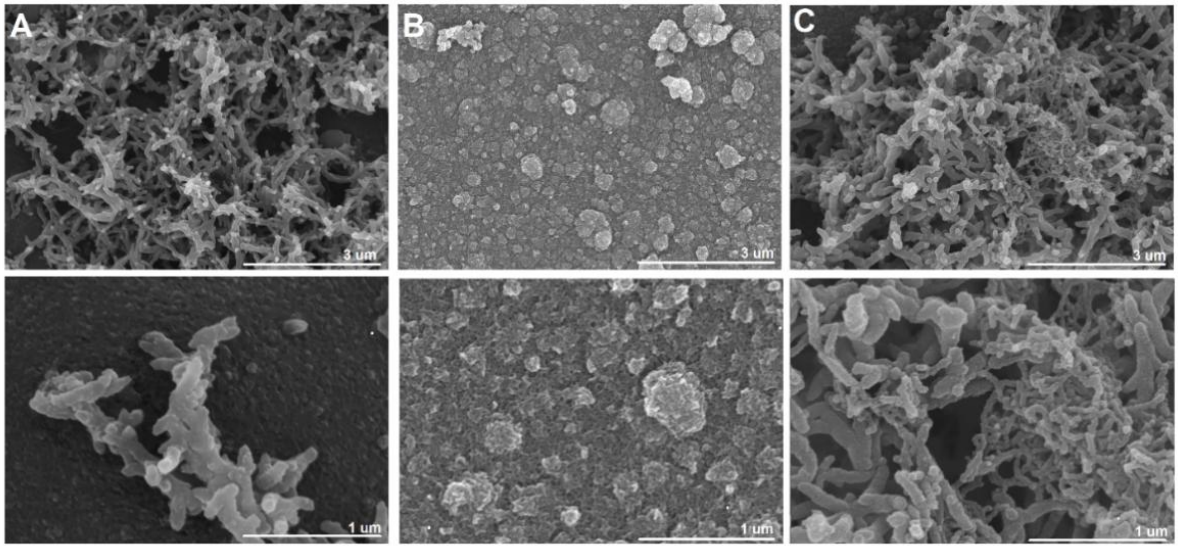


Figure 26. SEM micrographs acquired at 10 kV of PANI (A), PEDOT (B), and PANI–PEDOT (C). The upper row shows images at a scale bar of 3 μm, while the lower row presents higher-magnification images with a 1 μm scale bar. Reprinted with permission from [95].

EDS measurements confirmed the coexistence of nitrogen and sulfur on the PANI–PEDOT surface (**Figure 27**); however, the technique does not allow a definitive assessment of coating uniformity. Based on the observed morphological changes, PEDOT is presumed to form a layer over the PANI fibrils, leading to an increase in the mean fibril diameter to 126 ± 33 nm. Such a hierarchical, mesh-like structure is expected to facilitate neurite penetration and interconnection within the polymer network, as previously demonstrated for similar systems [148].

Given that effective electrode–tissue integration is critical for neural interface performance, the fibrillar architecture of the PANI–PEDOT coating is anticipated to enhance charge transfer at the biointerface and improve both stimulation and recording efficiency. Moreover, the observed morphology is likely to contribute to the electrochemical behavior of the material. As reported by Aurian-Blajeni et al. [260], CSC is strongly influenced by surface morphology, with increased effective surface area enhancing electrolyte contact and promoting more efficient charge transfer processes. Consistent with this mechanism, the PANI–PEDOT coatings exhibited higher CSC values compared with PANI alone, confirming the beneficial impact of the hybrid fibrillar structure on electrochemical performance.

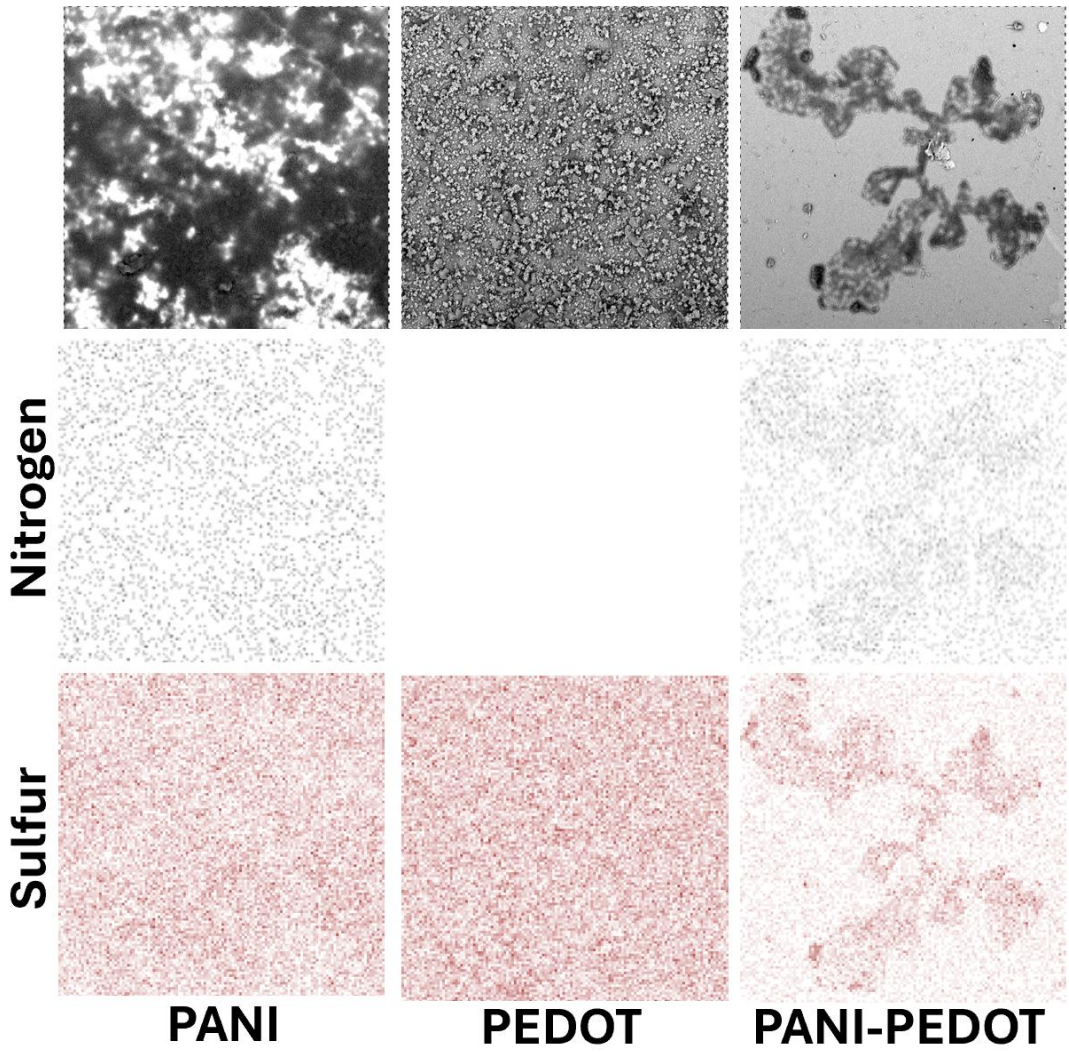


Figure 27. SEM micrographs and corresponding EDS elemental mapping of sulfur (S) and nitrogen (N) on PANI, PEDOT, and PANI–PEDOT surfaces. Reprinted with permission from [95].

Raman spectroscopy was used to analyze the chemical composition, and functional groups present on the modified electrode surfaces [261]. Unlike infrared spectroscopy, Raman measurements do not require sample drying, enabling direct investigation of surface chemistry while preserving the native three-dimensional morphology of the coatings.

The Raman spectrum of PANI-modified electrodes (**Figure 28A**) displays characteristic bands associated with emeraldine base and other oxidation states of polyaniline, in agreement with previously reported data [262]. A prominent peak at 1592 cm^{-1} is assigned to C=C stretching vibrations in quinonoid ring structures. In addition, the band observed at 1234 cm^{-1} corresponds to C–N stretching in semiquinoid and quinonoid units [263]. The signal at 1510 cm^{-1} is attributed to N–H deformation modes, while weaker features around 1375 cm^{-1} are related to C–N stretching vibrations in amine groups [264] [265]. A distinct band at 1178 cm^{-1} is associated with in-plane C–H deformation of the quinonoid structure [263] [108]. The spectral region between 400 and 1000 cm^{-1} provides further information on benzene ring deformations, including both in-plane and out-of-plane vibrational modes. Specifically, peaks at 810, 518, and 424 cm^{-1} are linked to vibrational modes of the protonated emeraldine form of PANI [266].

The Raman spectrum of PEDOT-modified electrodes (**Figure 28A**) is characterized by a strong band at 1430 cm^{-1}, attributed to symmetric stretching of the Cα=Cβ bond within the thiophene ring. This vibration is highly sensitive to conformational changes and doping level and is typically enhanced in oxidized PEDOT structures [267]. Additional bands at 1364 cm^{-1} and 1096 cm^{-1} correspond to Cβ–Cβ stretching and C–O–C deformation, respectively. The peaks at 1244 cm^{-1} and 990 cm^{-1} are assigned to inter-ring Cα–Cα stretching and oxyethylene ring deformation. Further features at 856 cm^{-1} and 700 cm^{-1} are attributed to C–H bending and symmetric C–S–C deformation, while signals at 580 cm^{-1} and 442 cm^{-1} correspond to additional oxyethylene and C–O–C vibrational modes [268]. Weak bands observed around 1520–1525 cm^{-1} are associated with asymmetric C–C stretching within the thiophene backbone [269] Collectively, these peaks confirm successful electropolymerization of PEDOT on the Pt electrode surface.

The Raman spectrum of the PANI–PEDOT hybrid coating largely resembles that of PEDOT, consistent with the deposition of PEDOT onto a pre-existing PANI layer. The main evidence of PANI contribution is limited to two characteristic bands at 1178 cm^{-1} and 1234 cm^{-1}, corresponding to C–H in-plane deformation of quinonoid structures and C–N stretching in semiquinoid/quinonoid units, respectively. Although SEM analysis suggests a fibrillar PANI

framework decorated with PEDOT structures, Raman results indicate that the PEDOT overlayer is sufficiently continuous and thick to dominate the surface spectral response. This suggests that the final hybrid architecture consists of a PANI fibrillar scaffold coated by a largely continuous PEDOT layer, which governs the overall surface chemistry detected by Raman spectroscopy.

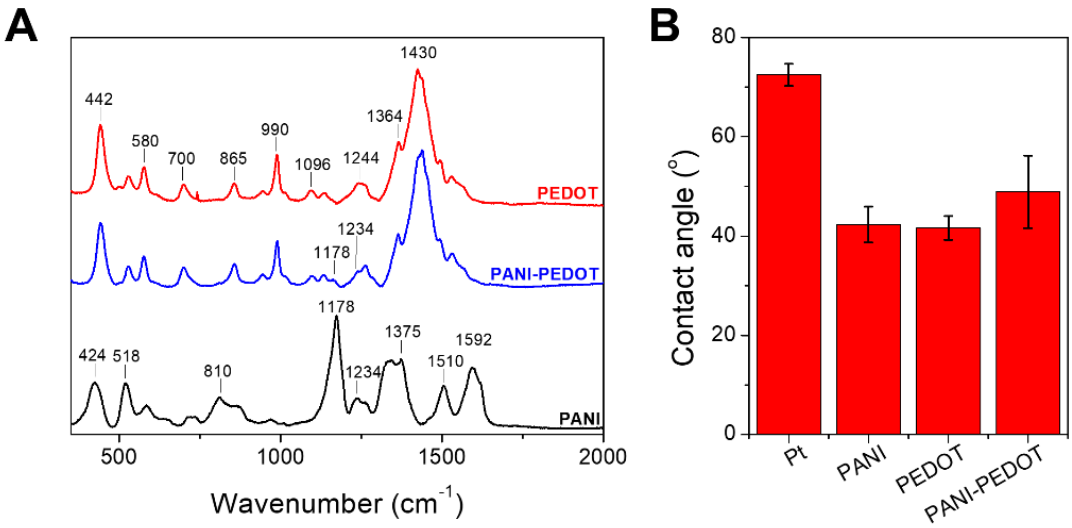


Figure 28. Structural and surface wettability characterization of electropolymerized thin films of PANI, PEDOT, and PANI–PEDOT. Raman spectra are shown in (A), while corresponding water contact angle measurements are presented in (B). Reprinted with permission from [95].

Surface wettability is another key parameter influencing cell–material interactions, as it is primarily governed by the chemical composition of the surface, the presence of functional groups, and its morphological features [268]. In the present study, all modified electrodes exhibited increased hydrophilicity compared with the unmodified Pt control (72.47 ± 2.2°), with relatively similar water contact angles measured for PEDOT (41.6 ± 2.4°), PANI (42.3 ± 3.6°), and PANI–PEDOT (48.9 ± 7.3°). This increased wettability can be attributed to the presence of hydrophilic amine functionalities within the PANI structure [270] [271], as well as the incorporation of sulfate (SO_4^{2-}) dopant ions in both PANI and PEDOT systems (**Figure 28B**) [268, 272]. It is well established that neither highly hydrophilic nor strongly hydrophobic surfaces are optimal for cell adhesion [271]. Instead, intermediate wettability has been reported to be most favorable for the adsorption and conformational stability of adhesion proteins, with an optimal water contact angle of approximately ~65° often cited in the literature [273] . In this

context, the PANI–PEDOT coating, with a contact angle of 48.9 ± 7.3°, presents a moderately hydrophilic surface that is expected to support favorable cell–surface interactions, particularly when compared with the more hydrophobic bare Pt electrode. Consequently, this level of wettability is considered suitable for promoting cell adhesion and enhancing overall electrode–tissue integration.

3.3.5. Biological Characterization

To evaluate the biocompatibility of the CP coatings, a mixed co-culture derived from ventral mesencephalon tissue of E14 rat embryos was cultured on both experimental and control electrodes for 3, 7, and 14 days. Representative fluorescence micrographs (**Figure 29A**) show neurons (red), astrocytes (green), and cell nuclei (blue). Although both cell types contribute to neural tissue function, astrocytes play a supportive role by maintaining neuronal homeostasis and facilitating neuronal survival through the secretion of growth factors and regulation of the extracellular environment [274]. At the same time, astrocytes are also implicated in glial scar formation during the foreign body response, which can ultimately hinder electrode performance by electrically isolating the implant surface and reducing signal quality *in vivo* [9]. Across all tested conditions, the investigated materials supported the adhesion of both neurons and astrocytes, as well as neurite extension and the formation of interconnected neural networks, indicating effective cytocompatibility and surface bioactivity.

An increase in the complexity and density of neural networks was observed with prolonged culture time, particularly after 14 days. **Figure 29B** presents the ratio of neurons to astrocytes over time. Initially, all substrates (Pt, PANI, and PANI–PEDOT) supported a predominantly neuronal population (~90%), with slightly lower neuronal proportions observed on PEDOT-modified surfaces (79 ± 3%). After 14 days, the neuron-to-astrocyte ratio shifted toward an approximate 70:30 balance, commonly considered a physiologically relevant "healthy" distribution [101], with a slight neuronal predominance maintained on PANI surfaces (81 ± 2%).

Neurite outgrowth was further quantified as an indicator of neuronal integration (**Figure 29C**). A progressive increase in neurite length was observed across all substrates at 3, 7, and 14 days of culture. However, at day 7, neurite extension on PEDOT and PANI–PEDOT surfaces was lower than that observed on Pt control samples. By day 14, however, neurons cultured on

PANI–PEDOT exhibited the greatest average neurite length (296 ± 7 µm), exceeding values measured on Pt (196 ± 8 µm), PEDOT (145 ± 6 µm), and PANI (206 ± 6 µm) substrates.

Neuronal outgrowth and regeneration are governed by a complex interplay of biochemical, physicochemical, and temporal factors. Surface chemistry (including functional groups, surface charge, and wettability) as well as topographical features strongly influence early cell adhesion and neurite extension [275] [276]. In addition, time-dependent cellular adaptation processes also play a crucial role in network maturation. In this study, the fibrillar morphology of PANI provided topographical guidance that enhanced early-stage cell adhesion and neurite extension compared with Pt controls. However, this effect appeared to be transient, as neurite lengths on PANI and Pt became comparable after 14 days. In contrast, although PEDOT and PANI–PEDOT surfaces initially supported less pronounced neurite extension—potentially due to reduced early protein adsorption during initial adhesion stages [277]—they demonstrated a stronger influence on long-term neural network development, particularly at later culture time points.

Overall, the PANI–PEDOT coating appears to combine the advantageous features of both materials, integrating the early-stage topographical benefits of PANI with the longer-term network-supporting effects associated with PEDOT. This synergistic behavior suggests improved suitability of the hybrid coating as a stable neural interface platform capable of supporting sustained neurite growth and functional network formation. However, a more detailed biochemical investigation would be required to fully elucidate the mechanisms underlying these time-dependent cellular responses on different substrates.

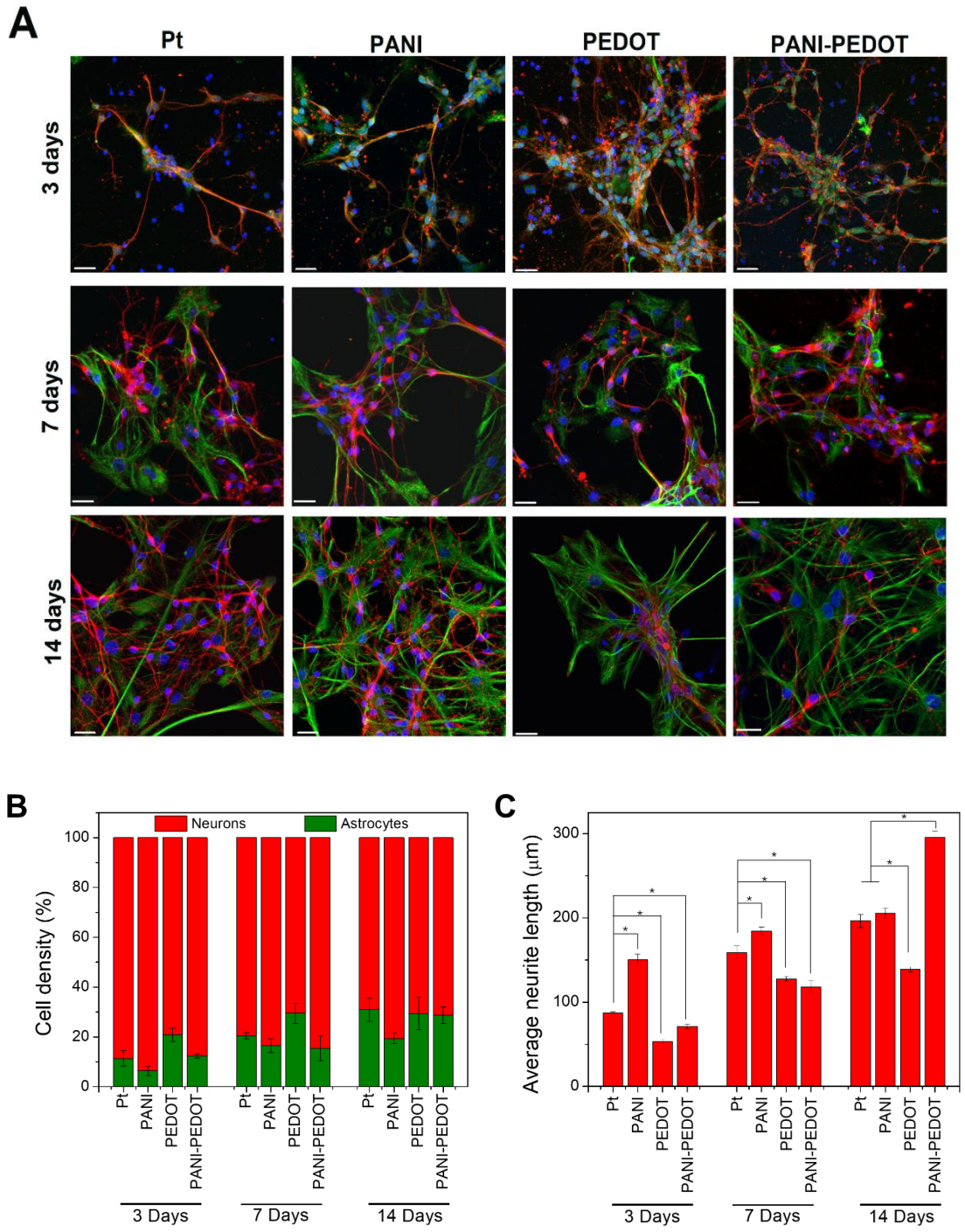


Figure 29. Fluorescence microscopy images of primary ventral mesencephalic (VM) mixed cell cultures on bare Pt and PANI-, PEDOT-, and PANI–PEDOT-coated electrodes at 3, 7, and 14 days *in vitro*. Neurons were labeled with anti-β-tubulin III (red), astrocytes with anti-GFAP (green), and nuclei with DAPI (blue); scale bar = 20 µm (A). Quantification of cell density (%) showing neuronal and astrocytic populations at each time point (B). Analysis of neurite length on Pt and polymer-coated electrodes (C), with statistical significance indicated as *$p < 0.05$. Reprinted with permission from [95].

Cell adhesion can be indirectly evaluated by analyzing the formation of FAs, which are dynamic multiprotein complexes that mechanically link the intracellular actin cytoskeleton to the extracellular matrix. **Figure 30A** presents fluorescence micrographs of a mixed VM co-culture grown on Pt control and PANI-, PEDOT-, and PANI–PEDOT-modified electrodes for up to 14 days, with cells immunostained for the focal adhesion protein paxillin. Punctate paxillin-positive structures were subsequently quantified after 14 days of culture (**Figure 30B**). Cells cultured on PANI–PEDOT surfaces exhibited a significantly higher number of FAs per cell (47 ± 7) compared with those grown on Pt controls (25 ± 3), as well as on PEDOT (35 ± 5) and PANI (23 ± 4) substrates. In addition to FA numbers, differences in FA morphology were also observed. On PANI–PEDOT coatings, both small nascent focal complexes (length < 1 μm) and more mature, elongated focal adhesions (length > 1 μm) were present, indicating a broader spectrum of adhesion maturation stages and more dynamic cell–substrate interactions.

Cell adhesion is primarily regulated by integrin-mediated signaling pathways, which govern the assembly and maturation of FAs through key adaptor proteins such as FAK and paxillin. These signaling cascades play an essential role in controlling cell spreading, morphology, and migration behavior [191]. Previous studies have shown that enhanced cell proliferation and growth are often correlated with increased substrate adhesiveness and stronger focal adhesion formation [278] [279]. In the present work, PANI alone produced a less pronounced effect on FA formation compared with PEDOT, suggesting that PEDOT plays a dominant role in promoting adhesion-related signaling within the hybrid system. However, the presence of fibrillar PANI contributes an important topographical component by increasing surface roughness and providing additional anchoring sites. As a result, the PANI–PEDOT coating benefits from a synergistic combination of surface chemistry PEDOT and fibrillar morphology (PANI), leading to enhanced focal adhesion formation.

This increase in focal adhesions is consistent with the observed enhancement in neurite outgrowth on PANI–PEDOT surfaces, suggesting a direct relationship between adhesion strength and neuronal extension. Overall, the results indicate that the high cellular adhesiveness of the PANI–PEDOT coating arises from the combined effects of its fibrillar architecture, electroactive surface chemistry, and favorable electrochemical properties, all of which contribute to improved cell–material interactions.

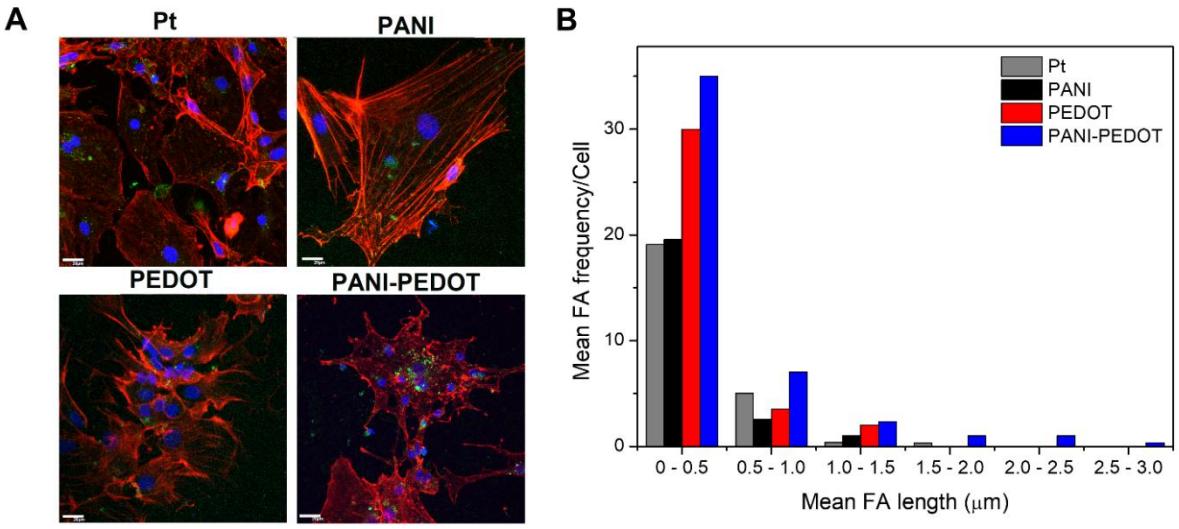


Figure 30. Immunofluorescence analysis of VM mixed cell cultures on bare Pt and PANI-, PEDOT-, and PANI–PEDOT-modified electrodes after 14 days in culture. F-actin (red), paxillin-positive focal adhesions (green), and nuclei (DAPI, blue) are shown; scale bar = 20 μm (A). (B) Distribution of focal adhesion contact numbers per astrocyte across the different substrates. Reprinted with permission from [95].

3.3.6. Perspectives and limitations

A key objective in neuroelectrode surface engineering is to preserve the electrical performance of the electrode while simultaneously enhancing its interaction with neural tissue. The developed electroactive coating is primarily intended for use as surface modifications of implantable neural electrodes employed in neuromodulation therapies. The growing prevalence of neurological disorders, driven in part by an aging population, has increased the demand for effective treatments for conditions such as Parkinson's disease, epilepsy, chronic pain, depression, and Alzheimer's disease. Electrical stimulation has become an established therapeutic approach for many of these disorders, relying on implantable electrodes to deliver controlled electrical pulses that modulate neural activity. The long-term success of these devices depends on the formation of a stable and functional interface between the electrode and the surrounding neural tissue. However, conventional metallic electrodes often exhibit limited electrochemical performance and inadequate tissue integration, which can compromise stimulation efficiency and recording quality [95].

Surface modification with nanostructured conductive polymer coatings offers a promising strategy to overcome these limitations. Such coatings increase the electrochemically active

surface area, reduce electrode impedance, enhance charge transfer and charge injection capacity, and improve signal quality during neural recording and stimulation. Furthermore, their physicochemical properties can promote neural cell adhesion and neurite outgrowth, contributing to a more stable electrode–tissue interface and reducing the foreign body response. Consequently, these coatings have the potential to improve the long-term performance, sensitivity, and reliability of implantable neural interfaces for both therapeutic stimulation and neural signal recording. Despite these promising findings, further preclinical evaluation is warranted to establish the mechanical robustness, structural stability, and long-term performance of the developed scaffolds. *In vivo* studies should subsequently be conducted to determine their biological safety and regenerative potential and to establish whether their use can promote meaningful functional recovery following spinal cord injury.

3.3.7. Conclusion

In this part of my studies, electrodes co-functionalized with a hybrid PANI-PEDOT coating were investigated for the first time as a strategy for neuroelectrode modification. Their electrochemical characteristics, surface morphology, and biocompatibility were comprehensively evaluated. The incorporation of the PANI-PEDOT coating resulted in a marked decrease in electrode impedance and a substantial increase in charge storage capacity, while maintaining electrochemical stability under physiological conditions. Biological performance was further examined using primary mixed neural cell cultures, with assessments focusing on cell proliferation, neurite outgrowth, and focal adhesion development. The results demonstrated that the hybrid conducting polymer coating supported favorable cellular responses and neural integration *in vitro*. Overall, the PANI-PEDOT films developed in this work establish a valuable foundation for future investigations into dual conducting polymer systems as functional coatings for neuroelectrodes, highlighting their potential to improve both electrochemical performance and biological compatibility.

3.4. Modification of nonconductive polymers using conducting polymers

3.4.1. Aims and objectives

The primary aim of this study was to elucidate how physicochemical surface properties, including porosity, surface chemistry, and electrostatic characteristics, regulate cell adhesion, spreading, proliferation, and surface coverage. To investigate these relationships, PPy-modified PCL fibrous scaffolds were fabricated via *in situ* pyrrole polymerization prior to electrospinning and employed as a model platform to establish structure–property–cell response relationships (**Figure 31**).

The specific objectives of this study were as follows:

1- To develop a simple and reproducible method for fabricating PPy-modified PCL fibrous scaffolds via in situ pyrrole polymerization followed by electrospinning.

2- To characterize the physicochemical properties of PPy-modified PCL fibers, including surface morphology, porosity, wettability, and surface charge.

3- To investigate the effect of PPy incorporation on cell–material interactions, with a focus on cell adhesion, spreading, proliferation, and surface coverage.

4- To assess the biological response of different human cell lines (SH-SY5Y neuroblastoma cells, NHDF fibroblasts, and U87 glioblastoma cells) cultured on the developed scaffolds.

5- To evaluate focal adhesion formation and cellular morphology as indicators of cell attachment strength and cytocompatibility.

6- To determine the suitability of PPy-modified PCL fibers as bioactive scaffolds for potential applications in neural tissue engineering and spinal cord injury repair.

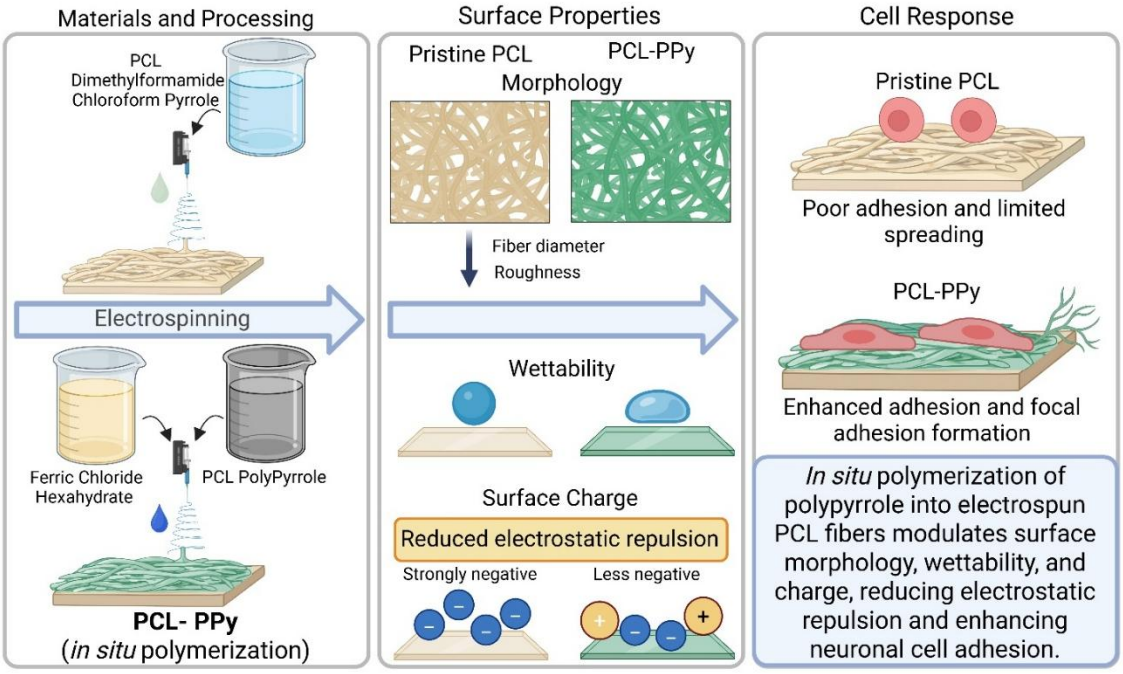


Figure 31. Schematic illustration of the study process for modification of the nonconductive PCL fiber using in-situ polymerization of the pyrrole.

3.4.2. Fabrication of fibers

PCL/PPy nanofibrous scaffolds were fabricated by combining in situ oxidative polymerization with electrospinning. Initially, a 10 wt% PCL solution was prepared by dissolving the polymer in a chloroform/DMF (9:1, v/v) solvent mixture under continuous stirring until complete dissolution was achieved. Pyrrole monomer was then introduced into the polymer solution at predetermined concentrations, followed by the addition of ferric chloride hexahydrate ($FeCl_3 \cdot 6H_2O$) as an oxidizing agent to initiate the oxidative polymerization of pyrrole within the polymer matrix. The reaction mixture was stirred continuously until a homogeneous dispersion was obtained, and the appearance of a characteristic dark coloration indicated successful formation of polypyrrole. Subsequently, the electroactive suspensions were processed by electrospinning under optimized conditions to produce uniform nanofibrous scaffolds. A detailed description of the solution composition, polymerization procedure, and electrospinning parameters is provided in the Methods section.

3.4.3. Morphology of fibers

Figure 32 presents SEM micrographs (**Figure 32A–C**) together with corresponding fiber diameter distributions (**Figure 32D**–**F**) for pristine PCL, PCL-1PPy, and PCL-3PPy samples. The pristine PCL fibers (**Figure 32A**) exhibited a uniform and well-defined morphology without bead formation. In contrast, both PPy-modified samples (**Figure 32B–C**) showed occasional bead-like defects embedded within the fibrous structure. Quantitative analysis revealed that pristine PCL fibers (**Figure 32D**) possessed relatively broad diameter variability, ranging from 1.04 μm to 2.14 μm, with an average diameter of 1.68 ± 0.14 μm. Following in situ pyrrole polymerization and incorporation into the electrospinning solution, a marked reduction in fiber diameter was observed. The average fiber size decreased to 618.36 ± 14.24 nm for PCL-1PPy (**Figure 32E**) and further to 396.16 ± 10.28 nm for PCL-3PPy (**Figure 32F**). In addition, PPy-containing samples exhibited a narrower diameter distribution compared with pristine PCL, with ranges of 0.29–0.94 μm and 0.26–0.63 μm for PCL-1PPy and PCL-3PPy, respectively.

The observed reduction in fiber diameter is most likely related to changes in the electrical conductivity of the spinning solution upon addition of PPy. During electrospinning, fiber formation is governed by electrostatic forces acting on the polymer jet, where surface charge induces stretching and elongation of the solution stream [130]. The process is strongly influenced by bending instabilities, which arise from the balance between Coulombic repulsion forces and the external electric field, both of which depend on surface charge density [280]. Since solution conductivity directly affects charge density, variations in conductivity can be used to tune fiber morphology. In general, higher conductivity leads to increased jet elongation due to enhanced charge repulsion, which in turn produces thinner fibers. Accordingly, increased solution conductivity resulting from the addition and in situ polymerization of pyrrole led to the formation of significantly finer fibers in PPy-modified PCL systems [127] [281].

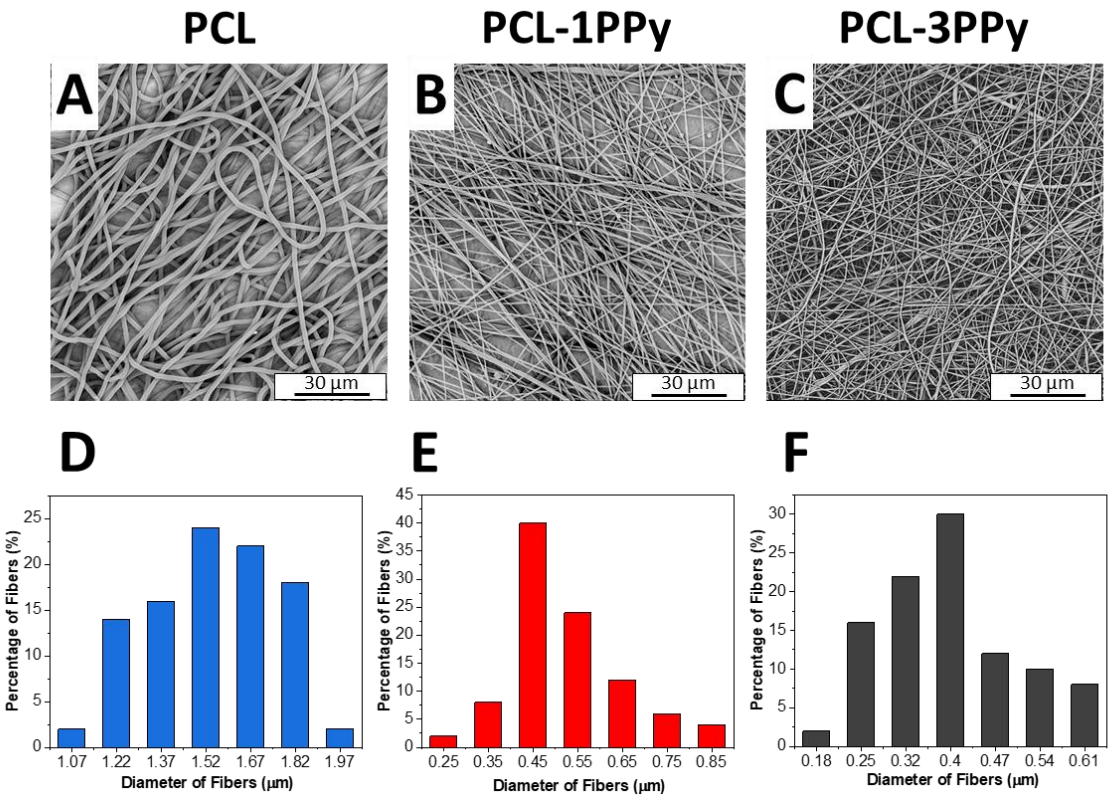


Figure 32. Representative scanning electron microscopy (SEM) images of polymeric fibers composed of pristine PCL, PCL-1PPy, and PCL-3PPy (A–C), along with the corresponding fiber diameter distribution histograms (n = 50) for each sample (D–F).

The fiber fraction, mass per unit area (mg/cm²), porosity percentage, and mean pore area for all samples are summarized in **Table 2**. The porosity of pristine PCL electrospun mats was measured at 89.54 ± 0.03%, and it increased significantly to 98.39 ± 0.01% for PCL-1PPy and 99.14 ± 0.01% for PCL-3PPy following PPy incorporation. This increase is consistent with the reduction in fiber diameter observed in PPy-modified samples, which is known to influence overall scaffold porosity [130].

A similar trend was observed for mass per unit area. Pristine PCL exhibited a value of 4.28 ± 1.43 mg/cm², whereas incorporation of PPy led to a substantial decrease to 0.53 ± 0.26 mg/cm² for PCL-1PPy and 0.37 ± 0.01 mg/cm² for PCL-3PPy. Despite comparable macroscopic surface areas, the reduction in fiber diameter results in lighter scaffolds, which correlates well with the observed increase in porosity. Previous studies by Soliman et al. [282] demonstrated that decreasing PCL fiber diameter leads to higher scaffold porosity and improved cell–material interactions. Using HUVEC cells, they showed that scaffolds with lower fiber density

supported enhanced cell proliferation and infiltration compared with denser structures. In highly porous scaffolds, increased interconnectivity facilitates cell migration throughout the 3D matrix, enabling uniform colonization and multilayer formation. In contrast, densely packed fibers restrict pore accessibility, limiting cell penetration and confining growth mainly to the surface. Once surface saturation occurs, further inward migration is hindered [282]. Since anchorage-dependent cells require suitable attachment sites, scaffolds with higher accessible surface area generally promote better adhesion, proliferation, and overall cellular density [283].

SEM-based analysis also indicated changes in fiber fraction with increasing PPy content. Pristine PCL showed a fiber fraction of 0.42 ± 0.03, with low variability indicating a uniform fiber distribution. A slight increase was observed for PCL-1PPy (0.44 ± 0.11), although the higher standard deviation suggests more heterogeneous fiber coverage, likely resulting from PPy influencing fiber formation and deposition. The highest fiber fraction was recorded for PCL-3PPy (0.48 ± 0.01), accompanied by the lowest variability, indicating a more consistent and homogeneous fibrous network. These findings suggest that PPy incorporation contributes to a more uniform scaffold architecture, which may be beneficial for cell attachment and growth.

In parallel, pore size analysis revealed a progressive decrease with increasing PPy content. Pristine PCL exhibited a mean pore area of 16.56 ± 9.31 µm², which decreased to 9.37 ± 3.64 µm² for PCL-1PPy and further to 3.49 ± 0.44 µm² for PCL-3PPy. This trend confirms that reductions in fiber diameter are directly associated with smaller pore formation within the scaffold structure [284].

Table 2. Overview of the physicochemical properties of electrospun fibers (n = 3).

Sample	Porosity (%)	Mass per unit area (mg/cm^2)	Fiber Fraction	Average Pore Size (µm^2)
PCL	89.54 ± 0.03	4.28 ± 1.43	0.42 ± 0.03	16.56 ± 9.31
PCL-1PPy	98.39 ± 0.01	0.53 ± 0.26	0.44 ± 0.11	9.37 ± 3.64
PCL-3PPy	99.14 ± 0.01	0.37 ± 0.01	0.48 ± 0.01	3.49 ± 0.44

3.4.4. Physicochemical characterization

Digital images (**Figure 7**) of the polymer solutions showed that the initially transparent PCL solution gradually changed to a greenish-black color after 48 hours. This pronounced color change in the PCL/PPy system is indicative of successful in situ oxidative polymerization of pyrrole within the polymer solution. The formation of a conducting polymer phase is further supported by FTIR spectroscopy results. As shown in **Figure 33A**, FTIR spectra were recorded for PPy, PCL, PCL-1PPy, and PCL-3PPy samples. All PCL-based spectra (PCL, PCL-1PPy, and PCL-3PPy) exhibited characteristic vibrational bands of polycaprolactone, including the carbonyl (C=O) stretching peak at 1720 cm^{-1}, asymmetric CH_2 stretching at 2946 cm^{-1}, symmetric CH_2 stretching at 2864 cm^{-1}, asymmetric C–O and C–C stretching at 1294 cm^{-1}, and asymmetric C–O–C stretching at 1243 cm^{-1} [173]. In the spectrum of pristine PPy, N–H stretching and bending vibrations were identified at 3290 cm^{-1} and 598 cm^{-1}, respectively [285]. Bands appearing in the 1300–1440 cm^{-1} region correspond to in-plane deformation modes of C–H and C–N bonds [286]. The peak at 1656 cm^{-1} is associated with carbonyl formation, which is likely due to nucleophilic attack by water during synthesis [287]. Additional bands at 1098 cm^{-1} and 734 cm^{-1} are attributed to N–H bending vibrations and out-of-plane C–H deformation modes, respectively [288] [289]. In the FTIR spectrum of PCL-3PPy (**Figure 33A'**), a distinct band at 1594 cm^{-1} is observed, which can be assigned to C–N and/or C=O-related vibrations associated with PPy [173]. Overall, samples containing PPy exhibit reduced peak intensities compared with pristine PCL [290]. Importantly, the characteristic FTIR features of PCL are retained after modification, while the emergence of PPy-related bands—particularly in PCL-3PPy—confirms the successful incorporation of polypyrrole into the electrospun fiber structure.

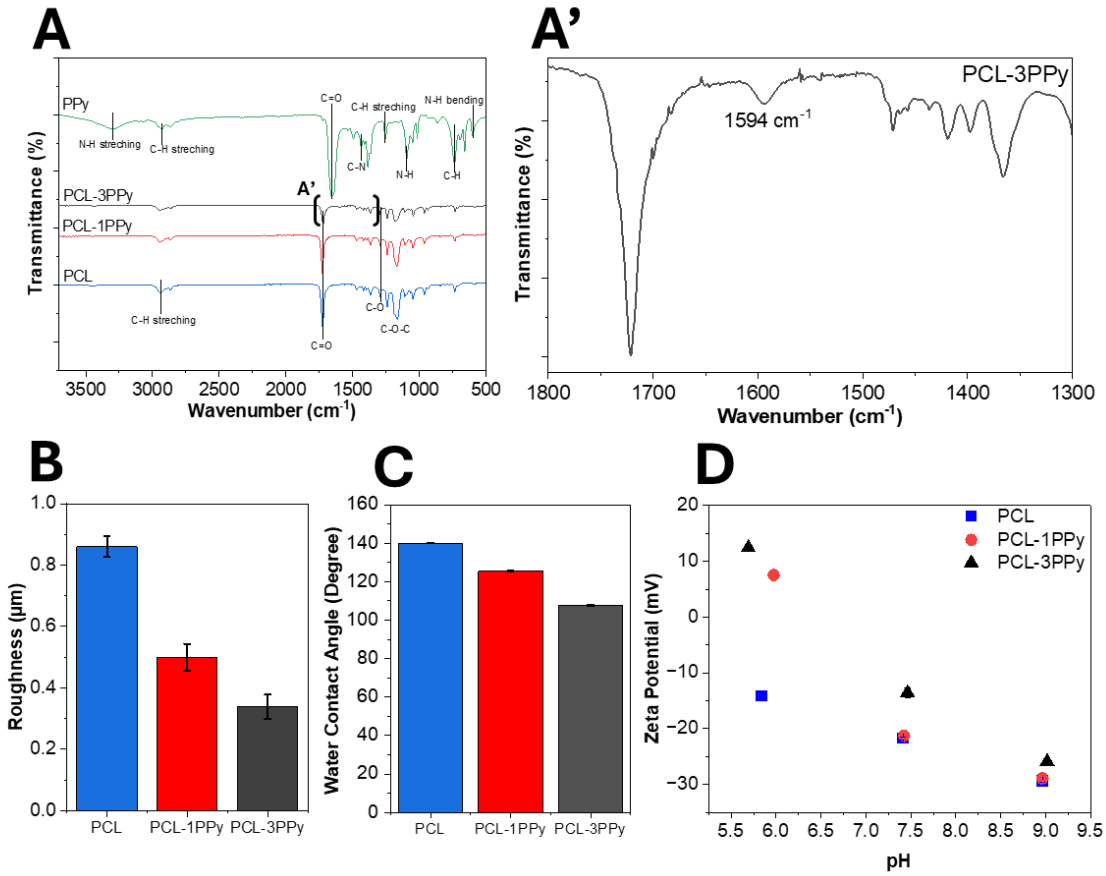


Figure 33. (A) FTIR spectra of PPy, PCL, PCL-1PPy, and PCL-3PPy, with characteristic N–H, C–H, C=O, C–N, and C–O–C vibrational bands indicated; magnified spectral regions for PCL-3PPy are shown in (A'). (B) Surface roughness (µm). (C) Static water contact angle (°). (D) Zeta potential (mV) as a function of pH.

The surface properties of the fibers were evaluated in terms of roughness and wettability. The average roughness (Ra) of pristine PCL fibers was measured at 0.860 ± 0.034 µm, and it progressively decreased to 0.499 ± 0.044 µm for PCL-1PPy and 0.338 ± 0.041 µm for PCL-3PPy (**Figure 33B**). This reduction in surface roughness can be associated with changes in fiber diameter, as larger fibers generally contribute to increased surface irregularities [291]. Water contact angle (WCA) measurements (**Figure 33C**) showed that pristine PCL exhibited a highly hydrophobic surface (140.1 ± 0.2°). After incorporation of PPy, the WCA decreased to 125.5 ± 0.1° for PCL-1PPy and further to 107.7 ± 0.4° for PCL-3PPy. This improvement in wettability is attributed to the inherently more hydrophilic nature of polypyrrole [292], which contains polar functional groups capable of hydrogen bonding with water molecules. Similar behavior has been previously reported by Sun et al. [289], where PPy incorporation enhanced

the hydrophilicity of poly (L-lactic acid-co-ε-caprolactone)/silk fibroin nanofibrous membranes.

It is also important to note that surface roughness and wettability are closely interrelated in electrospun fiber systems. The topographical features arising from randomly oriented fibers can influence apparent wettability, even in the absence of chemical modifications [293]. In such systems, wettability is governed not only by surface chemistry but also by the fraction of fiber area in contact with the liquid phase. The air pockets trapped between fibers contribute to wetting behavior consistent with the Cassie–Baxter regime [293]. Consequently, variations in fiber diameter affect fiber packing density, where smaller fibers increase fiber fraction at the surface and can lead to reduced water contact angles.

Zeta potential analysis (**Figure 33D**) further demonstrated a clear pH-dependent surface charge behavior for all samples. Pristine PCL exhibited consistently negative surface charge across the tested pH range, reflecting its chemically inert and hydrophobic nature. It has been previously reported that the isoelectric point (IEP) is strongly dependent on surface chemistry; acidic functional groups shift the IEP toward lower pH values, whereas basic groups shift it toward higher pH values [294]. The addition of PPy, particularly at higher content (PCL-3PPy), resulted in a noticeable shift toward less negative and even positive zeta potential values under acidic conditions. At pH ~6.0, PCL-3PPy exhibited a zeta potential of +12.41 ± 0.44 mV, while PCL-1PPy reached +7.53 ± 0.67 mV, both significantly higher than pristine PCL (-14.18 ± 0.09 mV). This behavior is attributed to the protonation of nitrogen atoms within the pyrrole ring, which become positively charged in acidic environments [295]. At physiological pH (7.4), all samples became more negatively charged due to deprotonation; however, PCL-3PPy retained a significantly less negative value (-13.57 ± 0.81 mV) compared with PCL (-21.80 ± 0.32 mV) and PCL-1PPy (-21.28 ± 0.63 mV). A similar trend was also observed under alkaline conditions (pH 9.0), where PCL-3PPy (-25.91 ± 0.50 mV) remained less negative than pristine PCL (-29.39 ± 0.18 mV). Overall, these findings indicate that PPy incorporation effectively modulates surface electrochemical properties and provides a tunable interface for controlling cell–material interactions. Since mammalian cell membranes are typically negatively charged, surface charge plays a crucial role in governing adhesion and spreading [296, 297]. In this context, the reduced negative charge of PCL-3PPy at physiological pH is expected to decrease electrostatic repulsion, thereby promoting initial cell attachment and supporting subsequent cellular processes. Cell adhesion generally occurs through sequential stages, including initial contact, spreading, and focal adhesion formation at the interface. Early-stage adhesion is

strongly influenced by electrostatic interactions, which facilitate surface binding and the initiation of focal adhesion assembly [6].

3.4.5. Cell viability and morphology

To investigate the influence of PPy incorporation into PCL fibers on cellular behavior, SH-SY5Y, NHDF, and U87 cells were cultured on electrospun scaffolds and evaluated with respect to morphology and surface coverage. The SH-SY5Y cell line, derived from human neuroblastoma, is widely used as an *in vitro* model for neuronal-like cells [298] [299]. These cells typically exhibit a neuroblast-like, non-polarized morphology [300], tending to form aggregates or clusters, while extending thin neurite-like processes into the surrounding environment. In densely populated areas, multilayered growth and partial stacking of cells can also be observed [298]. It has been demonstrated that surface charge strongly influences SH-SY5Y adhesion, proliferation, and differentiation, making it a key parameter for tuning their biological response [301].

Similarly, surface roughness modulates cell adhesion by altering the effective cell–substrate contact area, thereby influencing interfacial adhesion forces [302]. SEM images (**Figure 34A–C and 34A'–C'**) illustrate the morphology of SH-SY5Y cells at low and high magnification. The micrographs confirm morphological features consistent with the known phenotype of this cell line [299]. On pristine PCL fibers, cells predominantly retained a rounded morphology with limited spreading. In contrast, PPy-modified samples induced a more elongated morphology, with neurite-like extensions suggestive of early neuronal differentiation [303]. On PPy-containing scaffolds, cells were also observed to infiltrate the fibrous network and bridge across pore structures (**Figure 34B', C'**, red arrows), indicating improved three-dimensional interaction with the substrate. Quantitative analysis further demonstrated enhanced spreading on PCL-3PPy scaffolds (**Figure 34D**), where cells covered a significantly larger area (6126 ± 4907 μm²) compared with pristine PCL (944 ± 480 μm²), while PCL-1PPy showed a comparable value (879 ± 682 μm²).

In addition to morphological changes, PPy incorporation also influenced overall biocompatibility (**Figure 34E**). All tested materials supported acceptable cell viability above 70% [304]. Pristine PCL exhibited a viability of 84.2 ± 7.7%, while PPy-modified scaffolds showed values of 87.1 ± 6.6% for PCL-1PPy and 77.6 ± 8.6% for PCL-3PPy. However, these differences were not statistically significant. Although PPy is generally considered

biocompatible and has been widely reported in biomedical applications [305] [306], some studies have also described concentration-dependent cytotoxic effects [307] [308]. This potential toxicity has been associated with pyrrole and its derivatives, which may form reactive pyrrolic metabolites in biological systems [309]. These metabolites can interact covalently with cellular macromolecules, including proteins and DNA, thereby disrupting normal cellular functions. Additionally, they may induce oxidative stress and deplete intracellular antioxidant defenses, ultimately contributing to cellular damage and reduced viability [309] [310].

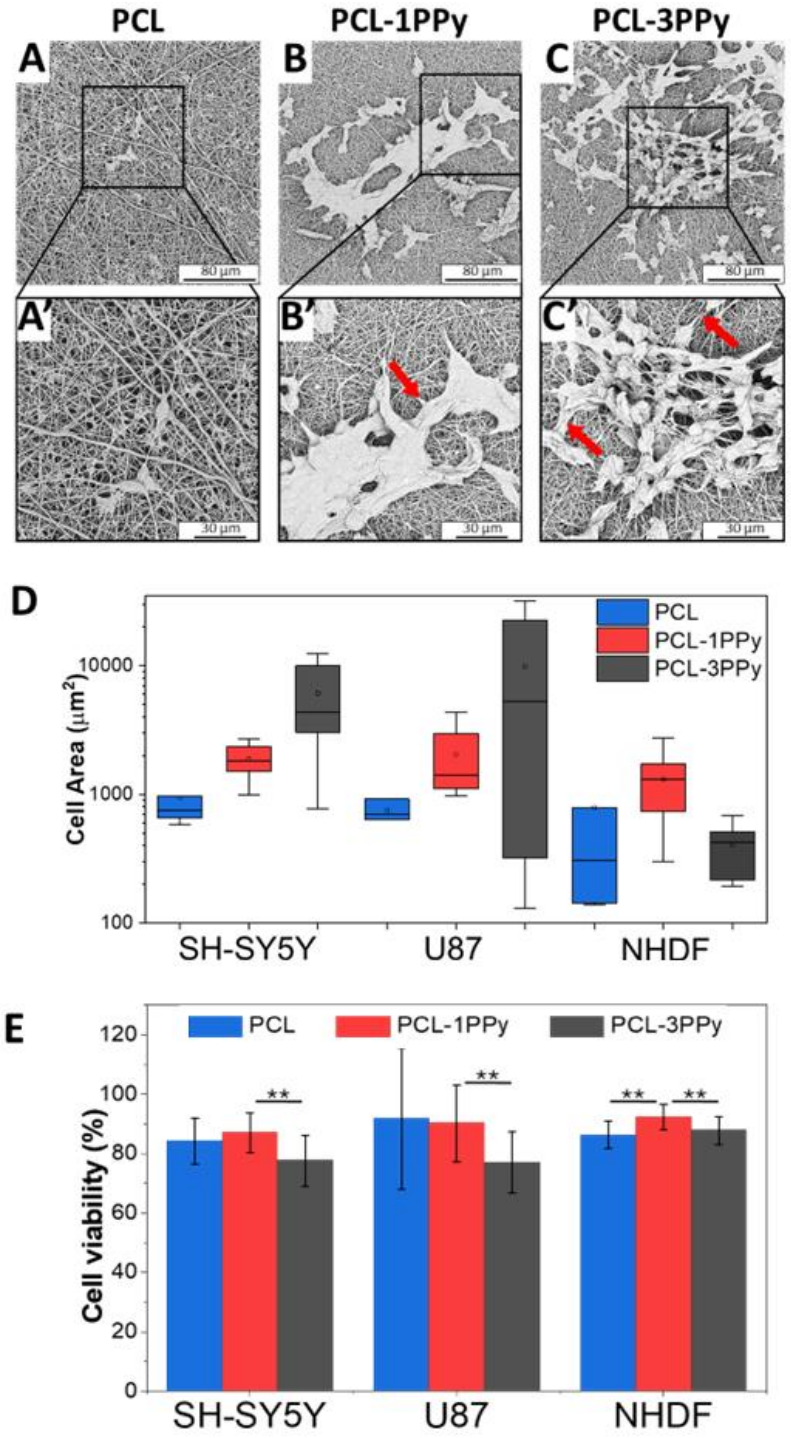


Figure 34. Morphological evaluation of SH-SY5Y cells on electrospun PCL and PPy-modified PCL fibers. Representative SEM images are shown for pristine PCL (A, A'), PCL-1PPy (B, B'), and PCL-3PPy (C, C'), with magnified regions indicating intercellular bridges (red arrows). (D) Cell spreading area (µm²). (E) Cell viability of SH-SY5Y, U87, and NHDF cells after 48 h of culture. Viability was normalized to tissue culture plastic (100%). Data are shown as mean ± SD; statistical analysis was performed using one-way ANOVA with significance defined (**$p \leq 0.05$).

The biological performance of the developed materials was further assessed using U87 and NHDF cell lines. The U87 cell line was selected as a model for glial cells, which are critically involved in the progression of SCI. Following the primary mechanical trauma, a cascade of secondary injury mechanisms develops over days to weeks, characterized by progressive degeneration of both neuronal and glial populations [311]. U87 glioma cells display a highly plastic and pleomorphic morphology, which can vary significantly depending on environmental conditions. Their structure and behavior are strongly influenced by external cues such as nutrient availability, ECM composition, and mechanical stimuli [312]. This pronounced cellular adaptability enables U87 cells to dynamically adjust their morphology and migratory activity in response to changes in their microenvironment [312].

In addition to neural and glial components, SCI pathology also involves the formation of a fibrotic scar at the lesion site [313]. For this reason, the interaction between the materials and NHDF fibroblast cells was also investigated [314]. Fibroblasts originate primarily from mesenchymal lineages and constitute the main cellular component of connective tissue. They are responsible for producing and maintaining ECM proteins, thereby ensuring structural integrity within mammalian tissues. Beyond their structural role, fibroblasts are actively involved in multiple physiological and pathological processes, including inflammation, angiogenesis, fibrosis, and tumor progression [315].

The *in vitro* response of U87 and NHDF cells to the fabricated scaffolds was evaluated in terms of both viability and morphology (**Figure 34D and 34E**). Both cell types showed relatively limited spreading and proliferation on pristine PCL fibers. For U87 cells, the highest surface coverage was observed on PCL-3PPy (9832.07 ± 12506), corresponding to approximately a 13-fold increase compared with PCL. In contrast, NHDF cells exhibited maximum coverage on PCL-1PPy (1320.94 ± 99.07), representing a 1.7-fold increase relative to pristine PCL. Regarding cell viability, U87 cells-maintained values above 70% across all samples, confirming overall cytocompatibility of the materials. Although PPy incorporation led to a reduction in viability, the differences were not statistically significant. Specifically, viability values were 91.7 ± 23.7% for PCL, 90.2 ± 12.9% for PCL-1PPy, and 77.1 ± 10.2% for PCL-3PPy. A similar trend was observed for NHDF cells (**Figure 34E**), where viability values remained within a biocompatible range. Pristine PCL supported 86.3 ± 4.6% viability, which increased slightly to 92.4 ± 4.2% for PCL-1PPy and remained comparable at 87.8 ± 4.7% for PCL-3PPy. However, none of these differences were statistically significant.

Several studies have reported that surface properties strongly influence NHDF and U87 cell behavior. For instance, Park et al. [316] demonstrated that NHDF cells exhibit enhanced gap-junctional communication on more hydrophilic substrates. In addition, surface charge has been identified as an important factor regulating fibroblast adhesion. Hamdan et al. [317] showed increased NHDF cell density on positively charged titanium surfaces, which was attributed to changes in the composition and organization of adsorbed protein layers that promote cell attachment. Similarly, Parikh et al. [318] reported enhanced proliferation of U87 cells on carbon nanotube-coated foams, linking this effect to improved wettability and increased available surface area for cell attachment.

3.4.6. Cell attachment

SH-SY5Y cells, widely used as a neuronal model in central nervous system and spinal cord injury research, were selected for detailed fluorescence microscopy analysis to investigate scaffold–neural cell interactions, whereas the remaining two cell lines served as general comparators [319] [320]. **Figure 35A–I** presents fluorescence images of SH-SY5Y cells after 48 h of culture, stained for the FA protein paxillin. Panels 4A, D, and G illustrate nuclear staining, revealing a clustered growth pattern across all scaffold types. **Figures 35B, E,** and **H** display F-actin staining, indicating well-organized cytoskeletal structures. Paxillin-labeled FA sites are shown in **Figures 35C, F,** and **I**. Quantitative analysis of punctate paxillin structures (**Figure 35J–L**) demonstrated that PPy incorporation influenced cell adhesion behavior. Pristine PCL fibers supported 151 ± 59 focal adhesions per cell, whereas this value increased substantially to 438 ± 168 on PCL-3PPy samples (**Figure 35J**). In contrast, PCL-1PPy samples showed 122 ± 28 focal adhesions per cell, slightly lower than unmodified PCL. Despite this, further evaluation indicated that PPy-containing scaffolds promoted the formation of larger FA structures. Additionally, cell density measurements revealed the highest level of surface attachment on PCL-1PPy (**Figure 35K**). Overall, the observed adhesion patterns align with the increased surface coverage previously identified in SEM analyses (**Figure 34D**). Figureure 4J further illustrates the distribution of FA sizes across the population. PCL-3PPy in particular exhibited a higher proportion of large adhesions compared to both PCL and PCL-1PPy samples.

FA size is known to vary depending on cell type, differentiation state, and the mechanical properties of the substrate, including stiffness and architecture [321]. Nascent adhesions

typically measure around 1 μm [322], while more mature focal contacts can extend to several micrometers and establish stronger connections with the cytoskeleton [323]. As mechanosensitive structures, focal adhesions continuously respond to external forces and substrate cues, thereby influencing key cellular behaviors such as migration, proliferation, and differentiation [321]. The geometry and organization of FAs also regulate cell motility, as their alignment and elongation can guide migration direction and speed. In general, larger and well-aligned adhesions are associated with more efficient cellular movement, and migration rate has been shown to correlate with adhesion size parameters, including length and area [321].

In this study, PCL-3PPy scaffolds exhibited a higher proportion of mature FAs (>2 μm in length [322]) compared to PCL and PCL-1PPy fibers. The improved interaction between cells and PPy-modified fibers can be explained by changes in key surface properties, including charge, wettability, and roughness. Previous studies have reported that more positively shifted zeta potentials enhance cell adhesion, likely due to stronger electrostatic interactions between the material surface and negatively charged cell membranes and serum proteins [324]. At the same time, both positively and negatively charged surfaces can support improved cell attachment when combined with moderate hydrophilicity [64] [325]. This suggests that protein adsorption is influenced by a balance of electrostatic interactions and surface wettability, both of which contribute to protein layer formation. However, optimal adhesion depends not only on the amount of adsorbed proteins but also on their structural integrity and biological activity at the interface [64].

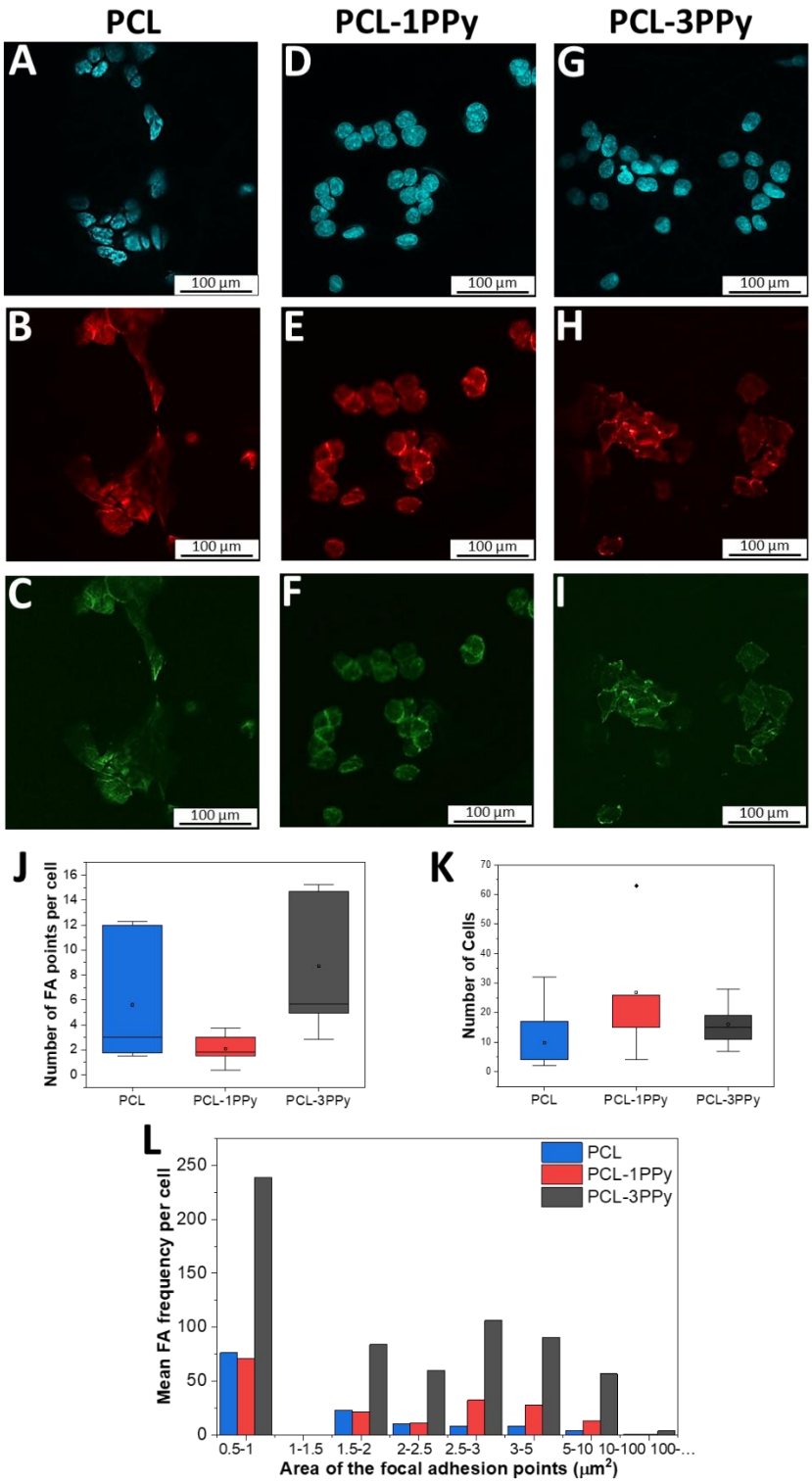


Figure 35. Immunofluorescence analysis of SH-SY5Y cells cultured on PCL, PCL-1PPy, and PCL-3PPy scaffolds. Representative images show nuclei (DAPI, blue), F-actin cytoskeleton (red), and paxillin-positive focal adhesions (green) for PCL (A–C), PCL-1PPy (D–F), and PCL-3PPy (G–I). Quantitative analysis includes the average number of focal adhesions per cell (J), scaffold surface cell occupancy (K), and mean focal adhesion frequency per cell (L).

The variations observed in cellular behavior may be linked to underlying molecular processes governing cell–material adhesion. Cell attachment is largely regulated through binding between transmembrane integrin receptors and ECM proteins [326]. Key ECM molecules, including laminin, fibronectin, and tenascin-C, facilitate cell adhesion and neurite extension via integrin-mediated signaling pathways [327]. Following spinal cord injury, however, the extracellular milieu becomes predominantly inhibitory, mainly due to the presence of chondroitin sulfate proteoglycans, which limit axonal regrowth and disrupt integrin-dependent cell–matrix interactions [328]. As a result, biomaterials that promote favorable adhesion-related interactions may enhance cellular responses. In this context, the amine groups associated with PPy may improve cell–material interactions, while enhanced protein adsorption and electrostatic effects are also likely to contribute to improved cell attachment at the scaffold interface [329].

3.4.7. *In vitro* degradation studies

In neural tissue engineering, scaffold degradation plays a crucial role in regulating axonal extension, cellular behavior, and the preservation of temporary structural support during regeneration processes [8,9]. Electrospun scaffolds designed for spinal cord repair are commonly engineered to exhibit tunable biodegradation, which is governed by polymer composition and blending ratios. Such materials provide transient mechanical support for regenerating axons and gradually degrade in coordination with tissue healing [330]. SCI progression is typically divided into acute, subacute, intermediate, and chronic stages, with the subacute phase defined as the period between 48 hours and 14 days post-injury [331]. Therefore, in this work, degradation behavior was assessed *in vitro* over 14 days, corresponding to the subacute phase of SCI.

Morphological evolution (**Figure 36A–C**), fiber diameter changes (**Figure 36D–F**), chemical structure alterations (**Figure 36G**), and mass loss (**Figure 36H**) were evaluated after immersion in PBS at 37°C for 14 days. All samples showed signs of degradation, with fiber diameter changes occurring in a non-uniform manner. The mean fiber diameters after degradation were 1.39 ± 0.45 μm for pristine PCL, 1.78 ± 1.09 μm for PCL-1PPy, and 1.48 ± 1.34 μm for PCL-3PPy. The relatively large standard deviations, particularly in PPy-containing samples, indicate heterogeneous degradation across the fiber network.

FTIR spectra recorded after 14 days (**Figure 36G**) revealed reduced overall band intensities for both PPy-modified samples compared with their pre-degradation state. No major spectral changes were observed for pristine PCL and PCL-3PPy before and after incubation. However, in PCL-1PPy, an increase in the intensity of bands corresponding to C=O and C–O stretching was detected, suggesting enhanced ester bond cleavage. Degradation of PCL is primarily driven by hydrolysis of ester linkages following water penetration into the polymer matrix [332]. Due to its hydrophobic nature, pristine PCL absorbs water slowly, which results in limited chemical degradation over the studied period [332]. In contrast, for PCL-3PPy, the disappearance of the band at 1594 cm^{-1} after incubation may indicate partial leaching of PPy during degradation. Overall, these observations suggest that while the PCL backbone in PCL-3PPy remained relatively stable chemically, degradation was likely dominated by physical processes such as PPy detachment or loss of loosely bound material, in addition to hydrolysis.

Mass loss measurements provide a direct indication of polymer degradation, as chain scission leads to fragmentation and a reduction in overall scaffold weight [289]. After 14 days, pristine PCL exhibited minimal weight loss (1.5 ± 0.4%), whereas significantly higher values were recorded for PCL-1PPy (16.5 ± 2.2%) and PCL-3PPy (21.7 ± 8.8%) (**Figure 36H**). When combined with FTIR data, these results suggest that degradation in the PCL-3PPy system is largely governed by physical mechanisms rather than purely chemical breakdown. Comparable findings were reported by Kai et al. [333], who investigated PPy-modified PCL/gelatin nanofibers for cardiac tissue engineering. In that study, higher PPy content led to reduced scaffold stability in PBS, with rapid loss of electrical and mechanical properties, whereas intermediate PPy levels improved degradation stability and were considered more suitable for tissue engineering applications. Overall, these results indicate that PPy incorporation significantly influences the degradation profile of PCL fibers in a concentration-dependent manner, increasing mass loss while largely maintaining fiber morphology over 14 days**.**

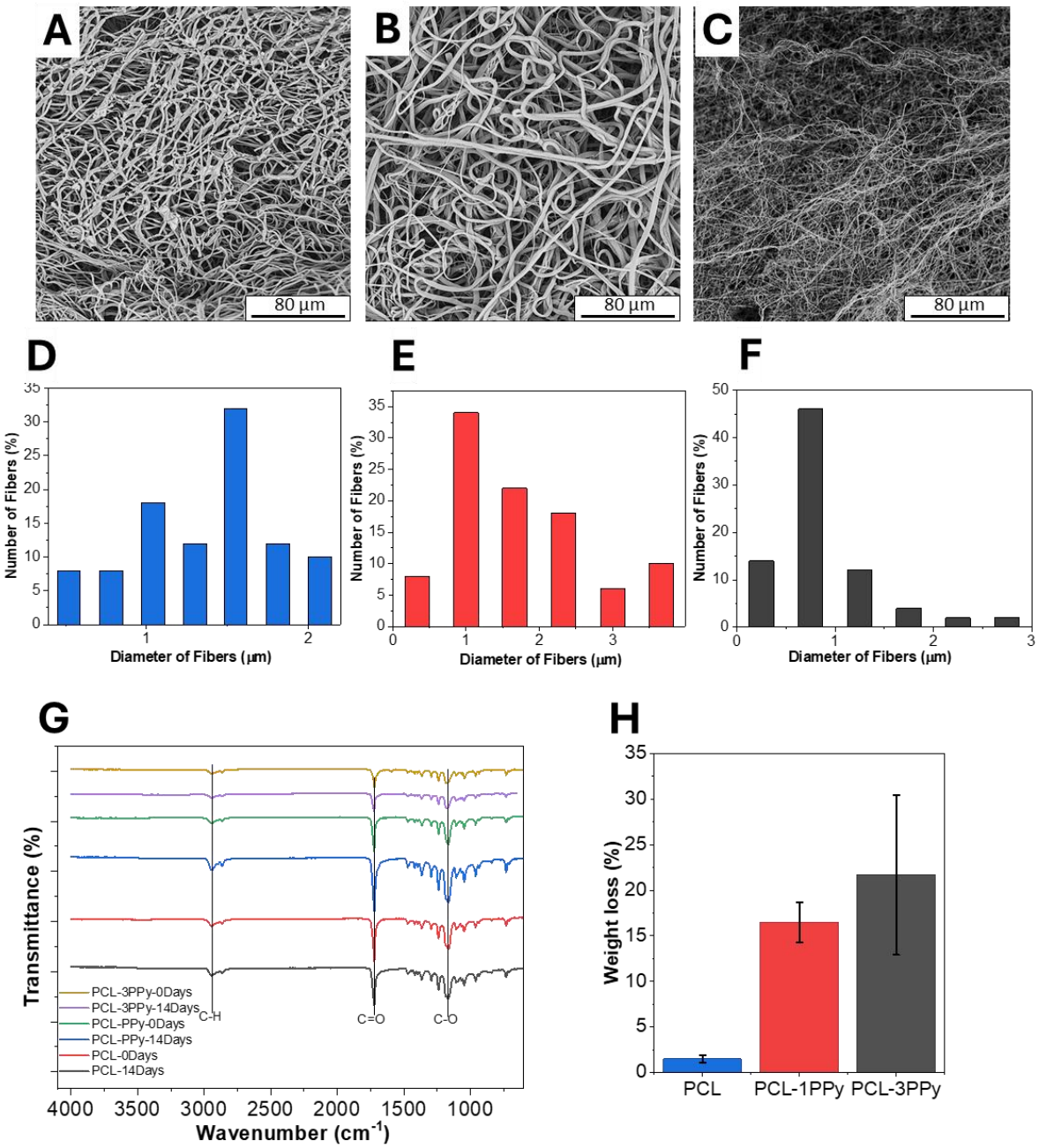


Figure 36 Morphological and physicochemical characterization of electrospun PCL-based fibers. SEM images of PCL (A), PCL-1PPy (B), and PCL-3PPy (C) are shown. (D–F) Fiber diameter distributions (n = 50) derived from SEM analysis. (G) FTIR spectra recorded at day 0 and after 14 days of incubation for PCL, PCL-1PPy, and PCL-3PPy. (H) Percentage mass loss following 14 days of degradation in PBS at 37 °C.

3.4.8. Perspectives and limitations

Polymeric scaffolds are widely investigated in tissue engineering, particularly for applications such as SCI repair, where they serve as structural and functional platforms to support cell attachment, growth, and network formation. Among these materials, PCL has attracted significant attention due to its excellent biocompatibility, mechanical stability, and ease of processing. However, its intrinsic hydrophobicity and lack of bioactivity limit its ability to support effective cell adhesion, which is a fundamental requirement for successful tissue integration and regeneration.

To address these limitations, surface modification strategies involving conducting polymers have emerged as a promising approach. PPy has been widely studied due to its electrical conductivity, biocompatibility, and ability to enhance cell–material interactions. Incorporation of PPy into polymer scaffolds can modulate key physicochemical properties such as surface charge, wettability, and morphology, all of which play critical roles in regulating cellular behavior. In this context, electrospun PCL fibers modified with PPy provide a simple yet effective platform for improving scaffold bioactivity.

Despite the promising outcomes reported for PPy-modified polymeric scaffolds, several limitations remain. Incorporation of conducting polymers such as PPy represents a promising strategy to introduce electroactive properties into otherwise non-conductive polymeric scaffolds. However, achieving a balance between enhanced electrical functionality and favorable biological performance remains challenging, as PPy incorporation can significantly modify surface physicochemical properties, including wettability, surface charge, and morphology, which directly influence cell–material interactions. Therefore, understanding how PPy-mediated modifications regulate cellular adhesion and scaffold biofunctionality is essential for the development of multifunctional scaffolds for tissue engineering applications.

3.4.9. Conclusions

Electrospun fibers containing PPy were successfully produced through a one-step fabrication approach using two different pyrrole concentrations. Detailed characterization of fiber morphology, wettability, surface roughness, porosity, zeta potential, and hydrolytic stability demonstrated that PPy incorporation markedly influenced the scaffold characteristics. In particular, the addition of PPy resulted in the formation of finer fibers, leading to lower surface roughness and increased porosity. Furthermore, increasing the PPy concentration reduced the water contact angle, indicating enhanced hydrophilicity of the scaffold surface. Measurements of zeta potential at pH values of 5.8, 7.4, and 9 showed that PPy modification shifted the surface charge toward less negative values. These alterations in surface properties were accompanied by improved cellular responses, including enhanced adhesion, spreading, and overall cell coverage. Cytocompatibility studies performed with SH-SY5Y neuroblastoma cells, NHDF fibroblasts, and U87 glioblastoma cells confirmed that all scaffold formulations-maintained cell viability above 70%, demonstrating acceptable biocompatibility. Compared with unmodified PCL scaffolds, PPy-containing fibers supported greater cell attachment and proliferation. For SH-SY5Y and U87 cells, this effect increased with PPy concentration, with the highest levels of cell coverage observed on the PCL-3PPy scaffolds. In contrast, NHDF fibroblasts exhibited the greatest surface coverage on PCL-1PPy samples. Fluorescence microscopy further demonstrated that SH-SY5Y cells cultured on PPy-modified fibers developed a greater number of focal adhesion sites than those grown on pristine PCL.

Overall, these results indicate that PPy-functionalized PCL scaffolds possess significant potential for spinal cord injury repair applications. The improved cellular behavior observed on the modified scaffolds can be attributed to changes in wettability, surface charge, porosity, and other physicochemical characteristics induced by PPy incorporation. By enhancing cell attachment, spreading, and proliferation while partially replicating features of the native extracellular matrix, these scaffolds may create a favorable environment for neural regeneration. Nevertheless, additional investigations, particularly concerning mechanical performance, are required before clinical translation can be considered. Future *in vivo* studies will also be necessary to verify their regenerative efficacy and ability to promote functional recovery following SCI.

Chapter 4

4. Conclusions

4.1. Conclusion

Cell–material interactions represent one of the fundamental determinants of the success of biomaterials used in tissue engineering, regenerative medicine, and implantable medical devices. Following implantation, the physicochemical properties of a biomaterial surface dictate the initial adsorption of proteins, which subsequently regulates cellular adhesion, morphology, proliferation, migration, differentiation, and ultimately tissue integration. Consequently, the rational design of biomaterial interfaces capable of directing specific cellular responses has become a central objective in modern biomaterials research. The work presented in this thesis demonstrates that precise engineering of electroactive, chemical, and topographical surface properties provides an effective strategy for modulating cell–material interactions and tailoring biological responses for biomedical applications, with particular emphasis on neural tissue engineering.

The central objective of this thesis was to investigate how modifications of surface physicochemical properties influence cellular behavior and to establish design principles for multifunctional biomaterial interfaces. To achieve this objective, several complementary surface engineering approaches were explored, including nanoscale topographical modification, bioactive chemical functionalization, electroactive conductive coatings, and modification of non-conductive electrospun fibrous scaffolds. Although each strategy relied on a different modification technique, all studies shared a common goal: understanding how the interplay between surface chemistry, roughness, wettability, electrical properties, surface charge, and nanoscale architecture governs cell adhesion and subsequent biological responses. Collectively, the findings demonstrate that cellular behavior is not controlled by a single surface characteristic but rather by the synergistic interaction of multiple physicochemical cues presented at the biomaterial interface.

The first part of this thesis focused on the influence of nanoscale surface topography on cellular behavior. Nanoengineered titanium surfaces containing highly ordered nanodimple structures demonstrated that subtle modifications of surface architecture can profoundly alter cell morphology, adhesion, migration, and cytoskeletal organization. The results revealed that nanotopography differentially regulates the behavior of distinct cell populations. Fibroblasts exhibited enhanced spreading and focal adhesion formation, while neuronal cells developed denser and more interconnected neurite networks. In contrast, astrocyte adhesion and migration were reduced, suggesting that nanotopographical cues may selectively suppress cellular responses associated with glial scar formation. These findings are particularly significant in the

context of neural tissue engineering, where successful integration of implanted devices requires simultaneous promotion of neuronal attachment while limiting excessive astrocyte activation. The study therefore demonstrates that nanotopography alone can provide selective regulation of cellular behavior without relying on biochemical or pharmacological interventions.

The second part of the thesis investigated chemical functionalization of titanium surfaces using bioactive polymer coatings. Incorporation of biologically active molecules into poly(vinyl alcohol)-based coatings enabled simultaneous modulation of cellular adhesion and enhancement of surface bioactivity. Beyond improving cell–material interactions, these coatings promoted mineralization, indicating their potential to facilitate long-term integration of titanium implants with surrounding tissues. The combination of selective cellular responses with enhanced bioactivity illustrates the advantages of multifunctional surface modifications over conventional passive implant surfaces. Rather than serving solely as structural materials, chemically functionalized coatings actively participate in regulating the biological microenvironment surrounding the implant. Such an approach may contribute to reducing complications associated with implant failure, fibrotic encapsulation, and inadequate tissue integration.

Electroactive conducting polymer coatings represented another important aspect of this research. Neural electrodes require materials that simultaneously exhibit excellent electrochemical performance and favorable biological compatibility. The results presented in this thesis demonstrate that conductive polymer coatings substantially improve electrode performance by increasing the electrochemically active surface area while reducing impedance and enhancing charge transfer properties. These electrochemical improvements were accompanied by enhanced neuronal adhesion and neurite extension, indicating that conductive coatings support the establishment of a more stable electrode–tissue interface. Considering that long-term performance of neural implants is often compromised by chronic inflammatory responses and poor electrical coupling, these findings highlight the considerable potential of electroactive polymers for next-generation neural interfaces. The ability to combine superior electrochemical functionality with biological compatibility represents an important step toward improving the reliability and longevity of implantable neuroprosthetic devices.

The final experimental chapter explored the modification of electrospun polycaprolactone scaffolds through in situ polymerization of polypyrrole prior to electrospinning. This strategy enabled homogeneous incorporation of conductive polymer throughout the electrospinning

solution while preserving the fibrous architecture. The resulting electroactive scaffolds demonstrated significant changes in surface charge, porosity, wettability, and electrical conductivity, which collectively enhanced initial cell attachment, spreading, and focal adhesion formation. These observations emphasize that conductive polymers influence cellular responses not only through electrical conductivity but also by altering several interconnected physicochemical properties that regulate protein adsorption and integrin-mediated adhesion.

An important outcome emerging from all studies is the recognition that cellular responses are governed by the combined influence of multiple surface characteristics rather than by individual parameters considered independently. Throughout this thesis, modifications in surface chemistry were frequently accompanied by changes in wettability, nanoscale roughness, electrochemical behavior, and surface charge. These parameters collectively determine the composition and conformation of adsorbed proteins, thereby influencing integrin binding, focal adhesion formation, cytoskeletal organization, and intracellular signaling pathways. Consequently, optimization of biomaterial surfaces requires consideration of these properties as an integrated system rather than as isolated variables. This integrated perspective represents one of the principal scientific contributions of this thesis and provides a conceptual framework for the rational design of advanced biomaterial interfaces.

Although the studies presented here primarily focused on neural tissue engineering, the underlying principles governing cell–surface interactions extend far beyond neural applications. The design strategies developed in this work are broadly applicable to numerous biomedical fields, including orthopedic implants, craniofacial reconstruction, cardiovascular devices, wound healing, and tissue-engineered scaffolds. The ability to selectively regulate different cell populations through rational surface engineering may facilitate the development of personalized biomaterials tailored to specific clinical requirements. Furthermore, combining electroactivity, bioactive chemistry, and nanoscale topography within a single multifunctional platform offers exciting opportunities for the next generation of smart biomaterials capable of dynamically interacting with the biological environment.

Despite these promising findings, several limitations should be acknowledged. The biological studies were primarily conducted using immortalized cell lines, which provide reproducible and well-established in vitro models but do not fully reproduce the complexity of native tissues. Primary cells, co-culture systems, organotypic models, and advanced three-dimensional tissue constructs would provide a more physiologically relevant assessment of cellular responses.

Similarly, while the present work successfully demonstrates proof-of-concept for several surface engineering strategies, comprehensive *in vivo* evaluation remains necessary to determine long-term implant integration, immune responses, biodegradation behavior, and functional performance under physiological conditions. Future investigations should also examine macrophage polarization, inflammatory signaling pathways, extracellular matrix remodeling, and vascularization, as these processes play essential roles in tissue regeneration and implant success.

Future research should also focus on integrating multiple surface engineering strategies into unified multifunctional platforms. Rather than considering topographical, chemical, and electroactive modifications independently, combining these approaches may generate synergistic effects that further improve biological performance. Advances in additive manufacturing, nanofabrication, biofabrication, and computational materials design offer exciting opportunities to develop customized biomaterial interfaces with spatially controlled physicochemical properties. In addition, emerging technologies such as artificial intelligence and machine learning may facilitate prediction of optimal surface characteristics capable of directing desired cellular responses, thereby accelerating the discovery and optimization of next-generation biomaterials.

In summary, this thesis demonstrates that rational engineering of biomaterial surfaces provides a powerful strategy for directing cellular behavior through precise control of electroactive, chemical, and topographical cues. The findings establish that modulation of cell adhesion is governed by the complex interplay between surface chemistry, nanotopography, wettability, electrochemical properties, and surface charge rather than by any single physicochemical parameter. By elucidating these relationships, this work contributes to a deeper understanding of cell–material interactions and advances the development of multifunctional biomaterial interfaces with improved biological and electrochemical performance. Collectively, the results presented in this thesis provide valuable design principles for future biomedical implants, neural interfaces, and tissue-engineered constructs, supporting the broader goal of developing biomaterials capable of actively guiding tissue regeneration and improving long-term clinical outcomes.

4.2. Applicability of results

The findings obtained in this thesis provide valuable insights into the rational design of biomaterial interfaces with tailored biological performance. By demonstrating that cellular responses can be modulated through precise control of surface physicochemical properties, this work provides a general framework for developing advanced biomaterials beyond conventional passive implant systems. The demonstrated effects of nanotopography, bioactive chemical modification, electroactive coatings, and polymer surface functionalization highlight the potential of surface engineering strategies to improve cell adhesion, tissue integration, and functional communication between implanted materials and biological systems. These principles can be applied to the development of next-generation biomedical implants where controlled cellular interactions are essential for long-term performance.

The outcomes of this research are particularly relevant for neural biomedical applications, including neural tissue engineering, neural stimulation platforms, and cranial implant technologies. The ability to promote neuronal adhesion and neurite extension while regulating undesirable cellular responses provides opportunities for improving the performance of neural scaffolds and implantable neurointerfaces. Furthermore, the demonstrated capability of modifying titanium and polymeric surfaces to regulate cell–material interactions may contribute to the development of improved cranial implants and other permanent medical devices by enhancing tissue compatibility and reducing adverse biological responses. Beyond neural applications, the design principles established in this thesis can be extended to orthopedic implants, cardiovascular devices, wound healing materials, and other tissue engineering platforms where precise regulation of cellular behavior is required.

Future translation of these findings will require further optimization and validation using advanced biological models, including primary human cells, multicellular systems, and in vivo studies. Nevertheless, the approaches developed in this work establish a foundation for designing multifunctional biomaterials that actively interact with the biological environment rather than merely providing structural support. The integration of physicochemical surface engineering with emerging fabrication technologies may enable the creation of patient-specific biomaterial interfaces with controlled biological functions, ultimately contributing to improved regenerative therapies and enhanced clinical outcomes.

4.3. Limitations

Despite the significant insights obtained regarding the regulation of cell–material interactions through surface engineering strategies, several limitations of this thesis should be acknowledged. First, the biological evaluations were primarily performed using established *in vitro* cell models, which provide controlled and reproducible systems for investigating specific aspects of cellular behavior but cannot fully replicate the complexity of native tissues. The interactions between biomaterials and cells *in vivo* involve dynamic processes including immune activation, vascularization, extracellular matrix remodeling, and communication between multiple cell types. Therefore, further validation using primary cells, co-culture systems, three-dimensional tissue models, and appropriate animal models is required to confirm the long-term biological performance and translational potential of the developed biomaterial platforms.

Another limitation is that, although this thesis demonstrated the influence of multiple physicochemical surface properties on cellular responses, these parameters are highly interconnected and difficult to completely decouple. Changes in one surface characteristic, such as chemical composition, often simultaneously affect wettability, surface charge, roughness, protein adsorption, and electrochemical behavior. Therefore, establishing direct cause–effect relationships between individual surface cues and specific cellular responses remains challenging. Future studies employing advanced surface characterization techniques, controlled model systems, and computational approaches could provide deeper mechanistic understanding of how individual physicochemical signals regulate protein–surface interactions, integrin activation, focal adhesion formation, and downstream cellular pathways.

Furthermore, the current work mainly focused on early cellular responses, including adhesion, morphology, spreading, and initial functional behavior. Although these parameters are critical determinants of biomaterial success, long-term biological outcomes such as chronic inflammation, immune response, tissue remodeling, and functional regeneration require additional investigation. In particular, evaluation of macrophage polarization, inflammatory signaling, glial responses, and vascular integration would provide a more comprehensive understanding of the performance of these materials under physiological conditions.

Finally, while the developed surface modification strategies successfully improved the biological performance of different biomaterial systems, further optimization is required to achieve multifunctional platforms suitable for specific clinical applications. Future research

should explore the integration of multiple surface cues within a single biomaterial system, together with scalable fabrication approaches and long-term stability assessments. Addressing these limitations will facilitate the translation of rationally engineered biomaterial interfaces from laboratory studies toward clinically relevant regenerative medicine and implantable biomedical applications.

Chapter 5

5. Scientific output

5.1. Overview of Scientific Output

The research conducted during this doctoral project resulted in a multidisciplinary body of scientific work focused on the modulation of cell–material interactions through the engineering of biomaterial surfaces. The research addressed three principal strategies for controlling cellular responses: topographical modification, chemical and bioactive functionalization, and electroactive surface engineering. These approaches were investigated using a range of metallic and polymeric biomaterials, including titanium, Ti-6Al-4V, conducting polymers, and electrospun polymeric scaffolds.

The scientific outcomes of the doctoral research include five journal manuscripts addressing different aspects of cell–material interactions, four international research internships, nine conference contributions, and three competitive research grants. The resulting publications collectively demonstrate the development and application of surface-engineering strategies for controlling cellular adhesion, morphology, proliferation, neurite outgrowth, and tissue–material interactions.

The publications arising from this doctoral research include two peer-reviewed journal articles published in international journals, two manuscripts currently under review or revision, and one review publication concerning the chemical regulation of cell–surface interactions. The research was further disseminated through presentations at international and national scientific conferences and supported by competitive funding for international research internships and the development of new research directions.

A detailed description of the scientific output and the author's individual contribution to each research study is provided below.

5.2. Journal Publications

Shakibania, S.; Niewolik, D.; Patel, T.; Bogusz, M.; Turczyn, R.; Basiaga, M.; Jaszcz, K.; Bednarczyk-Cwynar, B.; Skonieczna, M.; Krukiewicz, K.

Prevention of brain scarring during cranial reconstruction through a bioactive polymer coating. Biomaterials Advances 182 (2026) 214696

DOI: 10.1016/j.bioadv.2025.214696.

This study investigated the development of a bioactive polymeric coating intended to regulate tissue–material interactions during cranial reconstruction and to reduce undesirable cellular adhesion associated with postoperative brain scarring. The coating consisted of electrospun poly(vinyl alcohol) nanofibers incorporating a betulin disuccinate-derived component and PEG-based polymeric structures.

I fabricated the PVA-based nanofibrous coatings using electrospinning, performed and analyzed the morphological and physicochemical characterization of the developed materials, including SEM and FTIR. I also performed the *in vitro* biological experiments using SH-SY5Y, NHDF, and U2OS cells. I conducted cell viability and cell adhesion studies and analyzed the resulting cellular responses in relation to the physicochemical characteristics of the developed coatings. In addition, I contributed to the evaluation of coating deposition on Ti-6Al-4V substrates and the interpretation of the coating–substrate interaction. I was responsible for the analysis and interpretation of a substantial proportion of the experimental results, preparation of figures and graphical representations, and preparation and revision of the manuscript.

The obtained results contributed to demonstrating the potential of the developed bioactive coating to selectively regulate cellular adhesion while maintaining cytocompatibility and compatibility with titanium-based substrates.

Shakibania, S.; Patel, T.; Turczyn, R.; Biggs, M. J. P.; Krukiewicz, K.
Hybrid conducting polymer films promote neural outgrowth and neural-electrode integration in vitro. Bioelectrochemistry 165 (2025) 108985
DOI: 10.1016/j.bioelechem.2025.108985.

This study investigated hybrid conducting polymer coatings based on PANI and PEDOT as functional interfaces for neural electrodes. The work aimed to combine the electrochemical properties of conducting polymers with surface characteristics favorable for neural cell interaction and neurite development.

I was involved in the development of the hybrid conducting polymer coating and performed the physicochemical, morphological, and electrochemical characterization of the modified electrodes. I conducted electrochemical measurements to evaluate electrode impedance, charge storage properties, and electrochemical stability. I also analyzed the morphology and surface characteristics of the polymer coatings. I processed and analyzed the acquired microscopy images and quantified the relevant cellular parameters. I contributed to the interpretation of the electrochemical and biological results, preparation of figures and data presentation, and writing and revision of the manuscript.

The study demonstrated that the PANI–PEDOT hybrid coating could simultaneously improve electrochemical performance and support favorable neural cell responses, highlighting its potential for neural-electrode applications.

Shakibania, S.; Biggs, M. J. P.; Krukiewicz, K.

Adjusting Cell–Surface Interactions Through a Covalent Immobilization of Biomolecules.

Advanced Materials Interfaces 12 (2024) 2400774

DOI: https://doi.org/10.1002/admi.202400774.

This study investigated the use of covalent immobilization of biomolecules as a strategy to tailor different surface properties in biomaterials and control the interactions between cells and biomaterial surfaces. The work focused on the relationship between surface functionalization and cellular responses, providing a chemical approach to the regulation of cell–material interactions.

I conducted a comprehensive literature search and critically evaluated published studies concerning covalent immobilization of biomolecules on biomaterial surfaces and their effects on cell–material interactions. I contributed to the identification and organization of the major surface-functionalization strategies discussed in the review and analyzed the relationships between surface chemistry, biomolecule immobilization, and cellular responses. I was also involved in the critical interpretation and synthesis of the available literature, with particular emphasis on how covalent surface functionalization can be employed to control surface properties and subsequently modulate protein adsorption, cell adhesion, and other cellular behaviors. I contributed substantially to the conceptual development, structure, writing, and revision of the manuscript, as well as to the preparation and organization of figures and tables summarizing the relevant literature.

Shakibania, S.; Abdullah; Bogusz, M.; Lipińska, W.; Grochowska, K.; Karczewski, J.; Karoń, K.; Skonieczna, M.; Krukiewicz, K.
Biointeractive Titanium Surface Templates for Programming Cellular Responses. Advanced Materials Interfaces, manuscript under review.

This study investigated the influence of nanoscale surface topography on cell–material interactions using engineered titanium surfaces. Titanium substrates were modified through electrochemical anodization followed by chemical etching to produce uniformly distributed nanoscale dimples. The biological response of different cell models was subsequently evaluated to determine whether nanoscale surface architecture could selectively regulate cell adhesion, morphology, migration, and cellular organization.

I performed the biological experiments using NHDF, SH-SY5Y neuroblastoma cells, and U87 glioblastoma cells. I conducted cell culture experiments and evaluated cell attachment, spreading, morphology, and surface coverage. For the neuronal cell model, I performed immunofluorescence staining to investigate cytoskeletal organization and focal adhesion-related structures. Confocal laser scanning microscopy was used to evaluate cellular distribution and focal adhesion formation, and the resulting images were analyzed quantitatively. I contributed to the interpretation of the relationship between nanoscale topography and cell-specific responses, including fibroblast adhesion, neuronal network formation, and astrocytic behavior. I was also involved in data analysis, preparation of figures, and manuscript writing and revision.

Shakibania, S.; Abdullah; Tomasiak, A.; Knapczyk-Korczak, J.; Stachewicz, U.; Skonieczna, M.; Krukiewicz, K.
Polypyrrole-Modified Polycaprolactone Fibers with Enhanced Cell Adhesion for Spinal Cord Regeneration. ACS Applied Polymer Materials, manuscript under revision.

This study investigated the modification of electrospun PCL fibers with PPy to improve their physicochemical and biological properties for potential application in neural tissue engineering and spinal cord injury repair. The incorporation of PPy was investigated as a strategy for modifying surface morphology, wettability, surface charge, porosity, and cellular interactions.

I was responsible for the development and experimental investigation of the PPy-modified PCL scaffolds. I prepared the polymer formulations and fabricated the electrospun PCL/PPy fibrous scaffolds using the developed processing approach. I performed comprehensive physicochemical characterization of the scaffolds, including morphological analysis, wettability measurements, surface roughness characterization, porosity assessment, zeta potential measurements, and evaluation of hydrolytic stability. I analyzed the influence of PPy incorporation and concentration on the structural and surface properties of the electrospun fibers. I also performed the biological experiments using SH-SY5Y neuroblastoma, NHDF fibroblast, and U87 glioblastoma cell lines. I evaluated cell viability, adhesion, spreading, proliferation, and surface coverage and analyzed fluorescence microscopy images to assess cellular organization and focal adhesion formation. I analyzed and interpreted the relationship between PPy incorporation, changes in surface physicochemical properties, and cellular responses. I contributed to data analysis, preparation of figures, interpretation of the results, funding acquisition and writing and revision of the manuscript.

5.3. Other publication

1. Szymon Smołka, Alicja Tomasiak, Sara Shakibania, Kamran Ayaz, Taral Patel, Ethan Cao, Zuzanna Siwy, Magdalena Skonieczna, Ewa Zablocka-Godlewska, Roman Turczyn, and Katarzyna Krukiewicz "Winning the 'Race for the Surface': Curcumin-Loaded PEDOT Coatings with Enhanced Biocompatibility and Antibacterial Capability." Journal of Materials Chemistry B (2026), https://doi.org/10.1039/d6tb01040g
2. Abdullah, Sara Shakibania, Ewa Zabłocka-Godlewska, Krzysztof Aniołek, and Katarzyna Krukiewicz. "Surfactant-doped PEDOT films as dual-function bioelectronic coatings with enhanced charge storage capacity and antibiofilm activity." Bioelectrochemistry 172 (2026) 109366. 10.1016/j.bioelechem.2026.109366
3. Angelika Banaś, Roman Turczyn, Maciej Krzywiecki, Izabela Matuła, Sara Shakibania, Katarzyna Krukiewicz, and Deivasigamani Ranjith Kumar. "Electrochemically Engineered PEDOT: PSS/MXene Composite Electrode for the Label-Free Procalcitonin Detection." Advanced Materials Interfaces 13 (2026) e70492, https://doi.org/10.1002/admi.70492
4. Muhammad Saad, Katarzyna Krukiewicz, Yannig Nedellec, Ethan Cao, Zuzanna Siwy, Sara Shakibania, Krzysztof Karoń, Szymon Ruczka, Wojciech Pudło, Sławomir Boncel, Serge Cosnier. "Boosting the performance of bioelectrocatalytic electrodes by modulating the permeability of buckypapers." Electrochemistry Communications 187 (2026) 108158. 10.1016/j.elecom.2026.108158
5. Kamran Ayaz, Ewa Zabłocka-Godlewska, Sara Shakibania, Taral Patel, Krzysztof Karoń, Katarzyna Krukiewicz. "Enhancing Microbial Adhesion and Electron Transfer of Shewanella oneidensis MR-1 with Polyaniline-Glucose-Gelatin Coating for Bioelectrochemical Applications." Journal of Environmental Chemical Engineering 14 (2026) 121546. https://doi.org/10.1016/j.jece.2026.121546
6. Abdullah, Szymon Smołka, Kamran Ayaz, Sara Shakibania, Sajida Maryam, Taral Patel, Roman Turczyn, Ewa Zabłocka-Godlewska, Katarzyna Krukiewicz, "Smart Antibacterial Coatings: Harnessing Bacterial Redox Activity for Infection Control." Advanced Materials Interfaces (2026) e70647. https://doi.org/10.1002/admi.70647
7. Sajida Maryam, Ihtisham Ul Haq, Karolina Wilk, Sara Shakibania, Divine Yufetar Shyntum, Sebastian Student, Janusz Szewczenko, Katarzyna Krukiewicz. "Antimicrobial efficacy of ultrasonically deposited poly (vinyl alcohol)/poly (l-lysine)-

based coatings for urinary catheters." Surface and Coatings Technology 521 (2025) 133094. doi.org/10.1016/j.surfcoat.2025.133094

8. Abdullah, Divine Yufetar Shyntum, Sara Shakibania, Taral Patel, Katarzyna Krukiewicz. "Engineering conducting polymer-based interfaces for high-performance microbial electrochemical systems." Bioelectrochemistry 168 (2025) 109142. 10.1016/j.bioelechem.2025.109142
9. Małgorzata Skorupa, Ethan Cao, Adrian Barylski, Sara Shakibania, Sandra Pluczyk-Małek, Zuzanna Siwy, Katarzyna Krukiewicz. "Layer-By-Layer Approach to Improve the Capacitance of Conducting Polymer Films." Advanced Electronic Materials 11 (2025) 2400761. doi.org/10.1002/aelm.202400761
10. Agata Wawoczny, Joanna Wilk, Divine Shyntum, Sara Shakibania, Katarzyna Krukiewicz, Joanna Gibas, Marcin Machulik, Joanna Płonka, Sylwia Bajkacz, Gabriela Dudek, Danuta Gillner "Valorization of waste tomato leaves with natural deep eutectic solvents." Food Chemistry 472 (2025) 142884. 10.1016/j.foodchem.2025.142884
11. Abdullah, Sara Shakibania, Taral Patel, Divine Yufetar Shyntum, Katarzyna Krukiewicz, " Surface-Functionalized PEDOT:PSS Interfaces for Improved Adhesion, Viability, and Extracellular Charge Transfer of Shewanella oneidensis MR-1", ACS Sustainable Chemistry & Engineering 12 (2024) 52. doi.org/10.1021/acssuschemeng.4c05458
12. Weronika Janik, Dominika Kluska, Natalia Staniek, Paweł Grzybek, Sara Shakibania, Barbara Guzdek, Klaudiusz Gołombek, Krzysztof Matus, Divine Yufetar Shyntum, Katarzyna Krukiewicz, Gabriela Dudek, "Advantageous effect of calcium carbonate and chestnut extract on the performance of chitosan-based food packaging materials", Industrial Crops and Products 219 (2024) 119088. 10.1016/j.indcrop.2024.119088

5.4 International Research Internships

International research internships undertaken during the doctoral studies provided opportunities to acquire complementary experimental skills, establish international collaborations, and conduct research in specialized scientific environments. The internships were particularly relevant to the development of expertise in biomaterials, polymer chemistry, microscopy, and cell–material interactions.

1. Biofisika Institute, CSIC, UPV/EHU, Bilbao, Spain

15–25 July 2026
Supervisor: Prof. Adai Colom Diego

Research training focused on advanced microscopy approaches and the investigation of cellular behavior and interactions.

2. Université Grenoble Alpes, Grenoble, France

1–13 December 2025
Supervisor: Prof. Sami Halila

Research activities focused on the development of conducting hydrogel-based electrodes for highly efficient neural interfaces.

3. École des Mines de Saint-Étienne, Gardanne, France

1 October–30 November 2025
Supervisor: Prof. Rodney O'Connor

Research activities focused on biological characterization of the eutectic gels based on PEDOT:PSS.

4. University of Auckland, Auckland, New Zealand

25 March–26 June 2025
Supervisor: Prof. Jadranka Travas-Sejdic

A three-month research internship focused on synthesis and electrochemical characterization of the eutectic gels based on PEDOT:PSS.

5.5. Conference Contributions

The results generated during the doctoral research were disseminated through presentations at international and national scientific conferences. These contributions provided opportunities for scientific discussion, dissemination of research findings, and development of international collaborations.

1. Shakibania, S., et al. *Rheological and Electrical Optimization of Eutectic Gels for Conductive Wound Dressings Application.* 35th Conference of the European Society for Biomaterials, Antwerp, Belgium, September 2026.
2. Shakibania, S., et al. *Enhanced Cell Adhesion on Polypyrrole-Modified Polycaprolactone Fibers for Neural Tissue Engineering.* Computational Oncology and Personalized Medicine: From Genome to Treatment: AI & Precision Medicine, Gliwice, Poland, June 2026.
3. Shakibania, S., et al. *PEDOT Eutectogels as a Promising Conductive Material for Tissue Engineering.* Applications of Chemistry in Nanosciences and Biomaterials Engineering – NanoBioMat 2025, Bucharest, Romania, November 2025.
4. Shakibania, S., et al. *Enhancing Biocompatibility of Titanium Biomaterials: Fibroblast Adhesion and Morphology on Engineered Surface Topographies.* 34th Conference of the European Society for Biomaterials, Torino, Italy, September 2025.
5. Shakibania, S., et al. *Electrospun PCL/Polypyrrole Scaffolds: Enhancing Biocompatibility and Functionalization for Bone Tissue Engineering.* XXVIII Gliwice Scientific Meetings, Gliwice, Poland, November 2024.
6. Shakibania, S., et al. *Multilayer Electroactive Coatings with a Hierarchical Structure for Controlled Delivery of Neurotransmitters.* 4th International Biennial Conference BioMaH: Biomaterials and Novel Technologies for Healthcare, Rome, Italy, October 2024.
7. Shakibania, S., et al. *In-situ Polymerization of PPy within PCL Nanofibers: A Conductive Scaffold for Enhanced Neuronal Tissue Engineering.* 8th China-Europe Symposium on Biomaterials in Regenerative Medicine, Nuremberg, Germany, September 2024.

8. Shakibania, S., et al. *Bioactive Betulin-PEG Loaded Poly(vinyl alcohol) Nanofibers as a Biodegradable Coating for Titanium Bone Implants.* Polish-Scandinavian Symposium on Biomaterials, Kraków, Poland, September 2023.

9. Shakibania, S., et al. *Effect of Time and Method of Crosslinking on the Morphology of PVA Fibers.* Computational Oncology and Personalized Medicine: Crossing Borders, Connecting Science, Gliwice, Poland, April 2023.

5.6. Research Grants and Competitive Funding

The doctoral research was supported by competitive funding that enabled international research mobility, acquisition of specialized expertise, and the initiation of new research directions.

1. University of Auckland Research Internship Grant

The author was awarded a competitive research grant supporting a three-month international research internship at the University of Auckland, New Zealand. The funding was awarded under the Programme of Excellence Initiative – Research University, grant no. 32/014/SDU/10-27-30, and supported advanced research activities, international scientific collaboration, and development of specialized research skills.

2. Campus France Research Internship Grant

The author received a competitive grant supporting a two-month research internship at École Nationale Supérieure des Mines de Saint-Étienne, France. The internship was funded through the Campus France programme, grant no. N° 184764N, and enabled interdisciplinary research collaboration and methodological training within an international research environment.

3. Programme of Excellence Initiative Research University – Research Grant

The author received competitive funding to initiate a new research direction entitled “In-situ polymerization of polypyrrole on electrospun nanofibers: a conductive membrane for bone tissue engineering.” The project was supported under the Programme of Excellence Initiative – Research University, grant no. 32/014/SDU/10-22-61. The project contributed to the development of expertise in conducting-polymer modification of electrospun scaffolds and subsequently supported the research direction developed in the PCL/PPy study.

5.7. Patent Applications

1. Polymer scaffold for bone tissue regeneration, method for its preparation and use, filed at the Silesian University of Technology.

References

[1] A.T. Nguyen, S.R. Sathe, E.K. Yim, From nano to micro: topographical scale and its impact on cell adhesion, morphology and contact guidance, Journal of Physics: Condensed Matter 28(18) (2016) 183001.

[2] L. Bacakova, E. Filova, M. Parizek, T. Ruml, V. Svorcik, Modulation of cell adhesion, proliferation and differentiation on materials designed for body implants, Biotechnology advances 29(6) (2011) 739-767.

[3] M.A. Tokmedash, C. Kim, A.P. Chavda, A. Li, J. Robins, J. Min, Engineering multifunctional surface topography to regulate multiple biological responses, Biomaterials 319 (2025) 123136.

[4] C. Frantz, K.M. Stewart, V.M. Weaver, The extracellular matrix at a glance, Journal of Cell Science 123(24) (2010) 4195.

[5] L. Marcotte, M. Tabrizian, Sensing surfaces: Challenges in studying the cell adhesion process and the cell adhesion forces on biomaterials, Irbm 29(2-3) (2008) 77-88.

[6] S. Metwally, U. Stachewicz, Surface potential and charges impact on cell responses on biomaterials interfaces for medical applications, Materials Science and Engineering: C 104 (2019) 109883.

[7] A. Ahmad Khalili, M.R. Ahmad, A review of cell adhesion studies for biomedical and biological applications, International Journal of Molecular Sciences 16(8) (2015) 18149-18184.

[8] P. Roach, D. Eglin, K. Rohde, C.C. Perry, Modern biomaterials: a review—bulk properties and implications of surface modifications, Journal of Materials Science: Materials in Medicine 18(7) (2007) 1263-1277.

[9] J. Andrade, V. Hlady, Protein adsorption and materials biocompatibility: a tutorial review and suggested hypotheses, Biopolymers/Non-Exclusion HPLC (2005) 1-63.

[10] C.J. Wilson, R.E. Clegg, D.I. Leavesley, M.J. Pearcy, Mediation of biomaterial–cell interactions by adsorbed proteins: a review, Tissue Engineering 11(1-2) (2005) 1-18.

[11] D.R. Schmidt, H. Waldeck, W.J. Kao, Protein adsorption to biomaterials, Biological interactions on materials surfaces: Understanding and controlling protein, cell, and tissue responses, Springer2009, pp. 1-18.

[12] S.-Y. Jung, S.-M. Lim, F. Albertorio, G. Kim, M.C. Gurau, R.D. Yang, M.A. Holden, P.S. Cremer, The Vroman effect: a molecular level description of fibrinogen displacement, Journal of the American Chemical Society 125(42) (2003) 12782-12786.
[13] L. Parisi, A. Toffoli, B. Ghezzi, B. Mozzoni, S. Lumetti, G.M. Macaluso, A glance on the role of fibronectin in controlling cell response at biomaterial interface, Japanese Dental Science Review 56(1) (2020) 50-55.
[14] Q. Wei, T. Becherer, S. Angioletti-Uberti, J. Dzubiella, C. Wischke, A.T. Neffe, A. Lendlein, M. Ballauff, R. Haag, Protein interactions with polymer coatings and biomaterials, Angewandte Chemie International Edition 53(31) (2014) 8004-8031.
[15] S.R. Benhabbour, H. Sheardown, A. Adronov, Cell adhesion and proliferation on hydrophilic dendritically modified surfaces, Biomaterials 29(31) (2008) 4177-4186.
[16] A. Hasan, G. Waibhaw, L.M. Pandey, Conformational and organizational insights into serum proteins during competitive adsorption on self-assembled monolayers, Langmuir 34(28) (2018) 8178-8194.
[17] F. Martino, A.R. Perestrelo, V. Vinarský, S. Pagliari, G. Forte, Cellular mechanotransduction: from tension to function, Frontiers in physiology 9 (2018) 824.
[18] D.E. Jaalouk, J. Lammerding, Mechanotransduction gone awry, Nature reviews Molecular Cell Biology 10(1) (2009) 63-73.
[19] D.E. Ingber, Cellular mechanotransduction: putting all the pieces together again, The FASEB Journal 20(7) (2006) 811-827.
[20] D.E. Discher, P. Janmey, Y.-l. Wang, Tissue cells feel and respond to the stiffness of their substrate, Science 310(5751) (2005) 1139-1143.
[21] M.A. Schwartz, D.W. DeSimone, Cell adhesion receptors in mechanotransduction, Current Opinion in Cell Biology 20(5) (2008) 551-556.
[22] B. Geiger, J.P. Spatz, A.D. Bershadsky, Environmental sensing through focal adhesions, Nature Reviews Molecular Cell Biology 10(1) (2009) 21-33.
[23] M. Barczyk, S. Carracedo, D. Gullberg, Integrins, Cell and Tissue Research 339(1) (2010) 269-280.
[24] K. Katoh, Integrin and its associated proteins as a mediator for mechano-signal transduction, Biomolecules 15(2) (2025) 166.
[25] K. Katoh, Mechanostimulation-Induced Cell Adhesion and Interaction with the Extracellular Matrix, Biomolecules 16(1) (2025) 60.
[26] J.C. Kuo, Mechanotransduction at focal adhesions: integrating cytoskeletal mechanics in migrating cells, Journal of Cellular and Molecular Medicine 17(6) (2013) 704-712.

[27] M. Millard, S. Odde, N. Neamati, Integrin targeted therapeutics, Theranostics 1 (2011) 154.
[28] X. Zhong, F.J. Rescorla, Cell surface adhesion molecules and adhesion-initiated signaling: understanding of anoikis resistance mechanisms and therapeutic opportunities, Cellular Signalling 24(2) (2012) 393-401.
[29] C.G. Gahmberg, M. Grönholm, How integrin phosphorylations regulate cell adhesion and signaling, Trends in Biochemical Sciences 47(3) (2022) 265-278.
[30] A.E. Aplin, A.K. Howe, R. Juliano, Cell adhesion molecules, signal transduction and cell growth, Current Opinion in Cell Biology 11(6) (1999) 737-744.
[31] M. Singh, M. Thakur, M. Mishra, M. Yadav, R. Vibhuti, A.M. Menon, G. Nagda, V.P. Dwivedi, T.C. Dakal, V. Yadav, Gene regulation of intracellular adhesion molecule-1 (ICAM-1): A molecule with multiple functions, Immunology Letters 240 (2021) 123-136.
[32] M. Conacci-Sorrell, J. Zhurinsky, A. Ben-Ze'ev, The cadherin-catenin adhesion system in signaling and cancer, The Journal of Clinical Investigation 109(8) (2002) 987-991.
[33] K.L. Mui, C.S. Chen, R.K. Assoian, The mechanical regulation of integrin–cadherin crosstalk organizes cells, signaling and forces, Journal of Cell Science 129(6) (2016) 1093-1100.
[34] A. Von Recum, T. Van Kooten, The influence of micro-topography on cellular response and the implications for silicone implants, Journal of Biomaterials Science, Polymer Edition 7(2) (1996) 181-198.
[35] L. Wang, C. Wang, S. Wu, Y. Fan, X. Li, Influence of the mechanical properties of biomaterials on degradability, cell behaviors and signaling pathways: current progress and challenges, Biomaterials Science 8(10) (2020) 2714-2733.
[36] M. Drobota, S. Ursache, M. Aflori, Surface functionalities of polymers for biomaterial applications, Polymers 14(12) (2022) 2307.
[37] M. Rahmati, E.A. Silva, J.E. Reseland, C. A. Heyward, H.J. Haugen, Biological responses to physicochemical properties of biomaterial surface, Chemical Society Reviews 49(15) (2020) 5178-5224.
[38] P. Kingshott, G. Andersson, S.L. McArthur, H.J. Griesser, Surface modification and chemical surface analysis of biomaterials, Current Opinion in Chemical Biology 15(5) (2011) 667-676.
[39] H. Rostam, S. Singh, N. Vrana, M. Alexander, A. Ghaemmaghami, Impact of surface chemistry and topography on the function of antigen presenting cells, Biomaterials science 3(3) (2015) 424-441.

[40] S. Shakibania, M.J. Biggs, K. Krukiewicz, Adjusting cell-surface interactions through a covalent immobilization of biomolecules, Advanced Materials Interfaces 12(14) (2025) 2400774.
[41] B.D. Ratner, Surface modification of polymers: chemical, biological and surface analytical challenges, Biosensors and Bioelectronics 10(9-10) (1995) 797-804.
[42] S. Roh, Y. Jang, J. Yoo, H. Seong, Surface modification strategies for biomedical applications: enhancing cell–biomaterial interfaces and biochip performances, BioChip Journal 17(2) (2023) 174-191.
[43] X. Liu, J. He, S. Zhang, X.M. Wang, H.Y. Liu, F.Z. Cui, Adipose stem cells controlled by surface chemistry, Journal of tissue engineering and regenerative medicine 7(2) (2013) 112-117.
[44] F.J. Harding, L.R. Clements, R.D. Short, H. Thissen, N.H. Voelcker, Assessing embryonic stem cell response to surface chemistry using plasma polymer gradients, Acta Biomaterialia 8(5) (2012) 1739-1748.
[45] C.D. Bain, G.M. Whitesides, Depth sensitivity of wetting: monolayers of. omega.-mercapto ethers on gold, Journal of the American Chemical Society 110(17) (1988) 5897-5898.
[46] T.-W. Chung, D.-Z. Liu, S.-Y. Wang, S.-S. Wang, Enhancement of the growth of human endothelial cells by surface roughness at nanometer scale, Biomaterials 24(25) (2003) 4655-4661.
[47] S.A. Hacking, N. Ashammakhi, A. Khademhosseini, Cells and surfaces in vitro, Biomaterials science, Elsevier2020, pp. 661-681.
[48] Q. Wang, P. Zhou, S. Liu, S. Attarilar, R.L.-W. Ma, Y. Zhong, L. Wang, Multi-scale surface treatments of titanium implants for rapid osseointegration: a review, Nanomaterials 10(6) (2020) 1244.
[49] L. Xiao, Y. Sun, L. Liao, X. Su, Response of mesenchymal stem cells to surface topography of scaffolds and the underlying mechanisms, Journal of Materials Chemistry B 11(12) (2023) 2550-2567.
[50] V.A. Schulte, M. Diez, M. Möller, M.C. Lensen, Surface topography induces fibroblast adhesion on intrinsically nonadhesive poly (ethylene glycol) substrates, Biomacromolecules 10(10) (2009) 2795-2801.
[51] Y. Arima, H. Iwata, Effect of wettability and surface functional groups on protein adsorption and cell adhesion using well-defined mixed self-assembled monolayers, Biomaterials 28(20) (2007) 3074-3082.

[52] B.D. Ratner, A.S. Hoffman, F.J. Schoen, J.E. Lemons, Biomaterials science: an introduction to materials in medicine, Elsevier2004.
[53] S.P. Mitra, Protein adsorption on biomaterial surfaces: subsequent conformational and biological consequences—a review, Surface Science and Technology 36(1-2) (2020) 7-38.
[54] R.A. Latour, Fundamental principles of the thermodynamics and kinetics of protein adsorption to material surfaces, Colloids and Surfaces B: Biointerfaces 191 (2020) 110992.
[55] A. Hamraoui, Cell adhesion and surface interactions: A comprehensive review of surface energy, wettability, and topography effects, Aip Advances 15(9) (2025).
[56] F. Karimi, A.J. O'Connor, G.G. Qiao, D.E. Heath, Integrin clustering matters: a review of biomaterials functionalized with multivalent integrin-binding ligands to improve cell adhesion, migration, differentiation, angiogenesis, and biomedical device integration, Advanced Healthcare Materials 7(12) (2018) 1701324.
[57] R.J. Hunter, Zeta potential in colloid science: principles and applications, Academic Press2013.
[58] V.V. Chebodaeva, Surface electric properties and their role in the bioactivity of implant materials: A comprehensive review, Crystals 15(6) (2025) 583.
[59] S. Ferraris, M. Cazzola, V. Peretti, B. Stella, S. Spriano, Zeta potential measurements on solid surfaces for in vitro biomaterials testing: surface charge, reactivity upon contact with fluids and protein absorption, Frontiers in Bioengineering and Biotechnology 6 (2018) 60.
[60] T. Rana, Y.A. Bangash, A. Baz, T.A. Rana, M.A. Imran, Incremental composition process for the construction of component-based management systems, Sensors 20(5) (2020) 1351.
[61] C.D. McCaig, Membrane surface charge, phospholipids, and protein localization, No Electricity, No Life: Electrical Forces Govern Great Swathes of Biology (2025) 89-101.
[62] B.G. Keselowsky, D.M. Collard, A.J. García, Surface chemistry modulates fibronectin conformation and directs integrin binding and specificity to control cell adhesion, Journal of Biomedical Materials Research Part A: An Official Journal of The Society for Biomaterials, The Japanese Society for Biomaterials, and The Australian Society for Biomaterials and the Korean Society for Biomaterials 66(2) (2003) 247-259.
[63] H.-Y. Chang, W.-L. Kao, Y.-W. You, Y.-H. Chu, K.-J. Chu, P.-J. Chen, C.-Y. Wu, Y.-H. Lee, J.-J. Shyue, Effect of surface potential on epithelial cell adhesion, proliferation and morphology, Colloids and Surfaces B: Biointerfaces 141 (2016) 179-186.
[64] S. Guo, X. Zhu, M. Li, L. Shi, J.L.T. Ong, D. Jańczewski, K.G. Neoh, Parallel control over surface charge and wettability using polyelectrolyte architecture: effect on protein adsorption and cell adhesion, ACS Applied Materials & Interfaces 8(44) (2016) 30552-30563.

[65] T. Marques-Almeida, C. Ribeiro, I. Irastorza, P. Miranda-Azpiazu, I. Torres-Alemán, U. Silvan, S. Lanceros-Méndez, Electroactive materials surface charge impacts neuron viability and maturation in 2D cultures, ACS Applied Materials & Interfaces 15(26) (2023) 31206-31213.
[66] S. Santillo, Patch-Clamp: Studying the Passive and Active Properties of Excitable Membranes, Patch Clamp Technique-Current Methods and Future Prospects, IntechOpen2024.
[67] A.H. Rajabi, M. Jaffe, T.L. Arinzeh, Piezoelectric materials for tissue regeneration: A review, Acta Biomaterialia 24 (2015) 12-23.
[68] H.B. Carter, D.S. Coffey, Cell surface charge in predicting metastatic potential of aspirated cells from the Dunning rat prostatic adenocarcinoma model, The Journal of Urology 140(1) (1988) 173-175.
[69] J.M. Tong, D. Hao, Electroactive Biomaterials for Cardiovascular Tissue Engineering: Mechanisms, Design Strategies, and Therapeutic Applications, Journal of Functional Biomaterials 17(6) (2026) 295-295.
[70] H.-S. Kim, T. Baby, J.-H. Lee, U.S. Shin, H.-W. Kim, Biomaterials-enabled electrical stimulation for tissue healing and regeneration, Med-x 2(1) (2024) 7.
[71] A. Casella, A. Panitch, J.K. Leach, Electroconductive agarose hydrogels modulate mesenchymal stromal cell adhesion and spreading through protein adsorption, Journal of Biomedical Materials Research Part A 111(5) (2023) 596-608.
[72] M. Barrejón, H. Vara, A. Alves-Sampaio, H. Uceta, J.E. Collazos-Castro, Electroactive covalent linkers for enhancing conducting polymer adhesion, charge transfer, and biological integration of PEDOT-coated carbon microfibers, Carbon 232 (2025) 119820.
[73] Z. Liu, X. Wan, Z.L. Wang, L. Li, Electroactive biomaterials and systems for cell fate determination and tissue regeneration: design and applications, Advanced Materials 33(32) (2021) 2007429.
[74] H. Yang, L. Yao, Y. Wang, G. Chen, H. Chen, Advancing cell surface modification in mammalian cells with synthetic molecules, Chemical Science 14(46) (2023) 13325.
[75] G. Mani, Surface properties and characterization of metallic biomaterials, Surface Coating and Modification of Metallic Biomaterials, Elsevier2015, pp. 61-77.
[76] E.P. Ivanova, K. Bazaka, R.J. Crawford, Metallic biomaterials: types and advanced applications, New Functional Biomaterials for Medicine and Healthcare (2014) 121-147.
[77] X. Chen, S.M. Argandona, F. Melle, N. Rampal, D. Fairen-Jimenez, Advances in surface functionalization of next-generation metal-organic frameworks for biomedical applications: design, strategies, and prospects, Chemistry 10(2) (2024) 504-543.

[78] K.B. Narayanan, Nanotopographical features of polymeric nanocomposite scaffolds for tissue engineering and regenerative medicine: a review, Biomimetics 10(5) (2025) 317.
[79] J. Gaviria, V. Gaviria, K.V. Silva, A. Alcudia Cruz, E. Padrón-Hernández, Y. Torres Hernández, Nanoparticle Architecture Governing Antibacterial and Osteoinductive Responses in Bone-Integrating Implants, Metals (2025).
[80] T. Sjöström, G. Lalev, J.P. Mansell, B. Su, Initial attachment and spreading of MG63 cells on nanopatterned titanium surfaces via through-mask anodization, Applied Surface Science 257(10) (2011) 4552-4558.
[81] M. Domanski, R. Luttge, E. Lamers, X. Walboomers, L. Winnubst, J. Jansen, J.G. Gardeniers, Submicron-patterning of bulk titanium by nanoimprint lithography and reactive ion etching, Nanotechnology 23(6) (2012) 065306.
[82] W. Lipińska, K. Siuzdak, J. Karczewski, A. Dołęga, K. Grochowska, Electrochemical glucose sensor based on the glucose oxidase entrapped in chitosan immobilized onto laser-processed Au-Ti electrode, Sensors and Actuators B: Chemical 330 (2021) 129409.
[83] K. Grochowska, K. Siuzdak, Ł. Macewicz, F. Skiba, M. Szkoda, J. Karczewski, Ł. Burczyk, G. Śliwiński, Nanostructuring of thin Au films deposited on ordered Ti templates for applications in SERS, Applied Surface Science 418 (2017) 472-480.
[84] D. Regonini, C.R. Bowen, A. Jaroenworaluck, R. Stevens, A review of growth mechanism, structure and crystallinity of anodized TiO2 nanotubes, Materials Science and Engineering: R: Reports 74(12) (2013) 377-406.
[85] S. Li, G. Zhang, D. Guo, L. Yu, W. Zhang, Anodization fabrication of highly ordered TiO2 nanotubes, The Journal of Physical Chemistry C 113(29) (2009) 12759-12765.
[86] A.A. Khan, J.-H. Kim, Recent advances in materials and manufacturing of implantable devices for continuous health monitoring, Biosensors and Bioelectronics 261 (2024) 116461.
[87] E. Mariani, G. Lisignoli, R.M. Borzì, L. Pulsatelli, Biomaterials: foreign bodies or tuners for the immune response?, International Journal of Molecular Sciences 20(3) (2019) 636.
[88] W. Cao, L.L. Hench, Bioactive materials, Ceramics International 22(6) (1996) 493-507.
[89] J.R. Smith, D.A. Lamprou, Polymer coatings for biomedical applications: a review, Transactions of the IMF 92(1) (2014) 9-19.
[90] L. Xu, A. Yamamoto, Characteristics and cytocompatibility of biodegradable polymer film on magnesium by spin coating, Colloids and Surfaces B: Biointerfaces 93 (2012) 67-74.
[91] S. Kunjukunju, A. Roy, M. Ramanathan, B. Lee, J.E. Candiello, P.N. Kumta, A layer-by-layer approach to natural polymer-derived bioactive coatings on magnesium alloys, Acta Biomaterialia 9(10) (2013) 8690-8703.

[92] A. Brenner, Electrodeposition of alloys: principles and practice, Elsevier2013.
[93] T. Pauporté, D. Lincot, Electrodeposition of semiconductors for optoelectronic devices: results on zinc oxide, Electrochimica Acta 45(20) (2000) 3345-3353.
[94] E.M. Abebe, M. Ujihara, Simultaneous electrodeposition of ternary metal oxide nanocomposites for high-efficiency supercapacitor applications, ACS Omega 7(20) (2022) 17161-17174.
[95] S. Shakibania, T. Patel, R. Turczyn, M.J. Biggs, K. Krukiewicz, Hybrid conducting polymer films promote neural outgrowth and neural-electrode integration in vitro, Bioelectrochemistry 165 (2025) 108985.
[96] P. Sebastián, V. Climent, J. Feliu, E. Gómez, Ionic liquids in the field of metal electrodeposition, (2018).
[97] Z. Zhang, G. Tian, X. Duan, H.-l. Chen, D.-H. Kim Richie, Nanostructured PEDOT coatings for electrode–neuron integration, ACS Applied Bio Materials 4(7) (2021) 5556-5565.
[98] X. Cui, J.F. Hetke, J.A. Wiler, D.J. Anderson, D.C. Martin, Electrochemical deposition and characterization of conducting polymer polypyrrole/PSS on multichannel neural probes, Sensors and Actuators A: Physical 93(1) (2001) 8-18.
[99] X. Cui, V.A. Lee, Y. Raphael, J.A. Wiler, J.F. Hetke, D.J. Anderson, D.C. Martin, Surface modification of neural recording electrodes with conducting polymer/biomolecule blends, Journal of Biomedical Materials Research: An Official Journal of The Society for Biomaterials, The Japanese Society for Biomaterials, and The Australian Society for Biomaterials and the Korean Society for Biomaterials 56(2) (2001) 261-272.
[100] Z. Tu, Z. Ma, J. Li, J. Liang, S. Li, Y. Shi, L. Pan, Prospective on doping engineering of conductive polymers for enhanced interfacial properties, Applied Physics Letters 119(15) (2021).
[101] K. Krukiewicz, A. Kowalik, R. Turczyn, M.J. Biggs, In vitro attenuation of astrocyte activation and neuroinflammation through ibuprofen-doping of poly (3, 4-ethylenedioxypyrrole) formulations, Bioelectrochemistry 134 (2020) 107528.
[102] K. Krukiewicz, M. Chudy, S. Gregg, M.J. Biggs, The synergistic effects of gold particles and dexamethasone on the electrochemical and biological performance of PEDOT neural interfaces, Polymers 11(1) (2019) 67.
[103] B. Guo, P.X. Ma, Conducting polymers for tissue engineering, Biomacromolecules 19(6) (2018) 1764-1782.
[104] T. Nezakati, A. Seifalian, A. Tan, A.M. Seifalian, Conductive polymers: opportunities and challenges in biomedical applications, Chemical Reviews 118(14) (2018) 6766-6843.

[105] C.L. Ferreira, C.A. Valente, M.L. Zanini, B. Sgarioni, P.H. Ferreira Tondo, P.C. Chagastelles, J. Braga, M.M. Campos, J.A. Malmonge, N.R. de Souza Basso, Biocompatible PCL/PLGA/polypyrrole composites for regenerating nerves, Macromolecular Symposia, Wiley Online Library, 2019, p. 1800028.
[106] V. Castagnola, C. Bayon, E. Descamps, C. Bergaud, Morphology and conductivity of PEDOT layers produced by different electrochemical routes, Synthetic Metals 189 (2014) 7-16.
[107] P. Zhang, B. Zhu, P. Du, J. Travas-Sejdic, Electrochemical and electrical biosensors for wearable and implantable electronics based on conducting polymers and carbon-based materials, Chemical Reviews 124(3) (2023) 722-767.
[108] A. Sanchez-Sanchez, I. del Agua, G.G. Malliaras, D. Mecerreyes, Conductive poly (3, 4-Ethylenedioxythiophene)(PEDOT)-based polymers and their applications in bioelectronics, Smart Polymers and Their Applications, Elsevier2019, pp. 191-218.
[109] H.-l. Chen, D. Yang, C.-r. Chen, G.-z. Tian, D.-H. Kim, In situ polymerization of conducting polymers around living neural cells: Cellular effect study, Colloids and Surfaces B: Biointerfaces 213 (2022) 112410.
[110] C. Vallejo-Giraldo, K. Krukiewicz, I. Calaresu, J. Zhu, M. Palma, M. Fernandez-Yague, B. McDowell, N. Peixoto, N. Farid, G. O'Connor, Attenuated glial reactivity on topographically functionalized poly (3, 4-ethylenedioxythiophene): P-toluene sulfonate (PEDOT: PTS) neuroelectrodes fabricated by microimprint lithography, Small 14(28) (2018) 1800863.
[111] B. Xu, T. Bai, A. Sinclair, W. Wang, Q. Wu, F. Gao, H. Jia, S. Jiang, W. Liu, Directed neural stem cell differentiation on polyaniline-coated high strength hydrogels, Materials Today Chemistry 1 (2016) 15-22.
[112] L. Di, L.-P. Wang, Y.-N. Lu, L. He, Z.-X. Lin, K.-J. Wu, Q.-S. Ren, J.-Y. Wang, Protein adsorption and peroxidation of rat retinas under stimulation of a neural probe coated with polyaniline, Acta Biomaterialia 7(10) (2011) 3738-3745.
[113] D.J. Ahirrao, A.K. Pal, V. Singh, N. Jha, Nanostructured porous polyaniline (PANI) coated carbon cloth (CC) as electrodes for flexible supercapacitor device, Journal of Materials Science & Technology 88 (2021) 168-182.
[114] D. Xu, L. Fan, L. Gao, Y. Xiong, Y. Wang, Q. Ye, A. Yu, H. Dai, Y. Yin, J. Cai, Micro-nanostructured polyaniline assembled in cellulose matrix via interfacial polymerization for applications in nerve regeneration, ACS Applied Materials & Interfaces 8(27) (2016) 17090-17097.

[115] G. Wang, W. Wu, H. Yang, P. Zhang, J.Y. Wang, Intact polyaniline coating as a conductive guidance is beneficial to repairing sciatic nerve injury, Journal of Biomedical Materials Research Part B: Applied Biomaterials 108(1) (2020) 128-142.
[116] P. Humpolicek, V. Kasparkova, P. Saha, J. Stejskal, Biocompatibility of polyaniline, Synthetic Metals 162(7-8) (2012) 722-727.
[117] L. Wang, Q. Huang, J.-Y. Wang, Nanostructured polyaniline coating on ITO glass promotes the neurite outgrowth of PC 12 cells by electrical stimulation, Langmuir 31(44) (2015) 12315-12322.
[118] S. Caponi, S. Mattana, M. Ricci, K. Sagini, L. Juarez-Hernandez, A. Jimenez-Garduño, N. Cornella, L. Pasquardini, L. Urbanelli, P. Sassi, A multidisciplinary approach to study the functional properties of neuron-like cell models constituting a living bio-hybrid system: SH-SY5Y cells adhering to PANI substrate, AIP Advances 6(11) (2016).
[119] S. Kim, W.-K. Oh, Y.S. Jeong, J.-Y. Hong, B.-R. Cho, J.-S. Hahn, J. Jang, Cytotoxicity of, and innate immune response to, size-controlled polypyrrole nanoparticles in mammalian cells, Biomaterials 32(9) (2011) 2342-2350.
[120] Q. Zeng, Z. Huang, Challenges and opportunities of implantable neural interfaces: from material, electrochemical and biological perspectives, Advanced Functional Materials 33(32) (2023) 2301223.
[121] J. Ding, J. Zhang, J. Li, D. Li, C. Xiao, H. Xiao, H. Yang, X. Zhuang, X. Chen, Electrospun polymer biomaterials, Progress in Polymer Science 90 (2019) 1-34.
[122] S. Zhang, X.-J. Wang, W.-S. Li, X.-L. Xu, J.-B. Hu, X.-Q. Kang, J. Qi, X.-Y. Ying, J. You, Y.-Z. Du, Polycaprolactone/polysialic acid hybrid, multifunctional nanofiber scaffolds for treatment of spinal cord injury, Acta Biomaterialia 77 (2018) 15-27.
[123] J.W. McDonald, C. Sadowsky, Spinal-cord injury, The Lancet 359(9304) (2002) 417-425.
[124] A.M. Muñoz-González, D. Clavijo-Grimaldo, S. Leal-Marin, B. Glasmacher, Optimizing Electroconductive PPy-PCL Scaffolds for Enhanced Tissue Engineering Performance, Journal of Biomedical Materials Research Part B: Applied Biomaterials 112(12) (2024) e35511.
[125] C.H. Kim, M.S. Khil, H.Y. Kim, H.U. Lee, K.Y. Jahng, An improved hydrophilicity via electrospinning for enhanced cell attachment and proliferation, Journal of Biomedical Materials Research Part B: Applied Biomaterials: An Official Journal of The Society for Biomaterials, The Japanese Society for Biomaterials, and The Australian Society for Biomaterials and the Korean Society for Biomaterials 78(2) (2006) 283-290.

[126] C.A. Short, E.A. Suarez-Zayas, T.M. Gomez, Cell adhesion and invasion mechanisms that guide developing axons, Current Opinion in Neurobiology 39 (2016) 77-85.
[127] J.W. McDonald, R.C.o.t.C.R.P. Foundation, Repairing the damaged spinal cord, Scientific American 281(3) (1999) 64-73.
[128] J.E. Karbowniczek, P. İlhan, P.K. Szewczyk, E.M. Namli, M. Polak, Z.G.l. Morçimen, J. Knapczyk-Korczak, E. Turunç, A. Şendemir, U. Stachewicz, A Sustainable Alternative to PVDF for Neural Tissue Engineering via Piezoelectric PHBV and Cellulose Acetate Fibers, ACS Biomaterials Science & Engineering (2026).
[129] N.J. Schaub, C.D. Johnson, B. Cooper, R.J. Gilbert, Electrospun fibers for spinal cord injury research and regeneration, Journal of Neurotrauma 33(15) (2016) 1405-1415.
[130] M. Keshvardoostchokami, S.S. Majidi, P. Huo, R. Ramachandran, M. Chen, B. Liu, Electrospun nanofibers of natural and synthetic polymers as artificial extracellular matrix for tissue engineering, Nanomaterials 11(1) (2020) 21.
[131] J.M. Anderson, Biological responses to materials, Annual review of materials research 31(1) (2001) 81-110.
[132] M.E. Schwab, S.M. Strittmatter, Nogo limits neural plasticity and recovery from injury, Current Opinion in Neurobiology 27 (2014) 53-60.
[133] D.R. Nisbet, K.E. Crompton, M.K. Horne, D.I. Finkelstein, J.S. Forsythe, Neural tissue engineering of the CNS using hydrogels, Journal of Biomedical Materials Research Part B: Applied Biomaterials: An Official Journal of The Society for Biomaterials, The Japanese Society for Biomaterials, and The Australian Society for Biomaterials and the Korean Society for Biomaterials 87(1) (2008) 251-263.
[134] S.F. Cogan, Neural stimulation and recording electrodes, Annu. Rev. Biomed. Eng. 10(1) (2008) 275-309.
[135] S. Shakibania, D. Niewolik, T. Patel, M. Bogusz, R. Turczyn, M. Basiaga, K. Jaszcz, B. Bednarczyk-Cwynar, M. Skonieczna, K. Krukiewicz, Prevention of brain scarring during cranial reconstruction through a bioactive polymer coating, Biomaterials Advances (2026) 214696.
[136] J.W. Fawcett, R.A. Asher, The glial scar and central nervous system repair, Brain Research Bulletin 49(6) (1999) 377-391.
[137] T. Manoli, L. Schulz, S. Stahl, P. Jaminet, H.E. Schaller, Evaluation of sensory recovery after reconstruction of digital nerves of the hand using muscle-in-vein conduits in comparison to nerve suture or nerve autografting, Microsurgery 34(8) (2014) 608-615.

[138] M. Curcio, F. Bradke, Axon regeneration in the central nervous system: facing the challenges from the inside, Annual Review of Cell and Developmental Biology 34(1) (2018) 495-521.
[139] C.E. Schmidt, J.B. Leach, Neural tissue engineering: strategies for repair and regeneration, Annual Review of Biomedical Engineering 5(1) (2003) 293-347.
[140] L.R. Doblado, C. Martínez-Ramos, M.M. Pradas, Biomaterials for neural tissue engineering, Frontiers in Nanotechnology 3 (2021) 643507.
[141] S. Kehoe, X. Zhang, D. Boyd, FDA approved guidance conduits and wraps for peripheral nerve injury: a review of materials and efficacy, Injury 43(5) (2012) 553-572.
[142] X. Hu, W. Xu, Y. Ren, Z. Wang, X. He, R. Huang, B. Ma, J. Zhao, R. Zhu, L. Cheng, Spinal cord injury: molecular mechanisms and therapeutic interventions, Signal Transduction and Targeted Therapy 8(1) (2023) 245.
[143] J. Chedly, S. Soares, A. Montembault, Y. von Boxberg, M. Veron-Ravaille, C. Mouffle, M.-N. Benassy, J. Taxi, L. David, F. Nothias, Physical chitosan microhydrogels as scaffolds for spinal cord injury restoration and axon regeneration, Biomaterials 138 (2017) 91-107.
[144] M. Namhongsa, D. Daranarong, M. Sriyai, R. Molloy, S. Ross, G.M. Ross, A. Tuantranont, J. Tocharus, S. Sivasinprasasn, P.D. Topham, Surface-modified polypyrrole-coated PLCL and PLGA nerve guide conduits fabricated by 3D printing and electrospinning, Biomacromolecules 23(11) (2022) 4532-4546.
[145] Y. Zhang, X. Fang, L. Yan, L. Wang, Fibroblasts as a ruler of the immune microenvironment: measurement and modulation in tissue homeostasis and disease, Frontiers in Immunology 16 (2025) 1752621.
[146] C. Feng, L. Deng, Y.-Y. Yong, J.-M. Wu, D.-L. Qin, L. Yu, X.-G. Zhou, A.-G. Wu, The application of biomaterials in spinal cord injury, International Journal of Molecular Sciences 24(1) (2023) 816.
[147] E. Castel-Lacanal, Sites of electrical stimulation used in neurology, Annals of Physical and Rehabilitation Medicine 58(4) (2015) 201-207.
[148] D. Czerwińska-Główka, M. Skonieczna, A. Barylski, S. Golba, W. Przystaś, E. Zabłocka-Godlewska, S. Student, B. Cwalina, K. Krukiewicz, Bifunctional conducting polymer matrices with antibacterial and neuroprotective effects, Bioelectrochemistry 144 (2022) 108030.
[149] S.A. Seyedkhani, S. Kalhor, M. Vafaiee, M. Taghipoor, R. Mohammadpour, Polydopamine-doped PEDOT interfaces improve cell-electrode interactions and neural signal transmission, Scientific Reports 16 (2026) 10443.

[150] C. Zhang, Historical Review and Current Progress of the Cranioplasty, Health Safe Environ Technol 54 (2023) 100-105.
[151] L. Sveikata, L. Vasung, A. El Rahal, A. Bartoli, M. Bretzner, K. Schaller, A. Schnider, B. Leemann, Syndrome of the trephined: clinical spectrum, risk factors, and impact of cranioplasty on neurologic recovery in a prospective cohort, Neurosurgical Review 45(2) (2022) 1431-1443.
[152] H. Mee, F. Anwar, I. Timofeev, N. Owens, K. Grieve, G. Whiting, K. Alexander, K. Kendrick, A. Helmy, P. Hutchinson, Cranioplasty: a multidisciplinary approach, Frontiers in Surgery 9 (2022) 864385.
[153] H. Mee, C. Clement, F. Anwar, G. Whiting, I. Timofeev, A. Helmy, P.J. Hutchinson, A.G. Kolias, Exploring the experiences and challenges for patients undergoing cranioplasty: a mixed-methods study protocol, BMJ open 12(4) (2022) e048072.
[154] A.M. Shah, H. Jung, S. Skirboll, Materials used in cranioplasty: a history and analysis, Neurosurgical Focus 36(4) (2014) E19.
[155] T. Brommeland, P.N. Rydning, A.H. Pripp, E. Helseth, Cranioplasty complications and risk factors associated with bone flap resorption, Scandinavian Journal of Trauma, Resuscitation and Emergency Medicine 23(1) (2015) 75.
[156] Y.H. Kim, C.H. Lee, C.H. Kim, D.W. Son, S.W. Lee, G.S. Song, S.K. Sung, Clinical efficacy and safety of silicone elastomer sheet during decompressive craniectomy: anti-adhesive role in cranioplasty, Brain Sciences 11(1) (2021) 124.
[157] C.-H. Lee, D.-S. Cho, S.-C. Jin, S.-H. Kim, D.-B. Park, Usefulness of silicone elastomer sheet as another option of adhesion preventive material during craniectomies, Clinical Neurology and Neurosurgery 109(8) (2007) 667-671.
[158] R. Shi, J. Xue, H. Wang, R. Wang, M. Gong, D. Chen, L. Zhang, W. Tian, Fabrication and evaluation of a homogeneous electrospun PCL–gelatin hybrid membrane as an anti-adhesion barrier for craniectomy, Journal of Materials Chemistry B 3(19) (2015) 4063-4073.
[159] M.A. Azab, K. Sarhan, A. Hernández-Hernández, O. Atallah, B. Kammoun, A. Hazim, Potential techniques to facilitate dissection in patients undergoing cranioplasty following decompressive craniectomy, Neurosurgical Review 48(1) (2025) 357.
[160] T. Kawaguchi, K. Hosoda, Y. Shibata, J. Koyama, Expanded Polytetrafluoroethylene Membrane for Prevention of Adhesions in Patients Undergoing External Decompression and Subsequent Cranioplasty—Technical Note—, Neurologia Medico-Chirurgica 43(6) (2003) 320-324.

[161] S. Nakagawa, T. Hayashi, S. Anegawa, S. Nakashima, S. Shimokawa, Y. Furukawa, Postoperative infection after duraplasty with expanded polytetrafluoroethylene sheet, Neurologia Medico-Chirurgica 43(3) (2003) 120-124.
[162] S. Daghighi, J. Sjollema, H.C. van der Mei, H.J. Busscher, E.T. Rochford, Infection resistance of degradable versus non-degradable biomaterials: an assessment of the potential mechanisms, Biomaterials 34(33) (2013) 8013-8017.
[163] Y. Matsumoto, H. Aikawa, M. Tsutsumi, S. Narita, H. Yoshida, H. Etou, K. Sakamoto, K. Kazekawa, Histological Examination of Expanded Polytetrafluoroethylene Artificial Dura Mater at 14 Years After Craniotomy—Case Report—, Neurologia Medico-Chirurgica 53(1) (2013) 43-46.
[164] M. Pierson, P.V. Birinyi, S. Bhimireddy, J.R. Coppens, Analysis of decompressive craniectomies with subsequent cranioplasties in the presence of collagen matrix dural substitute and polytetrafluoroethylene as an adhesion preventative material, World Neurosurgery 86 (2016) 153-160.
[165] K.Y. Wu, J.K. Fujioka, P. Daigle, S.D. Tran, The use of functional biomaterials in aesthetic and functional restoration in orbital surgery, Journal of Functional Biomaterials 15(2) (2024) 33.
[166] M. Cabraja, M. Klein, T.-N. Lehmann, Long-term results following titanium cranioplasty of large skull defects, Neurosurgical Focus 26(6) (2009) E10.
[167] J.T. Jegadeesan, M. Baldia, B. Basu, Next-generation personalized cranioplasty treatment, Acta Biomaterialia 154 (2022) 63-82.
[168] S. Zhu, Y. Chen, F. Lin, Z. Chen, X. Jiang, J. Zhang, J. Wang, Complications following titanium cranioplasty compared with nontitanium implants cranioplasty: a systematic review and meta-analysis, Journal of Clinical Neuroscience 84 (2021) 66-74.
[169] P. Jeyaraj, Efficacy and versatility of the 3-D titanium mesh implant in the closure of large post-craniectomy osseous defects, and its therapeutic role in reversing the syndrome of the trephined: clinical study of a case series and review of literature, Journal of Maxillofacial and Oral Surgery 15(1) (2016) 82-92.
[170] T. Patel, M. Skonieczna, R. Turczyn, K. Krukiewicz, Modulating pro-adhesive nature of metallic surfaces through a polypeptide coupling via diazonium chemistry, Scientific Reports 13(1) (2023) 18365.
[171] D. Niewolik, B. Bednarczyk-Cwynar, P. Ruszkowski, G. Dzido, K. Jaszcz, Highly Branched Betulin Based Polyanhydrides for Self-Assembled Micellar Nanoparticles Formulation, International Journal of Molecular Sciences 23(19) (2022) 11462.

[172] N. Kumar, R.S. Langer, A.J. Domb, Polyanhydrides: an overview, Advanced Drug Delivery Reviews 54(7) (2002) 889-910.
[173] B. Maharjan, V.K. Kaliannagounder, S.R. Jang, G.P. Awasthi, D.P. Bhattarai, G. Choukrani, C.H. Park, C.S. Kim, In-situ polymerized polypyrrole nanoparticles immobilized poly (ε-caprolactone) electrospun conductive scaffolds for bone tissue engineering, Materials Science and Engineering: C 114 (2020) 111056.
[174] J. Lipus, K. Krukiewicz, Challenges and limitations of using charge storage capacity to assess capacitance of biomedical electrodes, Measurement 191 (2022) 110822.
[175] H.H. Lu, A. Tang, S.C. Oh, J.P. Spalazzi, K. Dionisio, Compositional effects on the formation of a calcium phosphate layer and the response of osteoblast-like cells on polymer-bioactive glass composites, Biomaterials 26(32) (2005) 6323-6334.
[176] G.W. O'Keeffe, P. Dockery, A.M. Sullivan, Effects of growth/differentiation factor 5 on the survival and morphology of embryonic rat midbrain dopaminergic neurones in vitro, Journal of Neurocytology 33(5) (2004) 479-488.
[177] W. Lipińska, K. Siuzdak, J. Ryl, P. Barski, G. Śliwiński, K. Grochowska, The optimization of enzyme immobilization at Au-Ti nanotextured platform and its impact onto the response towards glucose in neutral media, Materials Research Express 6(11) (2019) 1150e3.
[178] I. Casanellas, J. Samitier, A. Lagunas, Recent advances in engineering nanotopographic substrates for cell studies, Frontiers in Bioengineering and Biotechnology 10 (2022) 1002967.
[179] W.-C. Peng, Y.-C. Chen, J.-L. He, S.-L. Ou, R.-H. Horng, D.-S. Wuu, Tunability of p- and n-channel TiOx thin film transistors, Scientific Reports 8(1) (2018) 9255.
[180] M.C. Biesinger, B.P. Payne, A.P. Grosvenor, L.W. Lau, A.R. Gerson, R.S.C. Smart, Resolving surface chemical states in XPS analysis of first row transition metals, oxides and hydroxides: Cr, Mn, Fe, Co and Ni, Applied Surface Science 257(7) (2011) 2717-2730.
[181] J. Stepanovska, R. Matejka, J. Rosina, L. Bacakova, H. Kolarova, Treatments for enhancing the biocompatibility of titanium implants, Biomedical Papers of the Medical Faculty of Palacky University in Olomouc 164(1) (2020).
[182] M. D'Urso, I. Jorba, A. van der Pol, C.V. Bouten, N.A. Kurniawan, Spatial regulation of substrate adhesion directs fibroblast morphotype and phenotype, PNAS nexus 3(8) (2024) pgae289.
[183] S. Litvinov, X. Hu, N. Adams, Numerical simulation of tethered DNA in shear flow, Journal of Physics: Condensed Matter 23(18) (2011) 184118.

[184] K. Kolind, A. Dolatshahi-Pirouz, J. Lovmand, F.S. Pedersen, M. Foss, F. Besenbacher, A combinatorial screening of human fibroblast responses on micro-structured surfaces, Biomaterials 31(35) (2010) 9182-9191.
[185] H. Jeon, S. Koo, W.M. Reese, P. Loskill, C.P. Grigoropoulos, K.E. Healy, Directing cell migration and organization via nanocrater-patterned cell-repellent interfaces, Nature Materials 14(9) (2015) 918-923.
[186] J.H. Smith, C. Rowland, B. Harland, S. Moslehi, R. Montgomery, K. Schobert, W. Watterson, J. Dalrymple-Alford, R. Taylor, How neurons exploit fractal geometry to optimize their network connectivity, Scientific Reports 11(1) (2021) 2332.
[187] I. Nissan, H. Schori, V.B. Kumar, M.A. Passig, O. Shefi, A. Gedanken, Topographical impact of silver nanolines on the morphology of neuronal SH-SY5Y Cells, Journal of Materials Chemistry B 5(47) (2017) 9346-9353.
[188] J. Litowczenko, B.M. Maciejewska, J.K. Wychowaniec, M. Kościński, S. Jurga, A. Warowicka, Groove-patterned surfaces induce morphological changes in cells of neuronal origin, Journal of Biomedical Materials Research Part A 107(10) (2019) 2244-2256.
[189] C. Vallejo-Giraldo, K. Krukiewicz, M.J.P. Biggs, Understanding the mechanobiology of gliosis may be the key to unlocking sustained chronic performance of bioelectronic neural interfaces, Advanced NanoBiomed Research 2(3) (2022) 2100098.
[190] W.Q. Yuan, W.P. Huang, Y.C. Jiang, H. Xu, C.S. Duan, N.H. Chen, Y.J. Liu, X.M. Fu, The function of astrocytes and their role in neurological diseases, European Journal of Neuroscience 58(9) (2023) 3932-3961.
[191] N.J. Sniadecki, R.A. Desai, S.A. Ruiz, C.S. Chen, Nanotechnology for cell–substrate interactions, Annals of Biomedical Engineering 34(1) (2006) 59-74.
[192] H. Wang, G. Song, H. Chuang, C. Chiu, A. Abdelmaksoud, Y. Ye, L. Zhao, Portrait of glial scar in neurological diseases, International Journal of Immunopathology and Pharmacology 31 (2018) 2058738418801406.
[193] C. Göritz, D.O. Dias, N. Tomilin, M. Barbacid, O. Shupliakov, J. Frisén, A pericyte origin of spinal cord scar tissue, Science 333(6039) (2011) 238-242.
[194] N.A. Ewing-Crystal, N.M. Mroz, A. Larpthaveesarp, C.O. Lizama, R. Pennington, P. Chiaranunt, J.I. Dennis, A.A. Chang, E.D. Merrill, S.E. Caryotakis, Dynamic fibroblast–immune interactions shape recovery after brain injury, Nature 646(8086) (2025) 934-944.
[195] D.N. Mitchell, J.A. Siegenthaler, Fibroblasts are not so scar-y in brain injury, Immunity 58(10) (2025) 2370-2372.

[196] J.H. Nieto, T.X. Hoang, E.A. Warner, B.T. Franchini, U. Westerlund, L.A. Havton, Titanium mesh implantation—a method to stabilize the spine and protect the spinal cord following a multilevel laminectomy in the adult rat, Journal of Neuroscience Methods 147(1) (2005) 1-7.
[197] P.T. McCarthy, R. Madangopal, K.J. Otto, M.P. Rao, Titanium-based multi-channel, micro-electrode array for recording neural signals, 2009 Annual International Conference of the IEEE Engineering in Medicine and Biology Society, IEEE, 2009, pp. 2062-2065.
[198] D. Tahal, K. Madhavan, L.O. Chieng, G.M. Ghobrial, M.Y. Wang, Metals in spine, World Neurosurgery 100 (2017) 619-627.
[199] D. Grob, S. Daehn, A.F. Mannion, Titanium mesh cages (TMC) in spine surgery, European Spine Journal 14(3) (2005) 211-221.
[200] Y.O. Kang, I.S. Yoon, S.Y. Lee, D.D. Kim, S.J. Lee, W.H. Park, S.M. Hudson, Chitosan-coated poly (vinyl alcohol) nanofibers for wound dressings, Journal of Biomedical Materials Research Part B: Applied Biomaterials: An Official Journal of The Society for Biomaterials, The Japanese Society for Biomaterials, and The Australian Society for Biomaterials and the Korean Society for Biomaterials 92(2) (2010) 568-576.
[201] W. Ding, S. Wei, J. Zhu, X. Chen, D. Rutman, Z. Guo, Manipulated electrospun PVA nanofibers with inexpensive salts, Macromolecular Materials and Engineering 295(10) (2010) 958-965.
[202] P. Kumar, A.K. Singh, V. Raj, A. Rai, A.K. Keshari, D. Kumar, B. Maity, A. Prakash, S. Maiti, S. Saha, Poly (lactic-co-glycolic acid)-loaded nanoparticles of betulinic acid for improved treatment of hepatic cancer: characterization, in vitro and in vivo evaluations, International Journal of Nanomedicine (2018) 975-990.
[203] D. Niewolik, B. Bednarczyk-Cwynar, P. Ruszkowski, T.R. Sosnowski, K. Jaszcz, Bioactive betulin and PEG based polyanhydrides for use in drug delivery systems, International Journal of Molecular Sciences 22(3) (2021) 1090.
[204] R. Beigmoradi, A. Samimi, D. Mohebbi-Kalhori, Controllability of the hydrophilic or hydrophobic behavior of the modified polysulfone electrospun nanofiber mats, Polymer Testing 93 (2021) 106970.
[205] D. Gupta, M. Jassal, A.K. Agrawal, The electrospinning behavior of poly (vinyl alcohol) in DMSO–water binary solvent mixtures, RSC Advances 6(105) (2016) 102947-102955.
[206] J. Pelipenko, P. Kocbek, J. Kristl, Nanofiber diameter as a critical parameter affecting skin cell response, European Journal of Pharmaceutical Sciences 66 (2015) 29-35.

[207] C.J. Bettinger, R. Langer, J.T. Borenstein, Engineering substrate topography at the micro- and nanoscale to control cell function, Angewandte Chemie International Edition 48(30) (2009) 5406-5415.
[208] B. Janković, J. Pelipenko, M. Škarabot, I. Muševič, J. Kristl, The design trend in tissue-engineering scaffolds based on nanomechanical properties of individual electrospun nanofibers, International Journal of Pharmaceutics 455(1-2) (2013) 338-347.
[209] S.N. Alhosseini, F. Moztarzadeh, M. Mozafari, S. Asgari, M. Dodel, A. Samadikuchaksaraei, S. Kargozar, N. Jalali, Synthesis and characterization of electrospun polyvinyl alcohol nanofibrous scaffolds modified by blending with chitosan for neural tissue engineering, International Journal of Nanomedicine (2012) 25-34.
[210] D. Niewolik, K. Krukiewicz, B. Bednarczyk-Cwynar, P. Ruszkowski, K. Jaszcz, Novel polymeric derivatives of betulin with anticancer activity, RSC Advances 9(36) (2019) 20892-20900.
[211] O.V. Demets, A.T. Takibayeva, R.Z. Kassenov, M.R. Aliyeva, Methods of betulin extraction from birch bark, Molecules 27(11) (2022) 3621.
[212] G. Zhao, W. Yan, D. Cao, Simultaneous determination of betulin and betulinic acid in white birch bark using RP-HPLC, Journal of Pharmaceutical and Biomedical Analysis 43(3) (2007) 959-962.
[213] T.M. Temel-Soylu, C. Kececiler-Emir, T. Rababah, C. Ozel, S. Yucel, Y. Basaran-Elalmis, D. Altan, O. Kirgiz, I.E. Secinti, U. Kaya, Green electrospun poly (vinyl alcohol)/gelatin-based nanofibrous membrane by incorporating 45S5 bioglass nanoparticles and urea for wound dressing applications: Characterization and in vitro and in vivo evaluations, ACS Omega 9(19) (2024) 21187-21203.
[214] R. Ramalingam, G. Jiang, H. Larjava, L. Häkkinen, Macromolecular crowding regulates matrix composition and gene expression in human gingival fibroblast cultures, Scientific Reports 13(1) (2023) 2047.
[215] J. Małaczewska, E. Kaczorek-Łukowska, B. Kazuń, High cytotoxicity of betulin towards fish and murine fibroblasts: Is betulin safe for nonneoplastic cells?, BMC Veterinary Research 17(1) (2021) 198.
[216] K. Pfarr, C. Danciu, O. Arlt, C. Neske, C. Dehelean, J.M. Pfeilschifter, H.H. Radeke, Simultaneous and dose dependent melanoma cytotoxic and immune stimulatory activity of betulin, PLoS One 10(3) (2015) e0118802.
[217] W.-Y. Lin, S. Sadhasivam, F.-H. Lin, The dose dependent effects of betulin on porcine chondrocytes, Process Biochemistry 44(6) (2009) 678-684.

[218] M. Şahin, G. Öncü, M.A. Yılmaz, D. Özkan, H. Saybaşılı, Transformation of SH-SY5Y cell line into neuron-like cells: Investigation of electrophysiological and biomechanical changes, Neuroscience Letters 745 (2021) 135628.
[219] G. Gonzalez, J. Hodoň, A. Kazakova, C.W. D'Acunto, P. Kaňovský, M. Urban, M. Strnad, Novel pentacyclic triterpenes exhibiting strong neuroprotective activity in SH-SY5Y cells in salsolinol-and glutamate-induced neurodegeneration models, European Journal of Medicinal Chemistry 213 (2021) 113168.
[220] W. Jiang, K. Hao, Protective action of betulinic acid on cerebral ischemia/reperfusion injury through inflammation and energy metabolic homeostasis, Applied Sciences 10(7) (2020) 2578.
[221] S.K. Pandey, H. Singh, S. Ahmad, R.K. Singh, Betulinic acid protects SH-SY5Y cells exposed to lipopolysaccharide and ferrous sulfate through p38MAPK/NF-κB/GPX4/Nrf2/keap-1/HO-1 signaling axis, Free Radical Research 59(8-9) (2025) 688-706.
[222] A.G. Abdelaziz, H. Nageh, M.S. Abdalla, S.M. Abdo, A.A. Amer, S.A. Loutfy, N.F. Abdel Fattah, A. Alsalme, D. Cornu, M. Bechelany, Development of polyvinyl alcohol nanofiber scaffolds loaded with flaxseed extract for bone regeneration: phytochemicals, cell proliferation, adhesion, and osteogenic gene expression, Frontiers in Chemistry 12 (2024) 1417407.
[223] G. Zhang, X. Hou, Z. Geng, M. Yusoff, N.A. Roslan, M.H. Razali, Enhanced bone regeneration using sodium alginate and polyvinyl alcohol incorporating TiO2 nanoparticles composite film for orthopedic application, Results in Chemistry 13 (2025) 102049.
[224] K. Anselme, L. Ploux, A. Ponche, Cell/material interfaces: influence of surface chemistry and surface topography on cell adhesion, Journal of Adhesion Science and Technology 24(5) (2010) 831-852.
[225] S.I. Jeong, M.D. Krebs, C.A. Bonino, S.A. Khan, E. Alsberg, Electrospun alginate nanofibers with controlled cell adhesion for tissue engineering a, Macromolecular Bioscience 10(8) (2010) 934-943.
[226] M.A. Schwartz, Integrins and extracellular matrix in mechanotransduction, Cold Spring Harbor Perspectives in Biology 2(12) (2010) a005066.
[227] R. Hiramatsu, S. Fukuhara, S. Mitsuda, T. Yokomichi, T. Kataoka, Betulinic acid and oleanolic acid, natural pentacyclic triterpenoids, interfere with N-linked glycan modifications to intercellular adhesion molecule-1, but not its intracellular transport to the cell surface, European Journal of Pharmacology 767 (2015) 126-134.

[228] M. Mizerska-Kowalska, A. Sławińska-Brych, K. Kaławaj, A. Żurek, B. Pawińska, W. Rzeski, B. Zdzisińska, Betulin promotes differentiation of human osteoblasts in vitro and exerts an osteoinductive effect on the hFOB 1.19 cell line through activation of JNK, ERK1/2, and mTOR kinases, Molecules 24(14) (2019) 2637.
[229] Y.-C. Lo, Y.-H. Chang, B.-L. Wei, Y.-L. Huang, W.-F. Chiou, Betulinic acid stimulates the differentiation and mineralization of osteoblastic MC3T3-E1 cells: involvement of BMP/Runx2 and β-catenin signals, Journal of Agricultural and Food Chemistry 58(11) (2010) 6643-6649.
[230] K.M. Agarwal, A. Singhal, A. Kapoor, D. Bhatia, Simulated analysis of Ti-6Al-4V processed through equal channel angular pressing for biomedical applications, Materials Science for Energy Technologies 4 (2021) 290-295.
[231] L. Bauer, L. Brandstäter, M. Letmate, M. Palachandran, F.O. Wadehn, C. Wolfschmidt, T. Grothe, U. Güth, A. Ehrmann, Electrospinning for the Modification of 3D Objects for the Potential Use in Tissue Engineering, Technologies 10(3) (2022) 66.
[232] I. Caloian, J. Trapp, M.W. Williams, R.A. Kim, M.E. Moustafa, E.H. Stwodah, C. Tang, Direct fabrication of functional shapes on 3D surfaces using electrospinning, Polymers 15(3) (2023) 533.
[233] C. McManamon, J.P. de Silva, P. Delaney, M.A. Morris, G.L. Cross, Characteristics, interactions and coating adherence of heterogeneous polymer/drug coatings for biomedical devices, Materials Science and Engineering: C 59 (2016) 102-108.
[234] N. Nhlapo, T.C. Dzogbewu, O. de Smidt, Nanofiber polymers for coating titanium-based biomedical implants, Fibers 10(4) (2022) 36.
[235] R. Zhao, L. Shi, L. Gu, X. Qin, Z. Song, X. Fan, P. Zhao, C. Li, H. Zheng, Z. Li, Evaluation of bioactive glass scaffolds incorporating SrO or ZnO for bone repair: In vitro bioactivity and antibacterial activity, Journal of Applied Biomaterials & Functional Materials 19 (2021) 22808000211040910.
[236] S.J. Kashyap, R. Sankannavar, G. Madhu, Hydroxyapatite nanoparticles synthesized with a wide range of Ca/P molar ratios and their structural, optical, and dielectric characterization, Journal of the Korean Ceramic Society 59(6) (2022) 846-858.
[237] U. Tariq, Z. Haider, K. Chaudhary, R. Hussain, J. Ali, Calcium to phosphate ratio measurements in calcium phosphates using LIBS, Journal of Physics: Conference Series, IOP Publishing, 2018, p. 012015.

[238] A.F. Khan, M. Awais, A.S. Khan, S. Tabassum, A.A. Chaudhry, I.U. Rehman, Raman spectroscopy of natural bone and synthetic apatites, Applied Spectroscopy Reviews 48(4) (2013) 329-355.
[239] V.V. Nosenko, A.M. Yaremko, V.M. Dzhagan, I.P. Vorona, Y.A. Romanyuk, I.V. Zatovsky, Nature of some features in Raman spectra of hydroxyapatite-containing materials, Journal of Raman Spectroscopy 47(6) (2016) 726-730.
[240] L. Sotelo, T. Fontanot, S. Vig, P. Herre, P. Yousefi, M.H. Fernandes, G. Sarau, G. Leuchs, S. Christiansen, Influence of initial surface roughness on LIPSS formation and its consecutive impact on cell/bacteria attachment for TiAl6V4 surfaces, Advanced Materials Technologies 8(12) (2023) 2201802.
[241] D. Zhao, H. Liang, C. Han, J. Li, J. Liu, K. Zhou, C. Yang, Q. Wei, 3D printing of a titanium-tantalum Gyroid scaffold with superb elastic admissible strain, bioactivity and in-situ bone regeneration capability, Additive Manufacturing 47 (2021) 102223.
[242] G. Toworfe, R. Composto, I. Shapiro, P. Ducheyne, Nucleation and growth of calcium phosphate on amine-, carboxyl-and hydroxyl-silane self-assembled monolayers, Biomaterials 27(4) (2006) 631-642.
[243] G. Pohan, S. Mattiassi, Y. Yao, A.M. Zaw, D.E. Anderson, M.F. Cutiongco, M.T. Hinds, E.K. Yim, Effect of ethylene oxide sterilization on polyvinyl alcohol hydrogel compared with gamma radiation, Tissue Engineering Part A 26(19-20) (2020) 1077-1090.
[244] O. Belgherbi, L. Seid, D. Lakhdari, D. Chouder, M. Akhtar, M. Saeed, Optical and morphological properties of electropolymerized semiconductor polyaniline thin films: effect of thickness, Journal of Electronic Materials 50 (2021) 3876-3884.
[245] K.R. Prasad, N. Munichandraiah, Electrocatalytic efficiency of polyaniline by cyclic voltammetry and electrochemical impedance spectroscopy studies, Synthetic Metals 126(1) (2002) 61-68.
[246] E.G. Cansu-Ergun, A. Cihaner, New EDOT containing polymers: Effect of ring size on the benzimidazole acceptor, Electrochimica Acta 188 (2016) 165-174.
[247] M. Skorupa, D. Więcławska, D. Czerwińska-Główka, M. Skonieczna, K. Krukiewicz, Dopant-dependent electrical and biological functionality of pedot in bioelectronics, Polymers 13(12) (2021) 1948.
[248] K. Krukiewicz, A. Kruk, R. Turczyn, Evaluation of drug loading capacity and release characteristics of PEDOT/naproxen system: Effect of doping ions, Electrochimica Acta 289 (2018) 218-227.

[249] R. Rauti, M. Musto, S. Bosi, M. Prato, L. Ballerini, Properties and behavior of carbon nanomaterials when interfacing neuronal cells: How far have we come?, Carbon 143 (2019) 430-446.
[250] C. Boehler, S. Carli, L. Fadiga, T. Stieglitz, M. Asplund, Tutorial: guidelines for standardized performance tests for electrodes intended for neural interfaces and bioelectronics, Nature Protocols 15(11) (2020) 3557-3578.
[251] H.-l. Chen, G.-z. Tian, H. Yan, S.-x. Yang, D.-H. Kim, Fabrication of vertically aligned PEDOT nanotube arrays on microelectrodes to interface neurons, Electrochimica Acta 404 (2022) 139583.
[252] S. Holm, T. Holm, Ø.G. Martinsen, Simple circuit equivalents for the constant phase element, PloS one 16(3) (2021) e0248786.
[253] F.-F. Pang, S. Li, W.-Q. Sun, G.-Z. Han, Reversible conductivity modulation of PEDOT: PSS based on pH, Materials Chemistry and Physics 186 (2017) 246-250.
[254] S. Kulandaivalu, Z. Zainal, Y. Sulaiman, A new approach for electrodeposition of poly (3, 4-ethylenedioxythiophene)/polyaniline (PEDOT/PANI) copolymer, International Journal of Electrochemical Science 10(11) (2015) 8926-8940.
[255] A.d.J. Motheo, J. Santos Jr, E.C. Venancio, L.H.C. Mattoso, Influence of different types of acidic dopant on the electrodeposition and properties of polyaniline films, Polymer 39(26) (1998) 6977-6982.
[256] H. Zhang, J. Wang, Z. Wang, F. Zhang, S. Wang, Electrodeposition of polyaniline nanostructures: A lamellar structure, Synthetic Metals 159(3-4) (2009) 277-281.
[257] A. Bonastre, P. Bartlett, Electrodeposition of PANi films on platinum needle type microelectrodes. Application to the oxidation of ascorbate in human plasma, Analytica Chimica Acta 676(1-2) (2010) 1-8.
[258] N.A. Oberheim, T. Takano, X. Han, W. He, J.H. Lin, F. Wang, Q. Xu, J.D. Wyatt, W. Pilcher, J.G. Ojemann, Uniquely hominid features of adult human astrocytes, Journal of Neuroscience 29(10) (2009) 3276-3287.
[259] A. Popov, B. Brasiunas, A. Damaskaite, I. Plikusiene, A. Ramanavicius, A. Ramanaviciene, Electrodeposited gold nanostructures for the enhancement of electrochromic properties of PANI–PEDOT film deposited on transparent electrode, Polymers 12(12) (2020) 2778.
[260] B. Aurian-Blajeni, A. Kimball, L. Robblee, G. Kahanda, M. Tomkiewicz, Correlation between charge storage capacity and morphology, Journal of The Electrochemical Society 134 (1987) 2637.

[261] R. Singh, A. Kumar, Effect of electrode surface on the electrochromic properties of electropolymerized poly (3, 4-ethylenedioxythiophene) thin films, Organic Electronics 30 (2016) 67-75.
[262] I. Šeděnková, M. Trchová, J. Stejskal, Thermal degradation of polyaniline films prepared in solutions of strong and weak acids and in water–FTIR and Raman spectroscopic studies, Polymer Degradation and Stability 93(12) (2008) 2147-2157.
[263] A.B. Rohom, P.U. Londhe, S. Mahapatra, S. Kulkarni, N. Chaure, Electropolymerization of polyaniline thin films, High Performance Polymers 26(6) (2014) 641-646.
[264] P. Bober, J. Stejskal, M. Trchová, J. Prokeš, Polyaniline–silver composites prepared by the oxidation of aniline with mixed oxidants, silver nitrate and ammonium peroxydisulfate: The control of silver content, Polymer 52(26) (2011) 5947-5952.
[265] R. Mažeikienė, G. Niaura, A. Malinauskas, A comparative Raman spectroelectrochemical study of selected polyaniline derivatives in a pH-neutral solution, Synthetic Metals 160(9-10) (2010) 1060-1064.
[266] H.S. Abdullah, Electrochemical polymerization and Raman study of polypyrrole and polyaniline thin films, Physical Science International Journal 7(38) (2012) 5468-5476.
[267] Q. Zhao, R. Jamal, L. Zhang, M. Wang, T. Abdiryim, The structure and properties of PEDOT synthesized by template-free solution method, Nanoscale Research Letters 9 (2014) 1-9.
[268] S. Nešpůrek, P. Kuberský, R. Polanský, M. Trchová, J. Šebera, V. Sychrovský, Raman spectroscopy and DFT calculations of PEDOT: PSS in a dipolar field, Physical Chemistry Chemical Physics 24(1) (2022) 541-550.
[269] I. Alessandri, F. Torricelli, B. Cerea, M. Speziani, P. Romele, Z.M. Kovacs-Vajna, I. Vassalini, Why PEDOT: PSS should not be used for Raman sensing of redox states (and how it could be), ACS Applied Materials & Interfaces 14(50) (2022) 56363-56373.
[270] J. Štulík, R. Polanský, A. Hamáček, S. Nešpůrek, P. Slepička, Z. Kolská, V. Švorčík, Comparison of organic thermistors based on PEDOT: PSS and PEDOT: Tos thin films under various thermal and humidity conditions, Sensors and Actuators B: Chemical 275 (2018) 359-366.
[271] S. Jafarzadeh, P.M. Claesson, J. Pan, E. Thormann, Direct measurement of colloidal interactions between polyaniline surfaces in a UV-curable coating formulation: the effect of surface hydrophilicity/hydrophobicity and resin composition, Langmuir 30(4) (2014) 1045-1054.

[272] F. Xu, S. Ren, J. Li, X. Bi, Y. Gu, Molecular assembly of a durable hrp-aunps/pedot: Bsa/pt biosensor with detailed characterizations, Sensors 18(6) (2018) 1823.
[273] M. Shakiba, M. Abdouss, S. Mazinani, M.R. Kalaee, Super-hydrophilic electrospun PAN nanofibrous membrane modified with alkaline treatment and ultrasonic-assisted PANI in-situ polymerization for highly efficient gravity-driven oil/water separation, Separation and Purification Technology 309 (2023) 123032.
[274] V. Vedam-Mai, E. Van Battum, W. Kamphuis, M. Feenstra, D. Denys, B. Reynolds, M. Okun, E. Hol, Deep brain stimulation and the role of astrocytes, Molecular Psychiatry 17(2) (2012) 124-131.
[275] W.-H. Lee, C.-Y. Loo, R. Rohanizadeh, A review of chemical surface modification of bioceramics: effects on protein adsorption and cellular response, Colloids and Surfaces B: Biointerfaces 122 (2014) 823-834.
[276] D.H. Kim, S.M. Richardson-Burns, J.L. Hendricks, C. Sequera, D.C. Martin, Effect of immobilized nerve growth factor on conductive polymers: electrical properties and cellular response, Advanced Functional Materials 17(1) (2007) 79-86.
[277] J. Wei, T. Igarashi, N. Okumori, T. Igarashi, T. Maetani, B. Liu, M. Yoshinari, Influence of surface wettability on competitive protein adsorption and initial attachment of osteoblasts, Biomedical Materials 4(4) (2009) 045002.
[278] S.B. Carter, Haptotaxis and the mechanism of cell motility, Nature 213(5073) (1967) 256-260.
[279] J. Folkman, A. Moscona, Role of cell shape in growth control, Nature 273(5661) (1978) 345-349.
[280] S. Siri, P. Wadbua, V. Amornkitbamrung, N. Kampa, S. Maensiri, Surface modification of electrospun PCL scaffolds by plasma treatment and addition of adhesive protein to promote fibroblast cell adhesion, Materials Science and Technology 26(11) (2010) 1292-1297.
[281] M. Ferrari, F. Cirisano, M.C. Morán, Mammalian cell behavior on hydrophobic substrates: influence of surface properties, Colloids Interfaces 3 (2019) 48, (2019).
[282] S. Soliman, S. Sant, J.W. Nichol, M. Khabiry, E. Traversa, A. Khademhosseini, Controlling the porosity of fibrous scaffolds by modulating the fiber diameter and packing density, Journal of Biomedical Materials Research Part A 96(3) (2011) 566-574.
[283] J. Dias, A. Sousa, A. Augusto, P. Bártolo, P. Granja, Electrospun polycaprolactone (PCL) degradation: an in vitro and in vivo study. Polymers 14 (16): 3397, 2022.

[284] J.L. Lowery, N. Datta, G.C. Rutledge, Effect of fiber diameter, pore size and seeding method on growth of human dermal fibroblasts in electrospun poly (ε-caprolactone) fibrous mats, Biomaterials 31(3) (2010) 491-504.
[285] R. Elashnikov, S. Rimpelová, L. Děkanovský, V. Švorčík, O. Lyutakov, Polypyrrole-coated cellulose nanofibers: influence of orientation, coverage and electrical stimulation on SH-SY5Y behavior, Journal of Materials Chemistry B 7(42) (2019) 6500-6507.
[286] J. John, P. Saheeda, K. Sabeera, S. Jayalekshmi, Doped polypyrrole with good solubility and film forming properties suitable for device applications, Materials Today: Proceedings 5(10) (2018) 21140-21146.
[287] N.V. Blinova, J. Stejskal, M. Trchová, J. Prokeš, M. Omastová, Polyaniline and polypyrrole: A comparative study of the preparation, European Polymer Journal 43(6) (2007) 2331-2341.
[288] A.H. Birniwa, A.S. Abubakar, A.O. Huq, H.N.M.E. Mahmud, Polypyrrole-polyethyleneimine (PPy-PEI) nanocomposite: An effective adsorbent for nickel ion adsorption from aqueous solution, Journal of Macromolecular Science, Part A 58(3) (2021) 206-217.
[289] B. Sun, T. Wu, J. Wang, D. Li, J. Wang, Q. Gao, M.A. Bhutto, H. El-Hamshary, S.S. Al-Deyab, X. Mo, Polypyrrole-coated poly (l-lactic acid-co-ε-caprolactone)/silk fibroin nanofibrous membranes promoting neural cell proliferation and differentiation with electrical stimulation, Journal of Materials Chemistry B 4(41) (2016) 6670-6679.
[290] N.L.G.D.d. Souza, G.S. Cavallini, T.T. Alves, M.M. Pereira, H.d.M. Brandão, L.F.C.d. Oliveira, Compatibility and cytotoxicity of poly (ε-caprolactone)/polypyrrole-block-poly (ε-caprolactone) blend films in fibroblast bovine cells, Polímeros 34(1) (2024) e20240007.
[291] V. Milleret, T. Hefti, H. Hall, V. Vogel, D. Eberli, Influence of the fiber diameter and surface roughness of electrospun vascular grafts on blood activation, Acta Biomaterialia 8(12) (2012) 4349-4356.
[292] S. Gabriel, M. Cécius, K. Fleury-Frenette, D. Cossement, M. Hecq, N. Ruth, R. Jérôme, C. Jérôme, Synthesis of adherent hydrophilic polypyrrole coatings onto (semi) conducting surfaces, Chemistry of Materials 19(9) (2007) 2364-2371.
[293] P.K. Szewczyk, D.P. Ura, S. Metwally, J. Knapczyk-Korczak, M. Gajek, M.M. Marzec, A. Bernasik, U. Stachewicz, Roughness and fiber fraction dominated wetting of electrospun fiber-based porous meshes, Polymers 11(1) (2018) 34.
[294] S. Metwally, S. Ferraris, S. Spriano, Z.J. Krysiak, Ł. Kaniuk, M.M. Marzec, S.K. Kim, P.K. Szewczyk, A. Gruszczyński, M. Wytrwal-Sarna, Surface potential and roughness

controlled cell adhesion and collagen formation in electrospun PCL fibers for bone regeneration, Materials & Design 194 (2020) 108915.
[295] X. Zhang, Bai, Surface electric properties of polypyrrole in aqueous solutions, Langmuir 19(26) (2003) 10703-10709.
[296] E. Fröhlich, The role of surface charge in cellular uptake and cytotoxicity of medical nanoparticles, International Journal of Nanomedicine (2012) 5577-5591.
[297] N. Maroudas, Adhesion and spreading of cells on charged surfaces, Journal of Theoretical Biology 49(2) (1975) 417-424.
[298] C. Correia, D. Peixoto, D.S. da Costa, R.L. Reis, I. Pashkuleva, N.M. Alves, Development and in vitro assessment of injectable, adhesive, and self-healing chitosan-based hydrogels for treatment of spinal cord injury, Biomaterials Advances 167 (2025) 214090.
[299] R. Perlikowska, J. Silva, C. Alves, P. Susano, R. Pedrosa, The therapeutic potential of naturally occurring peptides in counteracting SH-SY5Y cells injury, International Journal of Molecular Sciences 23(19) (2022) 11778.
[300] J. Kovalevich, D. Langford, Considerations for the use of SH-SY5Y neuroblastoma cells in neurobiology, Neuronal cell culture: methods and protocols, Springer2013, pp. 9-21.
[301] T. Marques-Almeida, H. Fernandes, S. Lanceros-Mendez, C. Ribeiro, Surface charge and dynamic mechanoelectrical stimuli improves adhesion, proliferation and differentiation of neuron-like cells, Journal of Materials Chemistry B 11(1) (2023) 144-153.
[302] S. Khan, G. Newaz, A comprehensive review of surface modification for neural cell adhesion and patterning, Journal of Biomedical Materials Research Part A: An Official Journal of The Society for Biomaterials, The Japanese Society for Biomaterials, and The Australian Society for Biomaterials and the Korean Society for Biomaterials 93(3) (2010) 1209-1224.
[303] A. Devyatov, I. Kozlov, V. Das, Differentiation of SH-SY5Y Cells into Cortical Neuron-like Cells for Tauopathy Modeling and Seeding Assays, Molecular Neurobiology (2025) 1-12.
[304] I. ISO, ISO 10993: Biological evaluation of medical devices, TIMIRI SHANMUGAM PS, THANGARAJU P, PALANI N, et al. Medical Device Guidelines and Regulations Handbook2022. Springer International Publishing (2001).
[305] P.M. George, A.W. Lyckman, D.A. LaVan, A. Hegde, Y. Leung, R. Avasare, C. Testa, P.M. Alexander, R. Langer, M. Sur, Fabrication and biocompatibility of polypyrrole implants suitable for neural prosthetics, Biomaterials 26(17) (2005) 3511-3519.
[306] A. Ramanaviciene, A. Kausaite, S. Tautkus, A. Ramanavicius, Biocompatibility of polypyrrole particles: an in-vivo study in mice, Journal of Pharmacy and Pharmacology 59(2) (2007) 311-315.

[307] M. Entezari, M. Mozafari, M. Bakhtiyari, F. Moradi, Z. Bagher, M. Soleimani, Three-dimensional-printed polycaprolactone/polypyrrole conducting scaffolds for differentiation of human olfactory ecto-mesenchymal stem cells into Schwann cell-like phenotypes and promotion of neurite outgrowth, Journal of Biomedical Materials Research Part A 110(5) (2022) 1134-1146.
[308] R.A. Osmani, E. Singh, H. Kazi, R. Bhosale, R. Vaghela, V. Patravale, Conductive polymers and composite-based systems: A quantum leap in the drug delivery arena and therapeutics, Smart Polymeric Nano-Constructs in Drug Delivery, Elsevier2023, pp. 485-522.
[309] P.P. Fu, Q. Xia, G. Lin, M.W. Chou, Pyrrolizidine alkaloids—genotoxicity, metabolism enzymes, metabolic activation, and mechanisms, Drug metabolism Reviews 36(1) (2004) 1-55.
[310] J. Ma, Q. Xia, P.P. Fu, G. Lin, Pyrrole-protein adducts–A biomarker of pyrrolizidine alkaloid-induced hepatotoxicity, Journal of Food and Drug Analysis 26(3) (2018) 965-972.
[311] F. Renault-Mihara, S. Okada, S. Shibata, M. Nakamura, Y. Toyama, H. Okano, Spinal cord injury: emerging beneficial role of reactive astrocytes' migration, The International Journal of Biochemistry & Cell Biology 40(9) (2008) 1649-1653.
[312] M.S. Andrade Mier, E. Bakirci, P. Stahlhut, R. Blum, P.D. Dalton, C. Villmann, Primary glial cell and glioblastoma morphology in cocultures depends on scaffold design and hydrogel composition, Advanced Biology 7(10) (2023) 2300029.
[313] X. Xue, X. Wu, Y. Fan, S. Han, H. Zhang, Y. Sun, Y. Yin, M. Yin, B. Chen, Z. Sun, Heterogeneous fibroblasts contribute to fibrotic scar formation after spinal cord injury in mice and monkeys, Nature Communications 15(1) (2024) 6321.
[314] C.E. Dorrier, H.E. Jones, L. Pintarić, J.A. Siegenthaler, R. Daneman, Emerging roles for CNS fibroblasts in health, injury and disease, Nature Reviews Neuroscience 23(1) (2022) 23-34.
[315] C. Buken, J. Sahana, T.J. Corydon, D. Melnik, J. Bauer, M. Wehland, M. Krüger, S. Balk, N. Abuagela, M. Infanger, Morphological and molecular changes in juvenile normal human fibroblasts exposed to simulated microgravity, Scientific Reports 9(1) (2019) 11882.
[316] J.U. Park, T. Tsuchiya, Increase in gap-junctional intercellular communications (GJIC) of normal human dermal fibroblasts (NHDF) on surfaces coated with high-molecular-weight hyaluronic acid (HMW HA), Journal of Biomedical Materials Research: An Official Journal of The Society for Biomaterials, The Japanese Society for Biomaterials, and The Australian Society for Biomaterials and the Korean Society for Biomaterials 60(4) (2002) 541-547.

[317] M. Hamdan, L. Blanco, A. Khraisat, I.F. Tresguerres, Influence of titanium surface charge on fibroblast adhesion, Clinical Implant Dentistry and Related Research 8(1) (2006) 32-38.
[318] S.D. Parikh, S. Dave, L. Huang, W. Wang, S.M. Mukhopadhyay, D.A. Mayes, Multi-walled carbon nanotube carpets as scaffolds for U87MG glioblastoma multiforme cell growth, Materials Science and Engineering: C 108 (2020) 110345.
[319] Z. Wei, J. Liu, H. Xie, B. Wang, J. Wu, Z. Zhu, MiR-122-5p mitigates inflammation, reactive oxygen species and SH-SY5Y apoptosis by targeting CPEB1 after spinal cord injury via the PI3K/AKT signaling pathway, Neurochemical Research 46(4) (2021) 992-1005.
[320] L.F. Hoffmann, A. Martins, F. Majolo, V. Contini, S. Laufer, M.I. Goettert, Neural regeneration research model to be explored: SH-SY5Y human neuroblastoma cells, Neural Regeneration Research 18(6) (2023) 1265-1266.
[321] D.-H. Kim, D. Wirtz, Focal adhesion size uniquely predicts cell migration, Biophysical Journal 104(2) (2013) 319a.
[322] P.M. Tsimbouri, Adult stem cell responses to nanostimuli, Journal of Functional Biomaterials 6(3) (2015) 598-622.
[323] T. Hiraiwa, T.G. Yamada, N. Miki, A. Funahashi, N. Hiroi, Activation of cell migration via morphological changes in focal adhesions depends on shear stress in MYCN-amplified neuroblastoma cells, Journal of the Royal Society Interface 16(152) (2019) 20180934.
[324] T. Patel, M. Skorupa, M. Skonieczna, R. Turczyn, K. Krukiewicz, Surface grafting of poly-L-lysine via diazonium chemistry to enhance cell adhesion to biomedical electrodes, Bioelectrochemistry 152 (2023) 108465.
[325] M.E. Buck, A.S. Breitbach, S.K. Belgrade, H.E. Blackwell, D.M. Lynn, Chemical modification of reactive multilayered films fabricated from poly (2-alkenyl azlactone) s: design of surfaces that prevent or promote mammalian cell adhesion and bacterial biofilm growth, Biomacromolecules 10(6) (2009) 1564-1574.
[326] M. Bachmann, S. Kukkurainen, V.P. Hytönen, B. Wehrle-Haller, Cell adhesion by integrins, Physiological Reviews 99(4) (2019) 1655-1699.
[327] R. Probstmeier, P. Pesheva, Tenascin-C inhibits β1 integrin-dependent cell adhesion and neurite outgrowth on fibronectin by a disialoganglioside-mediated signaling mechanism, Glycobiology 9(2) (1999) 101-114.
[328] J. Jin, S. Tilve, Z. Huang, L. Zhou, H.M. Geller, P. Yu, Effect of chondroitin sulfate proteoglycans on neuronal cell adhesion, spreading and neurite growth in culture, Neural Regeneration Research 13(2) (2018) 289-297.

[329] I.N. Serratos, R. Olayo, C. Millán-Pacheco, J. Morales-Corona, J.O. Vicente-Escobar, A.M. Soto-Estrada, J.G. Córdoba-Herrera, O. Uribe, T. Gómez-Quintero, M.Á. Arroyo-Ornelas, Modeling integrin and plasma-polymerized pyrrole interactions: chemical diversity relevance for cell regeneration, Scientific Reports 9(1) (2019) 7009.
[330] B. Vigani, S. Rossi, G. Sandri, M.C. Bonferoni, F. Ferrari, Design and criteria of electrospun fibrous scaffolds for the treatment of spinal cord injury, Neural Regeneration Research 12(11) (2017) 1786-1790.
[331] J. Cao, J. Wu, J. Mu, S. Feng, J. Gao, The design criteria and therapeutic strategy of functional scaffolds for spinal cord injury repair, Biomaterials Science 9(13) (2021) 4591-4606.
[332] Y. Wan, J. Gao, J. Zhang, W. Peng, G. Qiu, Biodegradability of conducting chitosan-g-polycaprolactone/polypyrrole conduits, Polymer Degradation and Stability 95(10) (2010) 1994-2002.
[333] D. Kai, M.P. Prabhakaran, G. Jin, S. Ramakrishna, Polypyrrole-contained electrospun conductive nanofibrous membranes for cardiac tissue engineering, Journal of Biomedical Materials Research Part A 99(3) (2011) 376-385.